Internal Report
DESY F35-83-01
April 1983

ELECTRON-PROTON COLLIDING BEAMS

THE PHYSICS PROGRAMME AND THE MACHINE

by

B.H. Wiik

II. Institut für Experimentalphysik, University of Hamburg

and

Deutsches Elektronen-Synchrotron DESY, Hamburg, Germany

Internal Report
DESY F35-83-01
April 1983

Electron-Proton Colliding Beams

The Physics Programme and the Machine

B.H.Wiik

II. Institut für Experimentalphysik, University of Hamburg

and

Deutsches Elektronen-Synchrotron DESY, Hamburg, Germany.

1. Introduction

At present we have a simple and appealing picture of nature. At distances down to 10^{-16} cm, the smallest distances explored, experiments have shown that matter is made of two species of fundamental, pointlike fermions, quarks and leptons. The weak, electromagnetic and strong force which act between these constituents is described by gauge fields and is mediated by the exchange of gauge bosons. These forces might result from a single force; there is strong indirect evidence that the weak and the electromagnetic force coalesce into a single electroweak force at center-of-mass energies above 100 GeV, this electroweak force may be unified with the strong force at c.m. energies on the order of 10^{15} GeV.

Much of the experimental basis for our present understanding of nature results from deep inelastic lepton-hadron experiments. Examples are the discovery of quarks as physical entities, the first indirect evidence of gluons, the carriers of the strong force, and the discovery of the neutral weak current. The lepton-hadron interaction can be studied at center-of-mass energies well above the electroweak unification energy of 100 GeV by colliding electrons and protons in a two ring colliding beam facility.

The possibility of colliding electrons and protons was first considered by Hereward et al.[1] and further investigated by Goldzahl and Michaelis[2] as an option for the ISR. The discovery of pointlike constituents in deep inelastic electron proton scattering promted a joint LBL-SLAC group[3] to investigate a dedicated electron-proton colliding beam facility in more detail. The study showed that the

center-of-mass energies and expected luminosities for such a facility would be sufficient to investigate deep inelastic processes in the kinematic range where the electromagnetic and weak interaction are expected to be of similar strength. This is well outside the reach of available and proposed fixed target machines. Since then similar studies[4] have been carried out in nearly all high energy laboratories, however, they have not led to the construction of an electron-proton colliding beam facility.

At present several proposals to construct electron-proton facilities are ready for decision.

DESY has proposed to construct HERA[5], a dedicated electron-proton colliding beam facility, on a site joining the present site. HERA is designed to collide 820 GeV protons with 30 GeV electrons in four interaction regions yielding 314 GeV in the center of mass which is equivalent to the kinematical region covered by a 52 TeV fixed target machine. The maximum momentum transfer squared is 98400 GeV^2. The predicted luminosity at 314 GeV in c.m. is $6 \cdot 10^{31} cm^{-2} s^{-1}$. The project has been submitted to the German Government and recommended for construction by a review panel. The project can be completed late 1989 if authorized in 1983.

KEK plans to construct Tristan[6] designed to collide 25 GeV electrons with 300 GeV protons in three interaction regions. The maximum momentum transfer squared is $3 \cdot 10^4$ GeV^2 with an expected luminosity of $1.8 \cdot 10^{31}$ $cm^{-2} s^{-1}$. KEK has proposed to first construct an e^+e^- colliding ring capable of reaching 60 GeV in c.m. and this part of the project has been approved. A decision on the ep part is expected after first operation of the e^+e^- ring scheduled for 1985.

In addition to the dedicated facilities, a group of physicists[7] has proposed to collide 5 GeV electrons with the proton beam from FNAL Tevatron. A decision on this proposal has been postponed and will be considered at a later date. The same group has also proposed[7] an ep option for ISABELLE.

CERN has the option[8] of colliding the electrons in LEP with the protons in the SPS in one interaction region. This option yields a maximum momentum transfer squared of $5.4 \cdot 10^4$ GeV^2 and a predicted luminosity of $4 \cdot 10^{29}$ cm^{-2}s^{-1} in the parasitic mode and $1.3 \cdot 10^{31}$ cm^{-2}s^{-1} when both LEP and SPS are operating only for ep collisions.

In these lectures I'll first discuss the physics programme which can be carried out at a large electron - proton colliding beam facility, and from this discussion we will derive some of the constraints which physics impose on the machine parameters.

In the main part of my talk I'll review the physical principles of circular accelerators. Since this is perhaps a new topic to most of you, I have tried to be pedagogical and have borrowed freely from the excellent literatur[9,10,11,12] available. A more in depth treatment including a complete set of references to the original work can be found in the literature listed above and in the references listed at the beginning of each chapter.

M.Sands[9] has given a translucent discussion of the physical principles of an e^+e^- colliding ring and J.LeDuff[13] has very abely reviewed the same subject in the previous SLAC summer school. In these lecture we will therefore put more emphasis on the behaviour of the protons and the problems associated with colliding electrons and protons.

This part of the lecture begins with an overview of an electron-proton colliding beam facility using HERA as an example. The physics of such a facility is then reviewed in more detail starting out with the transverse and longitudinal motion of a single particle in the magnetic guide field and the accelerating r.f. field. The influence of the synchrotron radiation on the single particle motion is discussed next. How to obtain transversely polarised electron and how to transform this into a longitudinally polarised electron beam in the interaction point is described in chapter 8. Limitations on the stored current caused by various kinds of instabilities are reviewed in chapter 9. HERA is discussed in more details in the last chapter, with emphasis on the layout of the interaction region and the optimalisation of the luminosity.

2. Electron-proton Interactions at High Energies

2.1 Introduction

It has been shown experimentally that the proton contains point-like quarks confined by the strong interaction and that an electron incident on a proton interacts directly with one of these quarks in accordance with Fig. 2.1. The interaction between a lepton and a quark is mediated by a neutral or charged spacelike current. The variables and the kinematic of the process is defined in Fig. 2.1.

The physics programme[14] at an ep collider may be summarized as follows:

1. Determine the properties of the spacelike electroweak current at a mass which is large compared to the characteristic mass of the weak interaction. Measurements with electrons and positrons in well defined helicity states can be used to determine the properties of both charged and

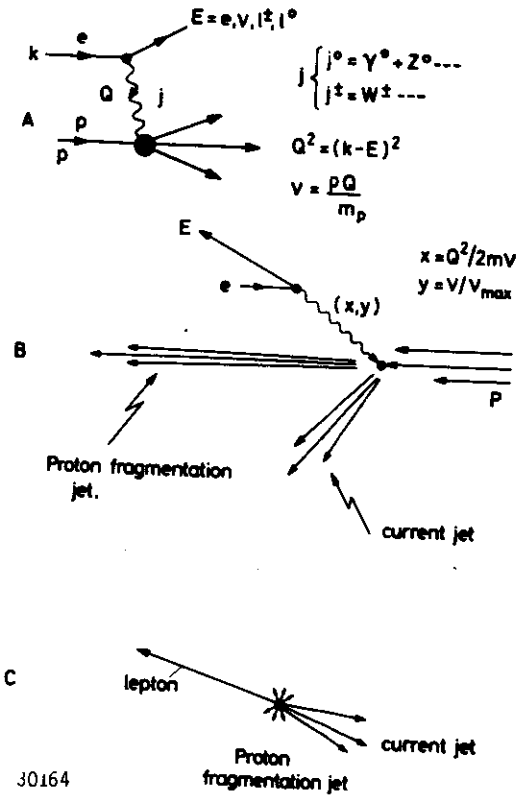

Fig. 2.1
Kinematics of deep inelastic electron proton collisions.

neutral currents in detail. For examples measurements with left handed positrons or right handed electrons are very sensitive probes for new weak currents.

2. Use the local, well defined electroweak current to explore the proton at distances down to 10^{-17} cm. Measurements of the structure functions will pose stringent tests of our present understanding of strong interaction. Such measurements may also reveal new constitu-

ents of the proton or they may show that quarks are composite objects.

3. Search for new phenomena. Examples are the search for free quarks, for supersymmetric particles, and for elementary particles with combined lepton and baryon numbers , the leptoquarks.

This programme demands a large kinematical area. The kinematical region available with HERA is equivalent to that of a 52 TeV fixed target machine and is shown in Fig. 2.2. The scale is set by the black dot in the left hand corner representing the region which can

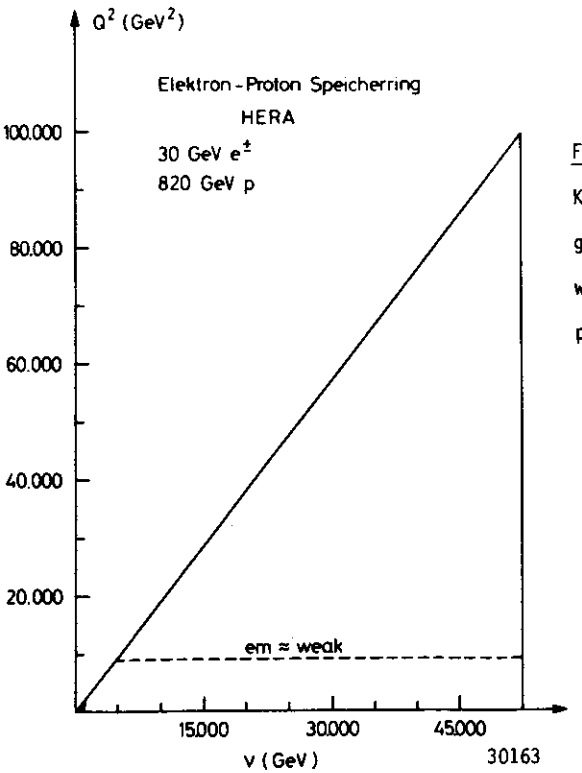

Fig. 2.2
Kinematical region in Q^2 and ν which can be explored with HERA.

be explored using a 1 TeV muon or neutrino beam on a fixed target. Lepton beams with somewhat lower energies will become available at the Tevatron[15] in 1983. It is clear that HERA opens a new kinematical region well outside that available with present or planned fixed target machines.

The Q^2-value corresponding to the characteristic mass of the weak interaction squared is shown as the dotted line. A large kinematical region is available beyond this Q^2-value.

The final state topology in deep inelastic electron-proton interactions is striking and easy to recognize. As indicated in Fig.2.1b and 2.1c the scattered lepton appears at a large angle with respect to the beam axis and the corresponding transverse momentum is balanced by the struck quark which fragments into a jet of hadrons appearing at large angles on the opposite side of the beam axis. The remains of the proton give rise to a foreward jet of hadrons focused along the proton beam axis with no net transverse momentum. Because of the imbalance between incident electron and proton momenta the particles will in general emerge in the forward hemisphere along the proton direction. The proton jet, the quark jet and the lepton defines a plane with small momenta transverse to the plane and large momenta in the plane.

The kinematic of the final lepton and of the current jet at nominal HERA energies of 30 GeV electrons on 820 GeV protons is shown in Figs.2.3a resp.2.3b. For a given Q^2 and x, the energy and the angle of the lepton, respectively, the current jet in the laboratory system is ob-

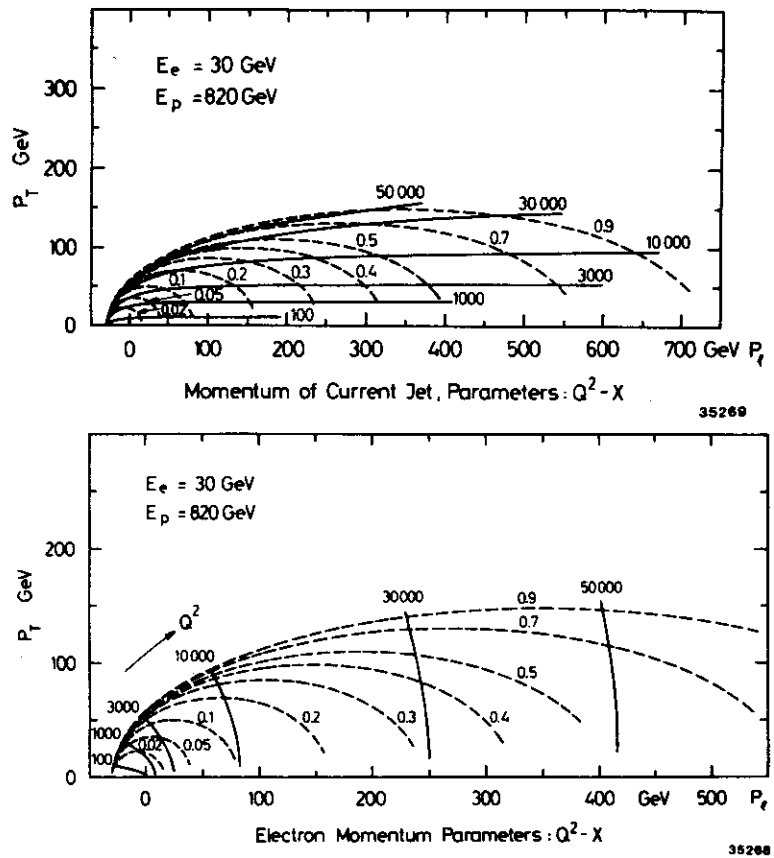

Fig. 2.3a,b - The laboratory momenta of the final lepton and the current jet with Q^2 and x as parameters. The laboratory angles and energies can be read off directly by connecting points with a given x and Q^2 with the origin.

tained by joining the relevant points with the origin. Note that the laboratory angles of the lepton and the current jet are in general large. Lowering the incident electron energy will focus the final state particles more strongly along the proton direction until particles belonging to the current jet are lost down the beam pipe. In this case Q^2 and x cannot be reconstructed from the current jet alone making it impossible to measure the form factors of the charged current.

Simply on the basis of topology it seems unlikely to confuse a deep inelastic electron-proton event with a background event such that the accessible Q^2-range appears not to be limited by the background. Note that particles from the lepton vertex and the quark vertex are kinematically well separated. In the standard model[16] only single neutrinos or electrons are allowed at the lepton vertex, such that the observation of jets emerging from the lepton vertex is a clear indication of new physics. It will therefore be possible to observe very rare exotic processes possessing this signature.

The Q^2-range which can be investigated is therefore only dependent on the rate - i.e. on the luminosity and the center-of-mass energy. In Fig. 2.4 the average luminosity needed to produce 100 charged current events a year with $Q^2 > Q_0^2$ is plotted versus Q_0^2 for various values of the center-of-mass energy. The year is assumed to have 5000 hrs and the rate is evaluated in the standard model with

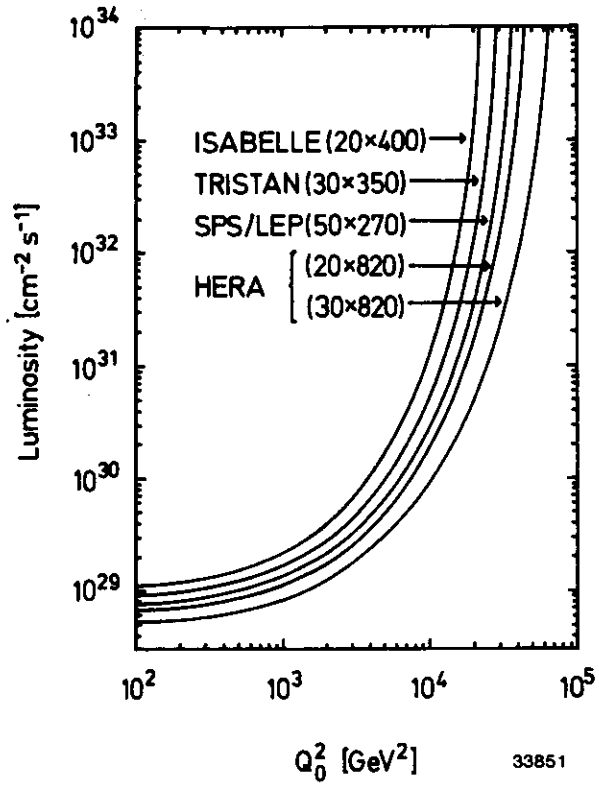

Fig. 2.4 - The average luminosity needed to produce 100 charged current events with $Q^2 > Q_0^2$ in 5000 hrs (1 year) of data taking versus Q_0^2 for various center-of-mass energies.

one charged vector boson. It is possible to explore Q^2-values up to say 3000 GeV^2 with a luminosity as low as $2 \cdot 10^{29}$ cm^{-2}s^{-1}. To produce 100 charged current events with $Q^2 > 10\,000$ GeV^2 per year requires a luminosity of $1.5 \cdot 10^{30}$ cm^{-2}s^{-1} - a factor of 40 below the HERA design luminosity. To obtain the same number of events with $Q^2 > 10\,000$ GeV^2 by colliding 20 GeV electrons with 400 GeV protons requires an average luminosity of $3 \cdot 10^{31}$ cm^{-2}s^{-1} - a factor 20 higher than the luminosity required at HERA. Note that for a luminosity of 10^{32} cm^{-2}s^{-1} we expect 100 events a year with $Q^2 \gtrsim 35\,000$ GeV^2.

2.2 Low Q^2-physics

The electron beam at HERA is equivalent to a well collimated bremsstrahlungsbeam with an endpoint energy of 52 TeV. The untagged photon-proton luminosity is typically on the order of a few percent of the electron-proton luminosity yielding some 10^7 hadronic events per day.

The photon has a dual character, it may convert into a vector meson and interact like a hadron. However, it has also a pointlike part and may induce hard processes like deep inelastic Compton scattering and the QCD analogues of Compton scattering and Bethe-Heitler processes as indicated in Fig. 2.5. Note that the QCD Bethe-Heitler process can be used to measure the gluon structure function (q = u,d,s) and to search for heavy quarks. A total of 10^5 $c\bar{c}$ pairs are expected to be produced per day at HERA via the QCD Bethe-Heitler process and some 20 $t\bar{t}$ pairs if $m_t = 50$ GeV.

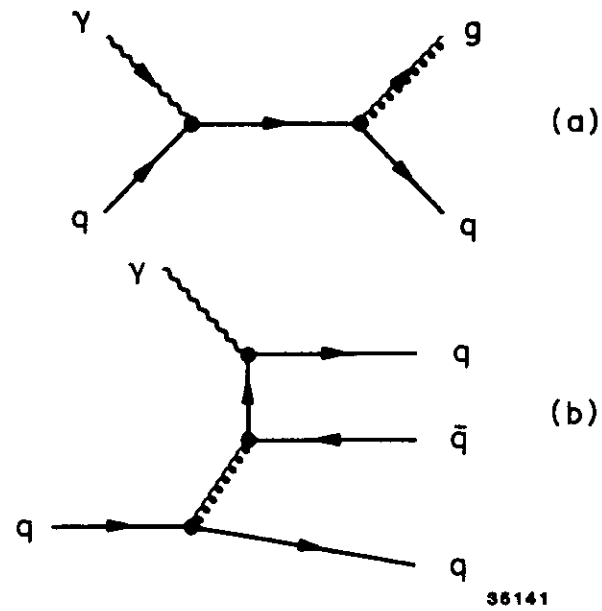

Fig. 2.5 - Hard processes induced by the pointlike part of the photon a) QCD Compton b) QCD Bethe-Heitler.

2.3 Properties of the currents

2.3.1 Charged currents

Present data are all consistent with a left handed current which is mediated by a single charged vector boson with a mass around 80 GeV. The observed simplicity of the charged current might well only reflect the static limit studied so far and a rich structure with many vector bosons, some perhaps giving rise to right handed

currents, might appear at high energies. From a purely experimental point HERA has some unique features compared to present fixed target experiments.

- Very high energy.

  The beam is equivalent to a monoenergetic neutrino beam with an energy up to 52 TeV.

- Choice of helicity.

  It will presumably be possible to change the helicity of the incident lepton - i.e. the cross section for left and right handed electrons (or positrons) can be measured directly.

- Visibility.

  The target is massless and can be surrounded by fine grained detectors including particle identification.

- Favourable kinematics.

  The lepton, the current jet and the target fragmentation jet are presumably well separated in space and the event is easily recognized.

The x, y distribution of charged current events in bins of dxdy = $(0.2)^2$ expected after one month of data taking with an unpolarised 30 GeV electron beam colliding with protons of 820 GeV is shown in Fig. 2.6. The rates were estimated in the standard model[16] with m_W = 78 GeV and formfactors parametrized according to Buras and Gaemers[16] and assuming a luminosity of 10^{32} $cm^{-2}s^{-1}$. Given the distinct signature of charged current events it seems possible to explore nearly the entire kinematic region.

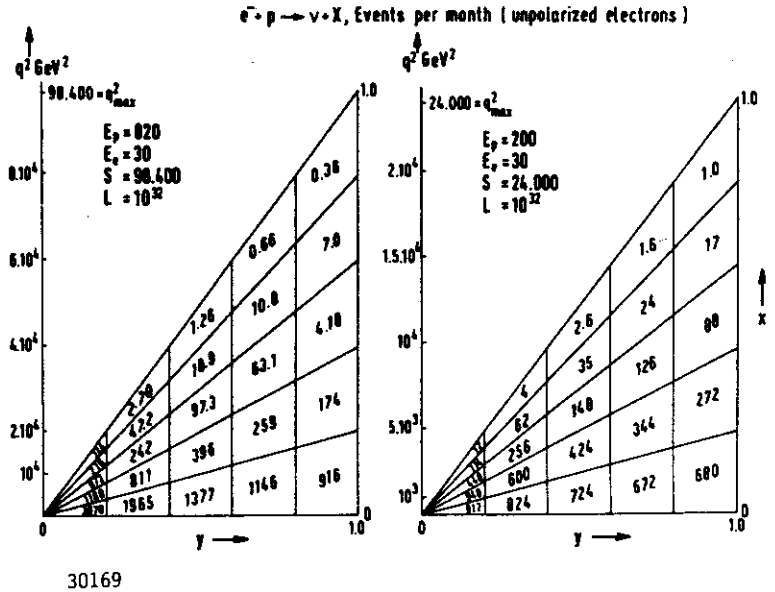

30169

Fig. 2.6 - Number of charged current events in bins of dxdy = $(0.2)^2$ produced per month of data taking assuming the standard model and a luminosity of $10^{32}cm^{-2}s^{-1}$. To obtain the number of events expected per year of data taking at the nominal HERA luminosity using left handed electrons multiply the left plot with a factor 8 and the right hand plot with a factor 5.

The expected number of events per year for the reaction $e_L^- + p \to \nu + x$, evaluated with the assumptions listed above, is plotted in Fig. 2.7 versus Q^2 for various propagator masses. It is clear that the mass of the propagator can be measured as long as it is below 500 GeV. The data can also be used to determine whether the charged current is damped by a single vector boson as presently believed or by several.

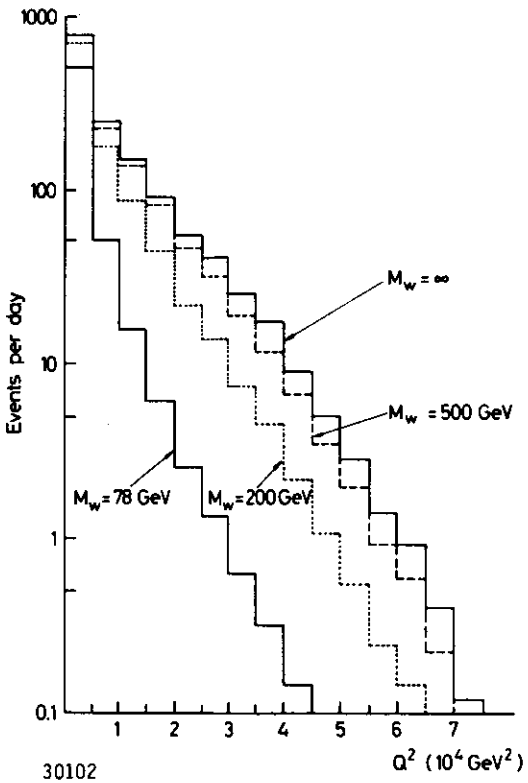

Fig. 2.7

Events per day for $e^- + p \to \nu + x$ in Q^2 bins of 5000 GeV^2 with the standard assumptions.

Right handed currents do not occur in the standard model. Sensitive searches for these currents may be carried out using right handed electrons and left handed positrons. Such measurements will reveal the existence of right handed currents if the mass of the right handed propagator is less than 600 GeV and the longitudinal beam polarisation is at least 80% known to an accuracy of 1%. This mass limit is valid even if the electron is partnered with a massive neutrino in a right handed doublet.

At $x > 0.4$ only valence quarks contribute to the cross section - i.e. $e^- + u \to d + x$ and $e^+ + d \to u + x$ are the dominant processes. This makes it possible to study the fragmentation of a well defined flavour. However, in principle it also opens the possibility of measuring the Kobayashi-Maskawa mixing angles[17] directly:

$$e^- + u \to s + x \quad \text{and} \quad e^- + u \to b + x$$
$$e^+ + d \to c + x \quad \text{and} \quad e^+ + d \to t + x \,.$$

2.3.2 Neutral currents

One photon exchange and Z^0 exchange contribute coherently to $e + p \to e' + x$ and both contributions are of similar strength at HERA energies. Measurements of this process can therefore decide if indeed the electromagnetic and weak interactions are manifestations of a single force and if this unification occurs as conjectured in the standard model[16] or if a more complicated mechanism involving many Z^0's is realized in nature. The number of neutral current events produced per day in a bin $dxdy = (0.2)^2$ is plotted in Fig. 2.8. Again due to the characteristic topology of deep inelastic events HERA can extend the Q^2 range from the present few hundred GeV^2 out to some 40 000 - 50 000 GeV^2.

The presence of a weak current in the amplitude has clear signatures:

1) Parity violation

$$\sigma(e_L^- + p \to e^{-\prime} + x) \neq \sigma(e_R^- + p \to e^{-\prime} + x)$$
$$\sigma(e_L^+ + p \to e^{+\prime} + x) \neq \sigma(e_R^+ + p \to e^{+\prime} + x)$$

This effect can only be caused by a neutral weak current.

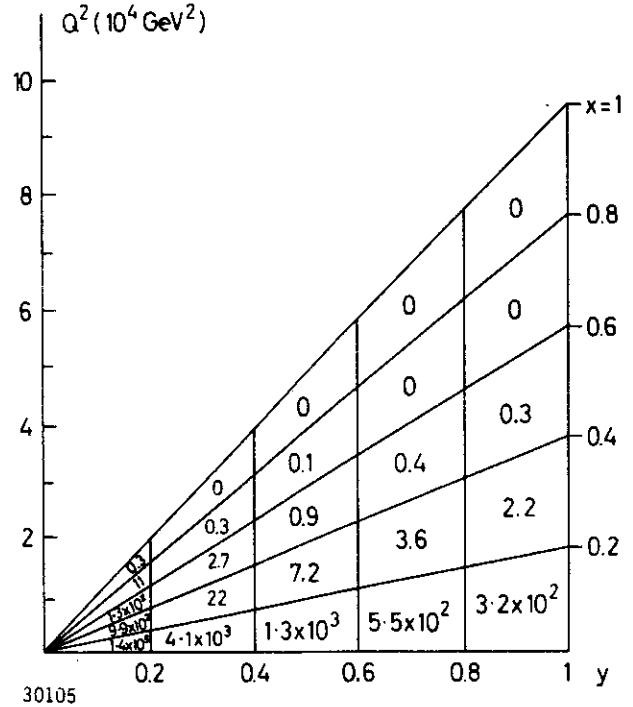

Fig. 2.8 - Number of events per day for $e^- + p \to e^- + x$ at $s = 9.6 \cdot 10^4$ GeV^2 and the standard assumptions.

2. Appearant C-violation

$$\sigma(e_L^- + p \to e^{-\prime} + x) \neq \sigma(e_L^+ + p \to e^{+\prime} + x)$$

$$\sigma(e_R^- + p \to e^{-\prime} + x) \neq \sigma(e_R^+ + p \to e^{+\prime} + x)$$

Two-photon exchange will also give rise to a charge asymmetry. This effect, however, is expected to be of order $\alpha/\pi \ln (Q^2/m^2)$ with $m \sim 300$ MeV. At large values of Q^2 this effect is small compared to the charge asymmetry caused by Z^0 exchange and it has furthermore a different Q^2 dependence.

3. The presence of a $1 - (1-y)^2$ term which is not allowed in the one photon exchange approximation. This effect cannot be caused by two photon exchange.

The size of these effects in the standard model is shown in Fig. 2.9 where the ratio

$$\frac{\sigma(\gamma + z^0)}{\sigma(\gamma)}$$

evaluated for left and right handed electrons and positrons is plotted as a solid line versus y for x = 0.25.

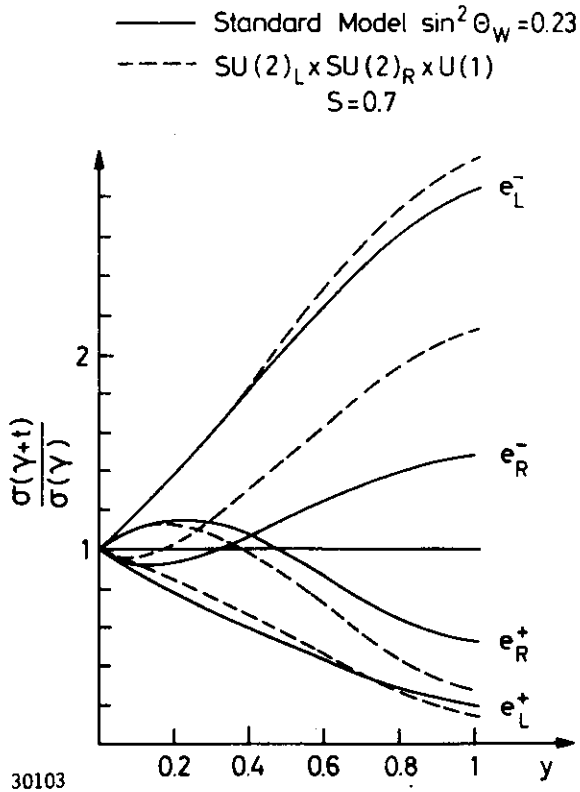

Fig. 2.9

The ratio $\sigma(\gamma+z^0)/\sigma(\gamma)$ plotted versus y for x = 0.25. The ratio is evaluated for two different weak interaction models.

The neutral current measurements at HERA are complementary to measurements at SLC and at LEP. For example it is easy to construct a senario in which the Z^0 peak is not observed in e^+e^- annihilation but propagator effects are seen in deep inelastic $e + p \to e' + x$.

The most trivial explanation would be to assume that the Z^0 peak is washed out by a large number of $\nu\bar{\nu}$ decays. A perhaps more exciting possibility has been put forward by Abbott and Fahri[19]. Usually $g_2^2/4\pi \ll 1$, where g_2 is the SU(2) coupling constant and hence SU(2) does not confine. Abbott and Fahri suggest that perhaps $g_2^2/4\pi$ is of order one and that SU(2) indeed does confine leading to composite fermions and bosons. Since

$$\frac{G_F}{\sqrt{2}} = \frac{g_2^2}{8m_W^2}$$

this would imply that the vector bosons in such a model are much heavier than the vector bosons in the standard model.

Flavour changing neutral currents like $e^- + d \to \tau^- + b$ may appear. In the example above the τ decay products will emerge on the lepton side instead of a single lepton. Such events would be spectacular and easy to observe.

2.4 Exploring the Proton

Measurements of the total electroweak cross section at values of Q^2 between a few GeV^2 and a few hundred GeV^2 have revealed[20] that the proton is made of pointlike fermions, the quarks. At short distances the quarks behave like free particles, yet the proton cannot be "ionized". The measurements further show that the quarks account for about a half of the proton momentum, the other half being carried by particles with only strong charge.

Measurements[21] at increasing values of Q^2 showed that the form factors are enhanced at low and depleted at high values of x. This observation is naturally explained in any field theory of strong interactions as shown schematically in Fig. 2.10. The resolving power of a spacelike electroweak current increases with Q such that the proton may be probed at shorter and shorter distances. Thus we may "see" the quark content of the gluon, or the quark after the emission of a gluon.

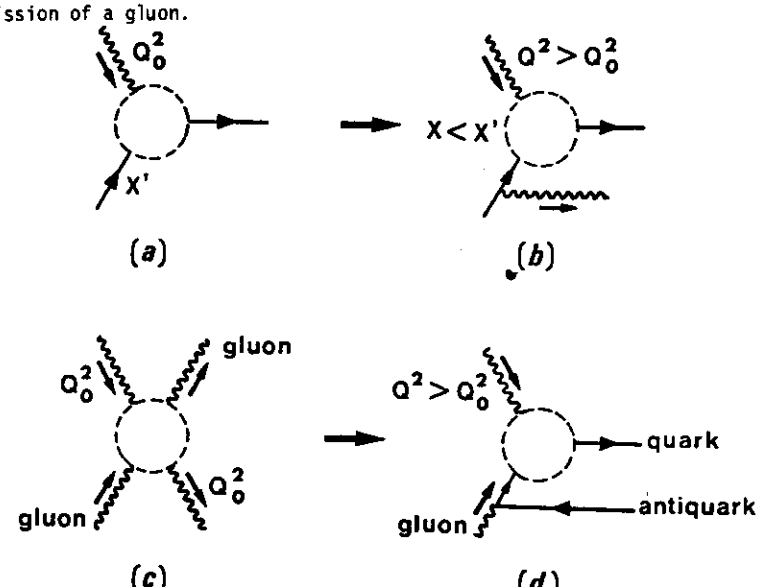

33681

Fig. 2.10 - a) A virtual photon with Q_0^2 striking a quark.
b) A virtual photon of higher Q^2 resolving the quark into a quark and a gluon.
c) A virtual photon with Q_0^2 traversing a gluon without interaction.
d) A virtual photon of higher Q^2 resolving the gluon into a quark-antiquark pair.

The experimental observations led to the formulation of Quantum Chromodynamics[22]. In this theory the strong interaction is mediated by eight coloured massless vector bosons, the gluons. The strong coupling constant α_s decreases with increasing values of Q^2 as

$$\alpha_s (Q^2) = \frac{12\pi}{(33 - 2n_f) \ln Q^2/\Lambda^2}$$

where n_f is the number of flavours and Λ the characteristic mass of the strong interaction.

The Q^2-evolution of the form factors can be unambigously computed in QCD. The result of such an computation is shown schematically in Fig. 2.11. Careful measurements of the cross section over wide range in Q^2 are needed to distinguish the logarithmic scaling violations inherent in QCD from a power series as would occur in a fixed point theory.

The correction factors needed to extract the cross section from the raw data must be small in order to determine the form factors with the required relative precision of a few percent. The results of a Monte Carlo calculations for charged current events are shown in Fig. 2.12. Plotted is the ratio between the extracted formfactor and the input form factor for values of Q^2 between 6 and 40 000 GeV^2. Note that for the HERA parameters the ratio approaches one - i.e. only small corrections must be applied to the raw data. This is no longer true if the electron energy is lowered say to 5 or 10 GeV keeping the proton energy fixed at 800 GeV. In this case hadrons from the current jet are lost down the beam pipe causing large corrections.

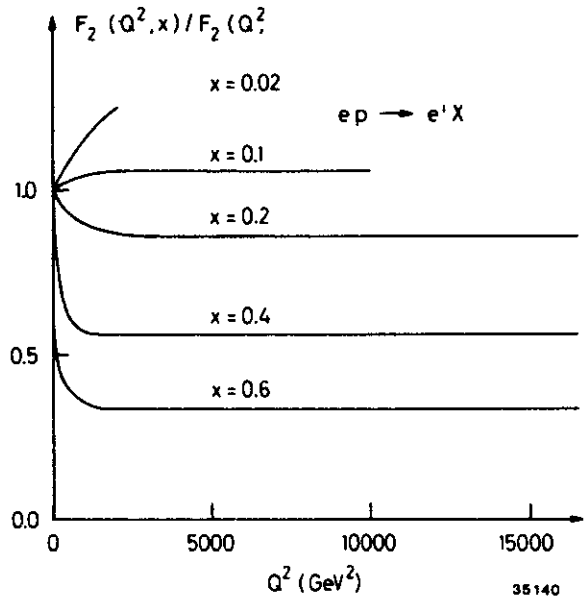

Fig. 2.11
The Q^2 dependence of the formfactors. plotted is the ratio $F_2(Q^2)/F_2(2,x)$ versus Q^2 for various values of $x = Q^2/2m\nu$.

The slow variation of the form factors with Q^2 as predicted in field theories makes it easy to search for new phenomena which may show up as scaling violations. Some possible sources of non QCD scaling violations are:

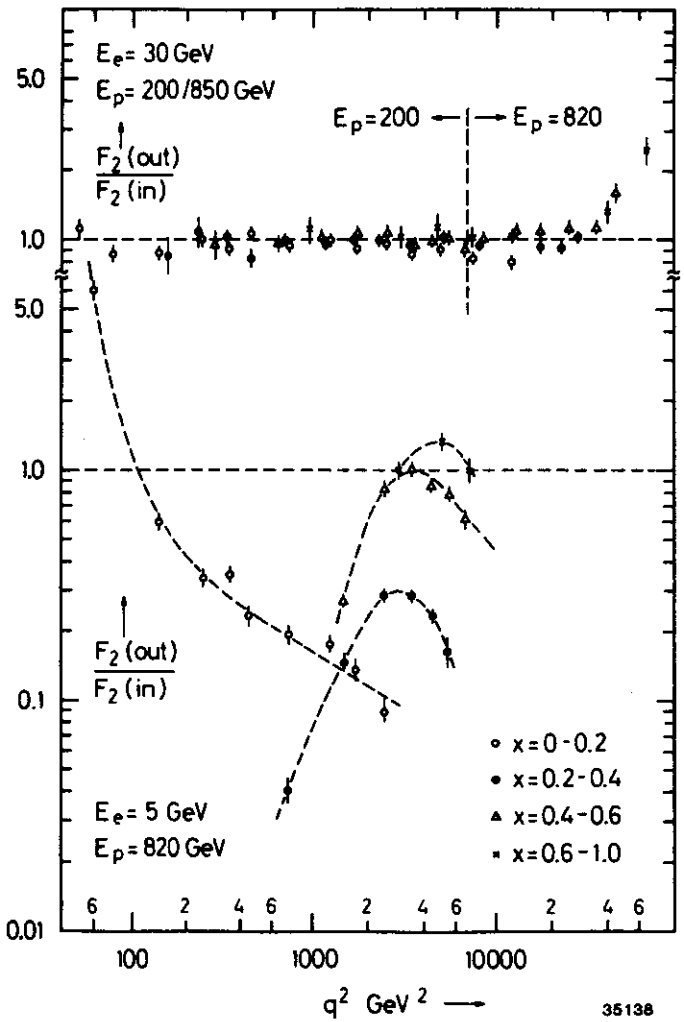

Fig. 2.12 - The correction factor which must be applied to be raw charged current data to extract the form factor $F_2(Q^2,x)$. Shown are the results of a Monte Carlo calculation of the ratio $F_2(out)/F_2(in)$ for various values of x plotted versus Q^2.

New constitutents in the proton. For example in supersymmetric models[23] the protons must contain, besides the normal quarks and gluons, scalar quarks and fermion gluinos. Thus the fraction of the momentum carried by the normal quarks will decrease at large values of Q^2 since the total proton momentum is now shared amongst more constituents. Scalar quarks will also contribute to the longitudinal form factor $F_L(x, Q^2) = F_2(x,Q^2) - 2xF_1(x,Q^2)$. Again precision measurements over a wide range in Q^2 are needed to extract information on new constituents.

Quarks and leptons may have finite size. Faced with the large number of leptons and quarks many physicists find it natural that these particles are composite[24] made of new building blocks. With HERA we can probe the fermion structure down to 10^{-17} cm. If the leptons have a size we would expect to observe a leptonic form factor and ultimately the production of excited leptons. The cross section would be modified by a form factor $F(Q^2) = \frac{1}{(1 + q^2/M^2)}$ giving rise of a scaling violation which is very different from that expected in QCD. A 10% measurement at $4 \cdot 10^4$ GeV^2 would be sensitive to a mass of the order of 1 TeV.

An excited lepton could decay into $e + \gamma$, $e + Z^0$ and $e^{\mp} + W^{\pm}$ leading to peaks in the invariant spectrum. Note that the topology of such a final state with several particles emerging from the lepton vertex makes it easy to find.

The cross section would be modified in a similar manner, if the quark has a structure - i.e. again one might probe down to distances of $(1\ \text{TeV})^{-1}$. In this case the formfactors may increase or de-

crease depending on the charges and the weak coupling constants of the new constituents.

The colour degree of freedom of quarks may also be excited[25] at small distances, and fractionally charged quarks resolved into integrally charged quarks of different colours:

$$u \to u_r\ (e = 1),\ u_y\ (e = 1),\ u_B\ (e = 0)$$

$$d \to d_r\ (e = 0),\ d_y\ (e = 0),\ u_B\ (e = -1)$$

Thus above the threshold for colour thaw:

$$\left(\frac{2}{3}\right)^2 u(x) \to \frac{1}{3}\left(1^2 + 1^2 + 0^2\right) u(x) = \frac{2}{3} u(x)$$

$$\left(\frac{1}{3}\right)^2 d(x) \to \frac{1}{3}\left(0^2 + 0^2 + 1^2\right) d(x) = \frac{1}{3} d(x)$$

In the valence quark approximation the electroproduction cross section would rise by a factor of 1.7. This model also contains charged gluons. The photon may interact with these gluons and this would contribute to the longitudinal cross section.

2.5 New Physics

The combination of high luminosity and the opening of a large kinematical region makes HERA well suited to search for new phenomena. Three obvious examples are discussed below:

2.5.1 New Fermions

Electron-proton collisions are ideally suited to produce electron-like charged or neutral leptons and new heavy quarks which couple to the u or d quarks in the proton. Such couplings are known to be rather weak in the standard model, however, new currents may exist. Indeed if the basic fermions are not pointlike they must have excited states which couple to the ground state. The rate for producing a heavy quark from a light quark is plotted in Fig. 2.13 with the mass of the outgoing lepton as a parameter. The rates were evaluated with the assumptions listed above plus the assumption that the new current couples with the same strength as the old one.

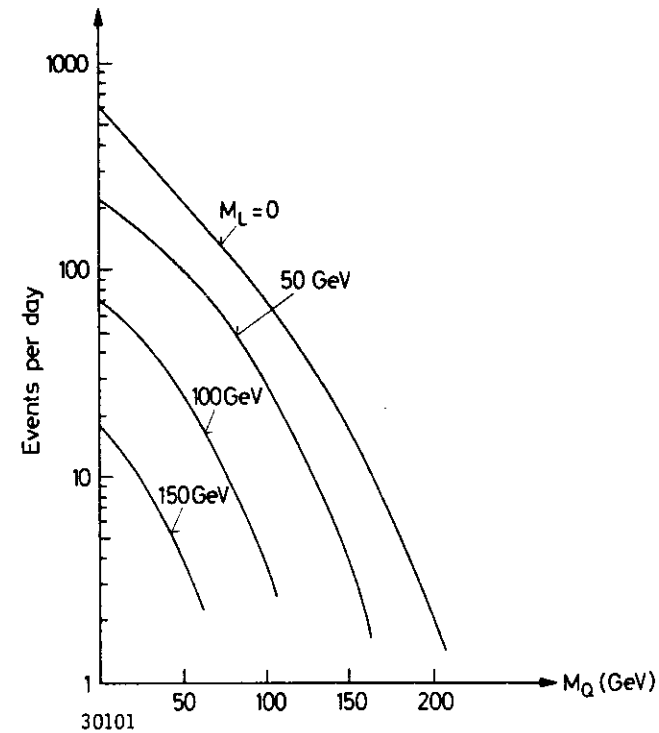

Fig. 2.13 - Number of events per day for $e^- + p \to L^- + Q + x$ at $s = 9.6 \times 10^4$ GeV^2 assuming left handed coupling, unpolarised electrons, m_{W_1} = 78 GeV, Buras-Gaemers paremetrization with Λ = 0.5 GeV and a luminosity of 10^{32} cm^{-2}s^{-1}.

Leptons and quarks with masses to 150 - 200 GeV can be found in this way. The deay of these particles leads to rather spectacular signatures on the lepton side: $L^0 \to e^- Q q'$, i.e. the single lepton emerging from the lepton vertex in the standard model will be replaced by a high multiplicity jet containing leptons.

2.5.2 Leptoquarks

It is generally accepted that the gauge symmetry must be spontanously broken to give mass to the intermediate vector bosons and to make the theory renormalizable. It has been proposed, as an alternative to the standard Higgs mechanism, that the symmetry breaking arises dynamically from the gauge interactions themselves. In this model a new set of unbroken non-Abelian gauge interactions [26] with a mass scale on the order of 1 TeV is introduced. This interaction gives rise to a complicated spectrum of technicolourless bound states with masses starting around 1 TeV. In addition, the technicolour interaction will result in leptoquarks, fundamental particles with combined lepton and baryon numbers and a mass predicted around 160 GeV.

The cross section resulting from the Feynman graphs in Fig.2.14a has been evaluated by Rudaz and Vermaseren [27] and is plotted in Fig. 2.14 versus the mass of the leptoquark. Roughly one event per day is expected for a leptoquark mass of 160 GeV and a suppression factor $\sin^2\theta_{et} \approx 0.05$. The topology of such an event is remarkable with a broad jet, resulting from the decay of the leptoquark (LQ) → e t, emerging at the lepton side.

2.5.3 Leptoproduction of supersymmetric particles

Gauging the isospin led to the successful unification of electromagnetic and weak interactions. In supersymmetric [23] theories the same story is repeated for the spin and this leads to a connection between fermions and bosons. Indeed the fundamental feature of supersymmetry is that it can generate fermions from bosons and vice versa. Thus for every particle with spin J there will in principle

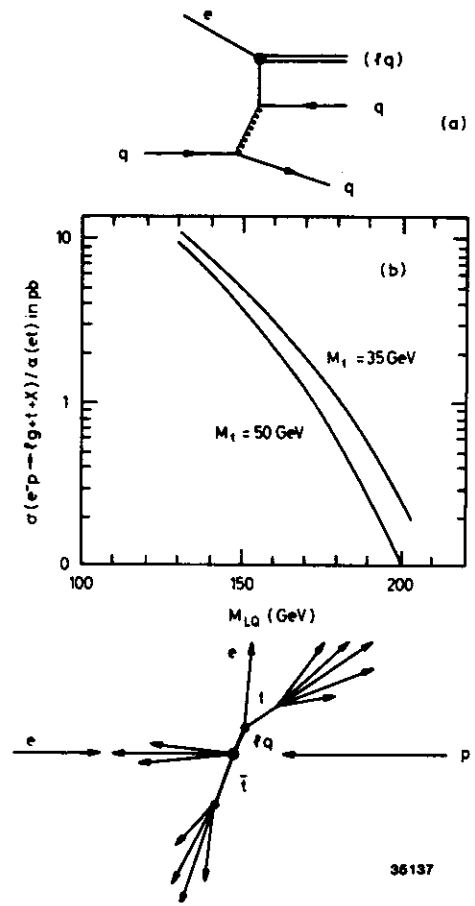

Fig. 2.14 - a) The Feynman graph for producing a leptoquark in deep inelastic ep reactions and the resulting topology.

b) The cross section for ep → (LQ) + x evaluated according to a).

be two new particles with spin $J \pm 1/2$.

A partial list[28] of such new particles is given in Table 2.1.

Table 2.1 - Possible supersymmetric particles

Types of conventional particles	Spin 1	Spin 1/2	Spin 0
Matter		quark q	scalar quarks $\tilde{q}$
		lepton ℓ	scalar lepton $\tilde{\ell}$
Massive Gauge Bosons	$W^{\pm}$,	supersymmetric heavy lepton	Higgs scalar
	Z^0	$\tilde{W}^{\pm}$, $\tilde{Z}^0$, H	H
Massless Gauge Boson		photino $\tilde{\gamma}$	
		nuinos $\tilde{\nu}$	
	g	gluino $\tilde{g}$	

Electron-proton collisions at high energies are well suited to search for supersymmetric particles:

Above threshold scalar quark and scalar leptons can be directly produced[29]

$$e + q \rightarrow \tilde{e} + \tilde{q}$$

$$e + q \rightarrow \tilde{\nu} + \tilde{q} .$$

The observable mass range for supersymmetric particles depends on the signature. If the scalar leptons decay into a jet of scalar particles then cross sections as low as 10^{-38} cm^{-2} corresponding to 10 events a year may be observable. If the dominant decay modes are of the type $\tilde{\ell} \rightarrow \ell + G$ and $\tilde{q} \rightarrow q + G$ where G is the undetectable

Goldstino, then the background will be more severe. In standard neutral current events, however, the direction and energies of the scattered lepton and the current jet are strongly correlated. Since in a supersymmetric neutral current event the electron and current jet results from decay processes this correlation is destroyed and the background can to a large extent be eliminated by suitable cuts.

Estimates[26] show that one may probe the mass range up to 100 - 150 GeV for the existance of supersymmetric quarks and leptons.

Scalar leptons can also be searched for in the process $e + p \rightarrow e^* + p \rightarrow G^0 + e + p \rightarrow e^- + p +$ missing energy and neutrino. The signature is very clear with only an electron and a proton in a final state. One should be able to observe this process if the mass of the produced supersymmetric particles are below 100 GeV.

2.6 Summary

To explore the Q^2 region above 10^4 GeV^2 requires center-of-mass energies on the order of 300 GeV or above. In principle the relativ electron and proton energies do not matter. However, the Q^2 and ν values of a charged current event must be determined from a measurement of the current jet and such a measurement can only be carried out if the electron energy is not too small. 30 GeV electrons colliding with 800 GeV protons is acceptable ; lowering the electron energy to 5 GeV keeping the proton energy constant is not.

The luminosity must approach 10^{32} cm^{-2}s^{-1} in order to be able to

explore the main fraction of the available kinematic region. Note from Fig. 2.4 that the event rate depends on both luminosity and center-of-mass energy - i.e. one may trade luminosity and versus center-of-mass energy.

The ability of using electrons and positrons in well defined helicity states is crucial for the determination of neutral current coupling constants and in the search for right handed currents.

3. Description of an Electron-Proton Colliding Beam Facility

In this part we give an overview of an electron-proton colliding beam facility using HERA [5] as an example. Some of the most important parameters are listed in Table 3.1. HERA consists of two circular accelerators, one for electrons (positrons) and one for protons arranged such that the counterrotating electron and proton beams collide in four points along the circumference. The accelerator has a fourfold symmetry; four 360 m long straight sections are joined by four arcs with a geometric radius of 779.2 m yielding a total circumference of 6336 m. The electrons and the protons collide in the middle of the four long straight sections. The layout of the machine is shown in Fig. 3.1.

Each of the circular accelerators is made of the following elements:

A guide field which bends the charged particles on a circular path and provides the necessary focusing to keep the particles transversely bunched over a distance of 10^{10} km. Nowadays most machines are of the separate function type - i.e. the bending by dipole fields,

1. Zunächst wurde die Drahtebene senkrecht zur Strahlachse (z-Achse) gestellt (Abbildung 21 auf Seite 34 a). Das Maß der Justierung ergab der Vergleich der Abstände Bolzen - Magnetjoch.

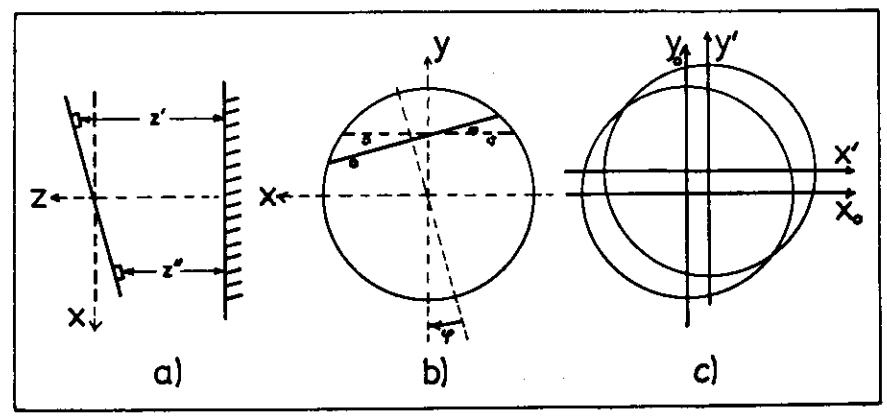

Abbildung 21. Drehachsen

2. Es folgte das Ausrichten der horizontalen Drähte in x-Richtung. Dazu wurde eine Präzisionsmetallschiene auf jeweils zwei Bolzen gelegt und mit Hilfe einer Wasserwaage justiert(Abbildung 21 b).

3. Alsdann wurden Drahtebenenmittelpunkt (= Kammermittelpunkt) und Strahlkoordinatensystem Nullpunkt (x=0, y=0) mit einem Theodoliten möglichst genau zur Übereinstimmung gebracht (Abbildung 21 c). Der Theodolit war dabei auf das Strahlkoordinatensystem justiert und es wurden die x- bzw. y-Abweichungen bzgl. des Nullpunktes zunächst zur Korrektur benutzt (Verschieben in x- bzw. y-Richtung), zuletzt vermessen.

Die Vermessung der z-Koordinaten der einzelnen Kammern erfolgte wiederum bzgl. der genau vermessenen PLUTO-Joch-Kanten (Abbildung 22 auf Seite 35)

Driftkammerkonstruktion

Table 3.1 - Basic parameters

	p-ring	e-ring	units
Nominal energy	820	30	GeV
$s = Q^2_{max}$	98400		GeV^2
Luminosity	0.6×10^{32}		$cm^{-2}s^{-1}$
Polarization time		20	min
Number of interaction points	4		
Length of straight sections	360		m
Free space for experiments	15		m
Circumference	6336		
Bending radius	603.8	540.9	m
Magnetic field	4.53	0.1849	T
Total number of particles	6.3×10^{13}	0.76×10^{13}	
Circulating current	480	58	mA
Energy range	200 → 820	10 → 35	GeV
Emittance (ϵ_x/ϵ_z)	0.47/0.24	1.6/0.16	10^{-8}m
Beta function β^*_x/β^*_z	3/0.3	3/0.15	m
Dispersion function D^*_x/D^*_z	0/0	0/0	m
Beam-beam tune shift $\Delta Q_x/\Delta Q_z$	0.0006/0.0009	0.008/0.014	
Beam size at crossing σ^*_x	0.12(0.91)**	0.22	mm
Beam size at crossing σ^*_z	0.027	0.013	mm
Number of bunches	210		
Bunch length	9.5	0.93	cm
RF frequency	208.189	499.667	MHz
Maximum circumferential voltage	100***	290	MV
Total RF power	4-6	13.2	MW
Filling time	20	15	min
Injection energy	40.0	14.0	GeV
Energy loss / turn	1.4×10^{-10}	142.3	MeV
Critical energy	10^{-6}	111	keV
Heat loss at 4.3 K	13.2		kW
Lead cooling gas rate	42.5		g/s
Design refrigeration power at 4.3K	20		kW
Design lead gas rate	64		g/s

* At the interaction point
** Including the bunch length
*** 25 MV is foreseen initially corresponding to 1 - 1.5 MW.

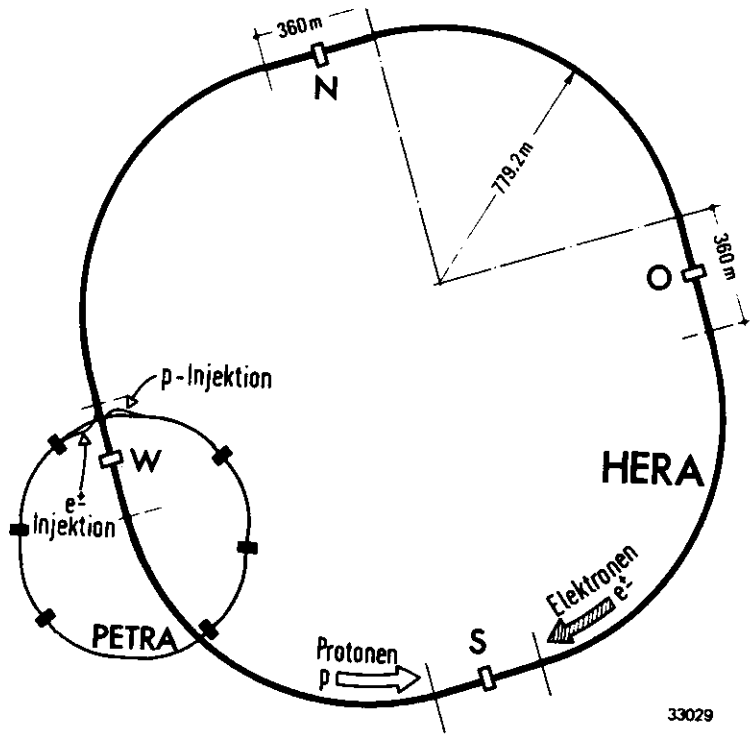

Fig. 3.1 - The layout of HERA.

the focusing by quadrupole fields and the corrections by higher multipole fields are provided by separate elements arranged in a repetitive pattern (cells).

An accelerating system made of a power source (klystron, tetrode) and resonating cavities. Energy is transferred to the particles by the longitudinal electric field oscillating in the cavities at a frequency which is an integer multiple of the particle revolution frequency. The r.f. system is used to accelerate particles from the injection energy to the final energy and - in the case of electrons - to compensate the average energy loss caused by synchrotron radiation. The r.f. system also provides longitudinal focusing of the beam.

A high vacuum system. A particle covers a distance of 10^{10} km during a typical storage time of 10 hrs such that a high vacuum system is mandatory to minimize the losses due to beam gas interactions. A pressure on the order of 10^{-11} torr is needed for the protons. The synchrotron radiation of the electron beam strikes the walls of the vacuum chamber leading to gas desorption which makes it difficult to maintain a pressure below 10^{-9} torr in the electron ring. However, this pressure is sufficient since the oscillation of electrons, excited by beam-gas interactions is damped by synchrotron radiation.

A monitor system to observe the behaviour of the particles and a sophisticated control system to supervise the operation of the accelerator and to take corrective action if needed.

An injection system capable of loading the rings with electrons

and protons in a time which is very short compared to the anticipated storage time of several hours. Not only the peak energy but also the minimum usuable energy of an accelerator is limited. For a machine made of superconducting magnets this limit is probably determined by the constant field errors caused by persistent currents in the superconductor. The strength of these higher multipole fields relativ to the dipole field increases with decreasing energy and they may well limit the injection energy of the protons to some 5% of the peak energy. The electron beam is rather stable due to the damping caused by the synchrotron radiation. The damping time is proportional to $1/E^3$. Thus the operating range of an electron ring, limited by instabilities at the lower end and by the available r.f. power at the higher end, is rather small compared to the range available for a proton ring. In the case of HERA, a chain consisting of linear accelerators, the DESY synchrotron and PETRA are used to boost the energy of the protons and the electrons to 40 GeV respectively 14 GeV before injecting into HERA.

An extraction system designed to eject the stored proton beam in a single turn. This is necessary since a localized loss of 10^{-4} of the design current, or some 10^{10} protons, in a magnet at 4.5 T will destroy the superconducting state and lead to a quench. Thus the proton beam must be ejected without a loss at the onset of an instability or at the end of a run.

The interaction region is presumably the most complex part of an electron proton collider. The two beams with rather different properties must be brought into a small angle, low beta (i.e. small

beam spot) collision geometry. The electron spin, which is perpendicular to the orbit in the arcs, must be turned to be either parallel or antiparallel to the beam direction in the interaction point and then be restored to its vertical direction upon entering the arcs. Furthermore the dispersion in the lattice must be made to disappear in the interaction point, and sufficient space for r.f. cavities, injection and ejection systems must be found.

The layout favoured for HERA is shown in Fig. 3.2. The beams cross in the horizontal plane of the electron ring at an angle of $\pm$ 10 mrad in middle of the 360 m long straight section. A horizontal crossing is advantagous since the radial size of the electron beam is much larger than its vertical size. The choice of a relatively large crossing angle makes it possible to design the machines without common elements such that the electron and proton energies can be chosen and varied independently. The resulting increase in the effective horizontal beam size can be compensated by bringing the proton quadrupoles closer to the interaction point with a resulting reduction in vertical beam size. A free distance of $\pm$ 7.5 m around the interaction point is available for experiments. In this design the spin is turned into the longitudinal direction by an 80 m long rotator installed at the end of the arcs and restored to the transverse direction by a similar rotator positioned at the entrance to the next arc. The large distance between the interaction point and the last bend in the rotator minimizes the amount of synchrotron radiation which reaches the detector. In each section roughly 200 m is available for the r.f. system and the injection and

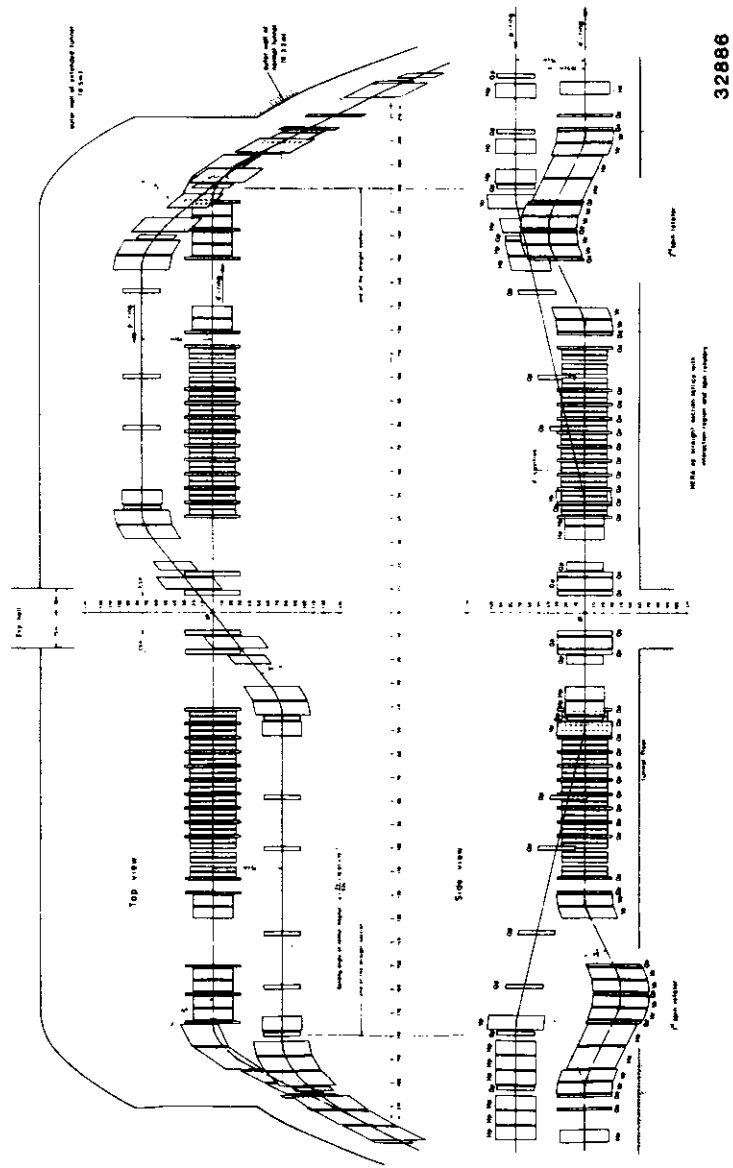

Fig. 3.2 - Layout of the interaction region.

ejection system.

Energy and luminosity are obviously two factors which determine the quality of an ep facility. The physics discussed in chapter 2 emphasized the importance of investigating the region of Q^2 greater than 10^4 GeV^2 and showed that luminosities of the order of 10^{31} cm^{-2}s^{-1} to 10^{32} cm^{-2}s^{-1} are needed to obtain a useful event rate at such large values of Q^2

The maximum momentum transfer squared Q^2_{max} which can be obtained in an ep colliding ring is given by

$$Q^2_{max} = 4\, E_e E_p \quad . \tag{3.1}$$

The maximum energy of the proton beam is determined by the product of the bending radius ρ and magnetic induction B

$$E_p\ (\text{GeV}) = \frac{B\,\rho\ (\text{T.m.})}{3.3356} \quad . \tag{3.2}$$

Thus, for a given radius, the energy is limited by the strength of the magnetic field. Due to the pioneering work at FNAL and BNL superconducting accelerator magnets can be massproduced with reproducible properties for an induction up to 5 T. The nominal induction of the superconducting dipolemagnets in HERA is 4.53 T yielding a proton energy of 820 GeV.

An electron of energy E (GeV) transversing a circle of radius ρ (m) radiates an average of e U_e(keV) per turn:

$$e\, U_o(\text{keV}) = 88.5\, \frac{E^4}{\rho} \quad . \tag{3.3}$$

This energy loss must be restored by the r.f. system and to this end the cavities must be fed the power P_o. This power is the sum of

the losses in the cavity and the energy radiated by the beam.

The cavity losses are given by $U^2/2R$ where U is the peak voltage in the cavity and R the total shunt impedance of the r.f. cavity system. In principle this term can be made negligible small by using superconducting cavities, however, the second term still remains. The radiation losses are given by $i \cdot U_o$. High luminosities require a large circulating current such that the radiation term tends to dominate. The peak electron energy is therefore not limited by the magnetic field strength but rather by the available r.f. power. To reach the nominal energy of 30 GeV in HERA with a stored current of 56 mA requires 13.2 MeV of r.f. power with 4 MW needed to establish the circumferential voltage and 8 MW to compensate for the synchrotron radiation. 1.2 MW are lost in the waveguides. The dipole field is only 0.18 T.

It is important to push the electron energy for two reasons. Firstly the electron energy must be on the order of several percent of the proton energy to avoid that particles from the current jet are lost down the beampipe making it difficult to reconstruct the final state. This point was illustrated in Fig.2.12 which shows the corrections which must be applied to the experimental data in order to determine the formfactor $F_2(x_1,Q^2)$ from charged current interactions. Whereas the corrections in the case of 30 GeV electrons colliding with 820 GeV protons (200 GeV) are small and presumably managable they become very large and probably unreliable in the case of 5 GeV electrons collding with 1000 GeV protons.

The synchrotron radiation in the arcs will polarise the circulating electrons transversely to the beam plane. The maximum polarisation P_o = 92.4% is approached as:

$$P(t) = P_o \, (1 - e^{-1/\tau_p}) \tag{3.4}$$

with a build-up-time τ_p in seconds given by:

$$\tau_p = \frac{98.7}{E^5} \rho^3 \left(\frac{R}{\rho} \right) \tag{3.5}$$

The beam energy E is in GeV and the bending radius ρ, respectively the geometric radius R in meter.

The electron energy should therefore be so large that τ_p is very short compared to the anticipated beam life time. At 30 GeV τ_p is of the order of 20 min.

The luminosity, assuming n_b bunches of protons and electrons is given by:

$$L = \left(\frac{N_e \, N_p}{A} \right) f_o \, n_b \tag{3.6}$$

Here N_e and N_p are the number of electrons respectively protons per bunch, f_o the resolution frequency and A the effective beam cross section.

The ultimate limit on the number of electrons and protons is given by the tune shift - i.e. the effect of the electron beam on the proton beam and opposite. However, the real limit may well be given by the available r.f. power for the electrons or by instabilities for the protons. - In HERA we expect a luminosity of $6 \cdot 10^{31}$ $cm^{-2}s^{-1}$ at a c.m. energy of 314 GeV.

4. The Transverse Motion[10,30)]

The magnet system of an circular accelerator is made of deflecting and focusing elements arranged in a repetitiv pattern around the ring. The reference particle sees only dipole fields and retraces its orbit on every turn. The other particles traverses the magnetic elements off axis and experiences a linear restoring force in addition to the deflecting force. An arbitrary particle executes quasi-harmonic oscillation (betatron oscillation) with respect to the closed orbit of the reference particle. In this chapter we discuss the properties of the betatron oscillation in the linear approximation.

4.1 The Equation of Motion

We will first derive the equations of motion for a charged particle travelling in a guide field made of a deflecting dipole field and a focusing quadrupole field. The particle motion is described using the coordinate system defined in Fig. 4.1. The position of the reference particle is given by the radius ρ and the distance s_o measured along the orbit from an arbitrary origin. The position of an arbitrary particle is given by the vector

$$\vec{t} = r \, \vec{n}_r + z \, \vec{n}_z \tag{4.1}$$

where $\vec{n}_r$ and $\vec{n}_z$ are unit vectors. Usually relative coordinates are used:

$$x = r - \rho \quad \text{and} \quad z. \tag{4.2}$$

We consider the motion in a time independent field. Along the reference orbit the induction $\vec{B}$ is normal to the horizontal plane i.e.

$$B_s = B_x = 0 \, . \tag{4.3}$$

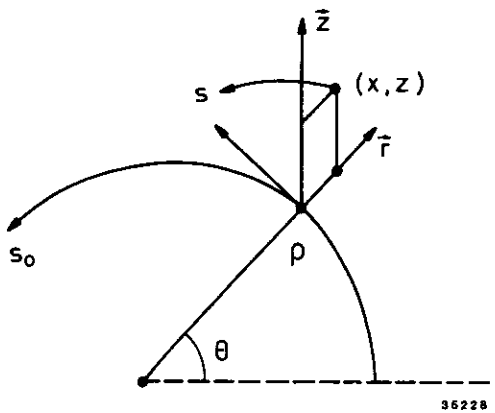

Fig. 4.1 - The coordinate system.

The magnetic induction is furthermore assumed to be symmetric with respect to the horizontal plane.

We consider particles oscillating with small amplitudes around the reference orbit. The induction can be expanded in a power series in x and z. Keeping only the first order terms yields:

$$B_z(s,x,z) = B_o(s) + \left(\frac{\partial B_z}{\partial x}\right)_o x + \ldots\ldots$$
$$B_x(s,x,z) = \left(\frac{\partial B_x}{\partial z}\right)_o z + \ldots\ldots \qquad (4.4)$$

In the median plane $\frac{1}{\mu_o}\nabla \times \vec{B} = \vec{j} = 0$ - i.e.

$$\frac{\partial B_z}{\partial x} = \frac{\partial B_x}{\partial z} \quad . \qquad (4.5)$$

It is convenient to normalize the dipole field and the gradient field to the momentum of the reference particle:

$$G(s) = \frac{1}{\rho_o} = \frac{e\,B_o}{o} \qquad (4.6)$$

$$K(s) = \frac{e}{p}\frac{\partial B}{\partial x} = \frac{1}{B\rho}\frac{\partial B_z}{\partial x} = \frac{1}{B\rho}\frac{\partial B_x}{\partial z} \qquad (4.7)$$

Note that both G(s) and K(s) are periodic functions with period L

$$G(s+L) = G(s)$$
$$K(s+L) = K(s) \qquad (4.8)$$

where L is the length of one turn.

The equation of motion of a charged particle in a magnetic field is given by the Lorentz force

$$\frac{d}{dt}(m\dot{\vec{t}}) = e(\vec{v} \times \vec{B}) \qquad (4.9)$$

We will first evaluate the left hand side. The time derivative of the position vector $\vec{t}$ is given by:

$$\dot{\vec{t}} = \dot{r}\vec{n}_r + r\dot{\vec{n}}_r + \dot{z}\vec{n}_z + z\dot{\vec{n}}_z \qquad (4.10)$$

The differentials of the unit vectors can be obtained from Fig. 4.1 by inspection.

$$d\vec{n}_r = \vec{n}_\theta d\theta \rightarrow \dot{\vec{n}}_r = \vec{n}_\theta \dot{\theta}$$
$$d\vec{n}_\theta = -\vec{n}_r\, d\theta \rightarrow \dot{\vec{n}}_\theta = -\vec{n}_r \dot{\theta} \qquad (4.11)$$
$$d\vec{n}_z = 0 \rightarrow \dot{\vec{n}}_z = 0$$

With the results of eqs. 4.10 and 4.11 the left hand side of eq. 4.9 yields:

$$\frac{d}{dt}(m\dot{\vec{r}}) = [\frac{d}{dt}(m\dot{r}) - mr\dot{\theta}^2]\vec{n}_r + [\frac{1}{r}\frac{d}{dt}(mr^2\dot{\theta})]\vec{n}_\theta + [\frac{d}{dt}(m\dot{z})\vec{n}_z] \qquad (4.12)$$

The right hand side of equation 4.9 in cylindrical coordinates is given by:

$$e(\vec{v} \times \vec{B}) = \begin{pmatrix} \vec{n}_r & \vec{n}_\theta & \vec{n}_z \\ \dot{r} & r\dot{\theta} & \dot{z} \\ B_r & B_\theta & B_z \end{pmatrix} \qquad (4.13)$$

The three components of the equation of motion can thus be written as:

$$(\ddot{r} - r\dot{\theta}^2) = (\frac{e}{m})(r\dot{\theta}B_z - \dot{z}B_\theta) \qquad (4.14a)$$

$$\frac{1}{r}\frac{d}{dt}(r^2\dot{\theta}) = (\frac{e}{m})(\dot{z}B_r - \dot{r}B_z) \qquad (4.14b)$$

$$\ddot{z} = (\frac{e}{m})(\dot{r}B_\theta - r\dot{\theta}B_r) \qquad (4.14c)$$

Equation 4.14a can be written as:

$$\frac{d^2x}{ds^2} = x'' = \frac{1}{r} + \frac{eB_o}{p}(1 + \frac{1}{B_o}\frac{\partial B_z}{\partial x}x) \qquad (4.15)$$

with the magnetic induction as defined above in eqs. 4.3 and 4.4 and the substitution:

$$\frac{d}{dt} = (\dot{r\theta})\frac{d}{ds} = v\frac{d}{ds} \qquad (4.16)$$

This can be simplified using:

$$\frac{1}{r} = \frac{1}{\rho + x} = \frac{1}{\rho}(1 - \frac{x}{\rho}), \quad \frac{1}{p} = \frac{1}{p_o + \Delta p} = \frac{1}{p_o}(1 - \frac{\Delta p}{p}) \qquad (4.17)$$

and

$$\frac{eB_o}{p_o} = -\frac{1}{\rho_o} .$$

Neglecting second order terms and using the definitions given in eqs. 4.6 and 4.7 yields the equation of motion in the horizontal plane:

$$x'' + (G^2(s) + K(s))x = G(s)\frac{\Delta p}{p} \qquad (4.18)$$

Note that in general $G^2(s) + K(s) \approx K(s)$.

The equation for the motion in the vertical plane follows from eq. 4.14c. With the approximations used above

$$z'' - K(s)z = 0 . \qquad (4.19)$$

Evaluation of eq. 4.14b yields:

$$\Delta p = \text{const.}$$

The transverse particle motion is described by two independent linear equations. The equations are of the harmonic oscillator form except that the restoring force K(s) is a function of the azimuthal coordinate.

4.2 The Magnetic Elements

The first strong focusing machines were made of combined function elements - i.e. the bending and the focusing field were produced by a single magnet.

This has several drawbacks:

- The average induction B_o must be low to avoid saturation of the pole tips.
- The ratio of the bending and the focusing strength is fixed by the shape of the polefaces and the machine tune can only be changed by additional independent quadrupoles.
- The emission of synchrotron radiation will cause the radial beam size to grow exponentially.

For these reasons most modern machines are designed as separate function machines. The bending and the focusing properties of the guide field are provided by independent elements arranged in a repetitive pattern of identical units - the cells. A standard FODO cell is shown in Fig. 4.2. The cell consists of a horizontal focusing quadrupol, bending magnets, a horizontal defocusing quadrupol and bending magnets. In general sextupol and octupol magnets for higher order corrections and dipole magnets to minimize closed orbit deviations are incorporated into the cell.

In a standard dipole the field shape is determined by the iron, and the induction is limited to 2T to avoid saturation. The next

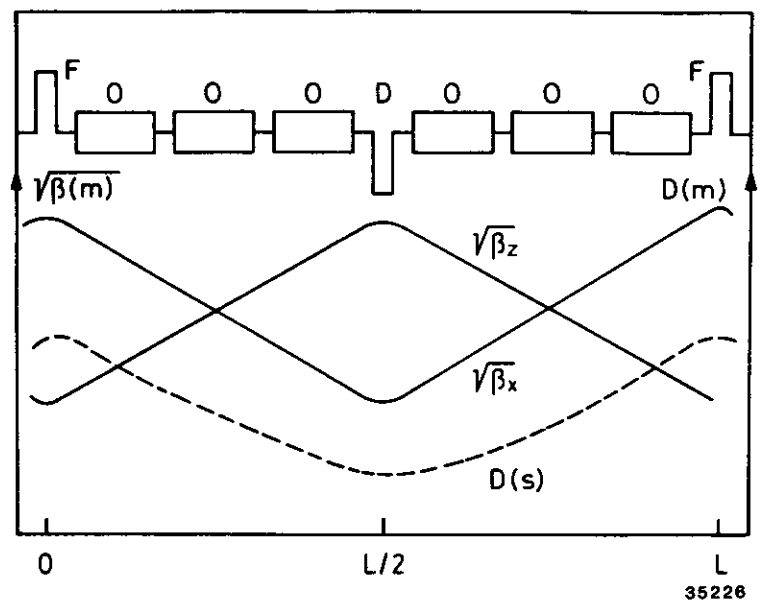

Fig. 4.2 - a) The magnet ordering in a simple FODO cell.
b) Variation of the betafunction and the dispersion over a cell.

generation of circular proton machines seeks to use superconducting coils to produce higher inductions. In this case the induction is determined by the current distribution and effects like persistent currents and production tolerances make the magnets rich in higher order multipoles. No accelerator exploiting this technology is operating although the FNAL Tevatron is nearly completed and long term tests involving strings of more than 100 magnets have been very encouraging. Indeed it seems possible to construct 5T superconducting dipole magnets of high and reproducible quality. The coils are wound using a Rutherford type helium transparent NbTi wire and magnets with an induction of 8 - 10 T seem feasible using this technology. Bending fields above 10 T require presumably a new conductor like $NbSn_3$.

The distribution of magnetic induction in a quadrupole lens is shown schematically in Fig. 4.3. The induction disappear on the axis and increases linearly with the distance from the beam axis in both the horizontal and vertical plane.

$$B_x = g\,z \qquad B_z = g\,x \tag{4.20}$$

with $g = \frac{\partial B_z}{\partial x} = \frac{\partial B_x}{\partial z}$.

A stream of parallel particles traversing a quadrupole of length l will be focused in one plane and defocused in the orthogonal plane with the same focal length f. In the focusing plane:

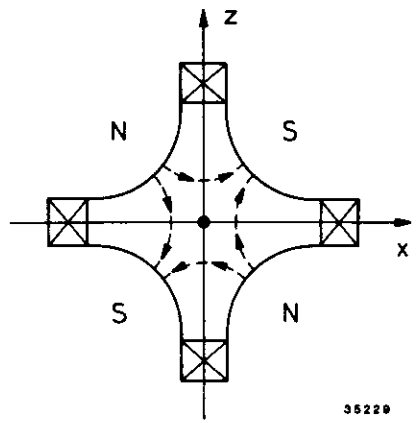

Fig. 4.3 - The magnetic induction pattern of a quadrupole lens.

$$x' = \frac{B_z\, l}{B_0\, \rho} = -\left(\frac{g\, l}{B_0 \rho}\right) x = -k\, l\, x = -\frac{x}{f} \tag{4.21}$$

f, the focal length is given by:

$$f = -\frac{1}{k\, l} \tag{4.22}$$

A charged particle beam traversing a quadrupole magnet is focused in one plane and defocused in the orthogonal plane. However, a pair of quadrupole lenses spaced at a distance L will focuse the beam in both plans provided f > L. To see this consider the transfer matrix for a quadrupole doublett in the thin lens approximation (see 4.5):

$$M_x = \begin{pmatrix} 1 & 0 \\ 1/f & 1 \end{pmatrix} \begin{pmatrix} 1 & L \\ 0 & 1 \end{pmatrix} \begin{pmatrix} 1 & 0 \\ -1/f & 1 \end{pmatrix} = \begin{pmatrix} 1-L/f & L \\ -L/f^2 & L/f+1 \end{pmatrix} \tag{4.23}$$

$$M_z = \begin{pmatrix} 1 & 0 \\ -1/f & 1 \end{pmatrix} \begin{pmatrix} 1 & L \\ 0 & 1 \end{pmatrix} \begin{pmatrix} 1 & 0 \\ 1/f & 1 \end{pmatrix} = \begin{pmatrix} 1+L/f & L \\ -L/f^2 & -L/f+1 \end{pmatrix}$$

Comparing the element m_{21} for both matrices yields:

$$f_x = f_z = -L/f^2 .$$

The focal length of a lens decreases with increasing momentum as:

$$f \sim 1/p .$$

Thus a machine made of only dipole and quadrupole magnets will have a strong chromatic abberation. This can be corrected with sextupole elements as discussed in chapter 5.3.

A sextupole lens is shown schematically in Fig. 4.4. The field distribution in carthesian coordinates x and z can be written as:

$$\begin{aligned} B_x(x, z) &= B'' \; x \; z \\ B_z(x, z) &= \frac{B''}{2}(x^2 - z^2) \end{aligned} \tag{4.24}$$

with $B'' = \dfrac{\partial^2 B_z}{\partial x^2}$.

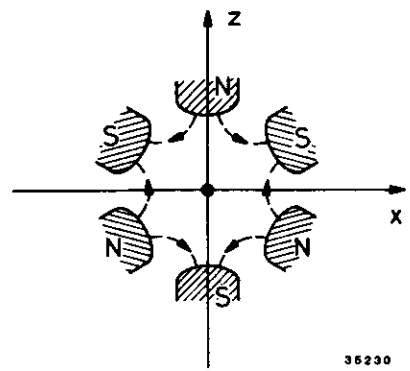

Fig. 4.4 - The magnetic induction pattern of a sextupole.

4.3 The Matrix Solution

The transverse motion in x and z for particles with $\Delta p = 0$ is described by the solutions to the linear homogenous equation

$$u''(s) + K(s)\, u(s) = 0 \tag{4.25}$$

The position u(s) and the slope u'(s) of a particle with azimuthal coordinate s can be written as a vector:

$$\vec{u}(s) = \begin{pmatrix} u \\ u' \end{pmatrix}_s \tag{4.26}$$

The value of u(s) at an arbitrary azimuth $s = s_1$ is related to its value at the origin s_0 by a linear transformation

$$\vec{u}(s_1) = M(s_1 \mid s_0)\, \vec{u}(s_0) \tag{4.27}$$

$M(s_1 \mid s_0)$ is a 2 x 2 matrix and the value of the maxtrix elements can be determined from the two particular solutions C(s) and S(s) of eq. 4.25.

The particular solutions are defined by their values and derivatives at the origin $s = s_0$.

$$\begin{aligned} C(s_0) &= 1 \qquad C'(s_0) = 0 \\ S(s_0) &= 0 \qquad S'(s_0) = 1 \end{aligned} \tag{4.28}$$

The general solution of eq. 4.25 is then the sum of the particular solutions:

$$\begin{aligned} u(s) &= u(s_0)\, C(s) + u'(s_0)\, S(s) \\ u'(s) &= u(s_0)\, C'(s) + u'(s_0)\, S'(s) \end{aligned} \tag{4.29}$$

This expression be verified for $s = s_0$ using the boundary conditions for C(s) and S(s) defined above.

The value at an arbitrary point $s = s_1$ is then given by eq. 4.27. Written in matrix form we find:

$$\begin{pmatrix} u \\ u' \end{pmatrix}_{s_1} = \begin{pmatrix} C(s_1) & S(s_1) \\ C'(s_1) & S'(s_1) \end{pmatrix} \begin{pmatrix} u \\ u' \end{pmatrix}_{s_0} \tag{4.30}$$

The transfer matrix $M(s_1 \mid s_0)$ for a particle between the azimuthal positions s_0 and s_1 is determined by the values of the particular solution at $s = s_1$.

4.3.1 Transfer matrices for $\Delta p = 0$

A separate function machine is made of dipole magnets, quadrupole magnets and drift distances. We will now evaluate the transfermatrices for these elements, each of length $L = s - s_0$. The transfermatrix for a string of elements is simply the product of the transfer matrices for individual elements:

$$M(s_n \mid s_0) = M(s_n \mid s_{n-1}) \cdots M(s_2 \mid s_1)\, M(s_1 \mid s_0) \tag{4.31}$$

a) Field free region

$K(s) = 0$ in a field free region and particles drift with constant slope. - The particular functions are now solutions of $u''(s) = 0$. These solutions are

$$\begin{aligned} C(s) &= 1 \qquad S(s) = s - s_0 = L \\ C'(s) &= 0 \qquad S'(s) = 1 \end{aligned} \tag{4.32}$$

Thus the transfer matrix is given by

$$M(s_1 \mid s_0) = \begin{pmatrix} 1 & L \\ 0 & 1 \end{pmatrix} \tag{4.33}$$

b) Focusing element

The particle motion in a focusing element is given by

$$u''(s) + K(s)\, u(s) = 0 \tag{4.34}$$

with $K(s) > 0$.

The resulting particular solutions are:

$$C = a \cos\sqrt{K}\, L \quad \text{and} \quad S = b \sin\sqrt{K}\, L \tag{4.35}$$

with the values of a and b determined by the boundary conditions above, i.e.

$$a = 1 \qquad b = \frac{1}{\sqrt{K}}\,.$$

The transfermatrix for a focusing element of length L is thus given by:

$$M(s_1 \mid s_0) = \begin{pmatrix} \cos\sqrt{K}\,L & \frac{1}{\sqrt{K}}\sin\sqrt{K}\,L \\ -\sqrt{K}\cdot\sin\sqrt{K}\,L & \cos\sqrt{K}\,L \end{pmatrix} \qquad (4.36)$$

c) Defocusing element

The particle motion in a defocusing element is given by:

$$u''(s) - K(s)\,u(s) = 0 \qquad (4.37)$$

The resulting particular solutions are:

$$C = a\cosh\sqrt{K}\,L \quad \text{and} \quad S = b\sinh\sqrt{K}\,L \qquad (4.38)$$

The boundary conditions yields:

$$a = 1 \quad \text{and} \quad b = \frac{1}{\sqrt{K}} \; .$$

The transfermatrix for a defocusing element of length L is thus given by:

$$M(s_1 \mid s_0) = \begin{pmatrix} \cosh\sqrt{K}\,L & (\frac{1}{\sqrt{K}})\sinh\sqrt{K}\,L \\ \sqrt{K}\cdot\sinh\sqrt{K}\,L & \cosh\sqrt{K}\,L \end{pmatrix} \qquad (4.39)$$

4.3.2 The Twiss matrix

The transfer matrix for a single cell or for a complete turn can be written in its most general form as:

$$T(s+L \mid s) = \begin{pmatrix} \cos\mu + \alpha\sin\mu & \beta\sin\mu \\ -\gamma\sin\mu & \cos\mu - \alpha\sin\mu \end{pmatrix}$$

$$= \begin{pmatrix} 1 & 0 \\ 0 & 1 \end{pmatrix}\cos\mu + \begin{pmatrix} \alpha & \beta \\ -\gamma & -\alpha \end{pmatrix}\sin\mu = I\cos\mu + \alpha\sin\mu \; . \qquad (4.40)$$

This matrix is called the Twiss matrix and the coefficients α, β and γ are periodic functions with the period L. The Twiss matrix must have unit determinand since it is the product of unit determinand matrices. This condition yields:

$$\beta\gamma - \alpha^2 = 1 \; . \qquad (4.41)$$

A particle executes stable betatron oscillation if the particular solutions C and S are bounded. The general stability condition can be conveniently expressed using the Twiss matrix.

The transfer matrix for two turns M_1M_2 is simply the product

$$M_1M_2 = (I\cos\mu_1 + J\sin\mu_1)(I\cos\mu_2 + I\sin\mu_2) \qquad (4.42)$$

Multiplying and inserting the relation $J^2 = -I$ yields:

$$M_1M_2 = I\cos(\mu_1 + \mu_2) + J\sin(\mu_1 + \mu_2) \qquad (4.43)$$

Eq. 4.43 can be easily generalized to n turns:

$$T_{n\ldots1} = I(\cos\mu_1 \ldots \cos\mu_n) + J(\sin\mu_1 \ldots \sin\mu_n) \qquad (4.44)$$

The betatron oscillations are bounded if the phase advance μ per turn is real:

$$\mathrm{Tr}\,|T| = 2\cos\mu \leq 2 \qquad (4.45)$$

4.4 The Betatron Function

The transverse motion of a charged particle ($\Delta p = 0$) in both planes with respect to the reference orbit is given by the solution to the equation

$$u''(s) + K(s)\,u(s) = 0 \; . \qquad (4.25)$$

This equation is rather famous, it was first investigated by the

astronomer Hill in conjunction with the orbitals of the moon. Below we sketch the solution[10] to this equation.

According to the theorem of Floquet, Hills equation has two independent particular solutions of the form

$$u_k(s) = p_k(s)\, e^{\pm i\mu \cdot s/L} \tag{4.47}$$

where $p_{1,2}(s)$ are periodic functions with period L:

$$p_{1,2}(s) = p_{1,2}(s + L) \tag{4.48}$$

The solution after one complete turn can be written as:

$$u_k(s + L) = p_k(s + L)\, e^{\pm i\mu(s+L)/L} = u_k(s)\, e^{\pm i\mu} \tag{4.49}$$

and it can be related to the Twiss matrix for one complete turn:

$$u_k(s)(\cos\mu \pm i\sin\mu) = (\cos\mu + \alpha\sin\mu)\, u_k(s) + \beta\sin\mu\, u_k'(s) \tag{4.50}$$

This equation must be valid for all values of the phase advance μ. Equating the $\cos\mu$ terms yield a trivial identidy whereas equating the $\sin\mu$ terms yield:

$$\frac{u_k'}{u_k} = \frac{\pm i - \alpha}{\beta} \tag{4.51}$$

Logarithmic differentiation leads to the expression:

$$\frac{u_k''}{u_k'} - \frac{u_k'}{u_k} = \frac{-\alpha'}{\pm i - \alpha}\,\frac{\beta'}{\beta} \tag{4.52}$$

An alternative expression for the right hand side of eq. 4.52 can be obtained by combining eq. 4.51 and Hill's equation. Multiply eq. 4.51 with K(s) and substitute $u_k'' = -Ku_k$ yields

$$\frac{u_k''}{u_k'} = -\frac{K\beta}{\pm i - \alpha} \tag{4.53}$$

Subtract eq. 4.51 from the equation above yield:

$$\frac{u_k''}{u_k'} - \frac{u_k'}{u_k} = -\frac{\pm i - \alpha}{\beta} - \frac{K\beta}{\pm i - \alpha} \tag{4.54}$$

Equating the right hand sides of eq. 4.52 and eq. 4.54 yields:

$$(\alpha^2 + K\beta^2 + \alpha\beta' - \alpha'\beta - 1) \mp i\,(\beta' + 2\alpha) = 0 \tag{4.55}$$

The real and the imaginary part must disappear independently and this yields the relations:

$$\begin{aligned} \beta' &= -2\alpha \\ \alpha' &= K\beta - \gamma\,. \end{aligned} \tag{4.56}$$

Substitute $\alpha = -\frac{1}{2}\beta'$ in eq. 4.51 results in a relationship between u_k, β and their derivatives

$$\frac{u_k'}{u_k} = \frac{i + \frac{1}{2}\beta'}{\beta} \tag{4.57}$$

Eq. 4.57 can be logarithmically integrated:

$$\begin{aligned} u_k(s) &= a\sqrt{\beta}\, e^{\pm i\mu} \\ u_k(s) &= a\sqrt{\beta}\cos(\mu(s) + \mu_0) \end{aligned} \tag{4.58}$$

with

$$\mu(s) = \int \frac{ds}{\beta} \tag{4.59}$$

$\beta(s)$ is called the betatron function and $\mu(s)$ the betatron phase.

The solution of Hills equation is a quasiharmonic oscillation with an instantaneous amplitude proportional to $\sqrt{\beta}$ and a reduced

wave length $\lambda = \beta(s)$. Q, the number of transverse oscillations per turn is given by eq. 4.59 integrated over one complete turn

$$Q = \frac{1}{2\pi} \oint \frac{ds}{\beta} \tag{4.60}$$

The Twiss matrix can be expressed using eqs. 4.41 and 4.56 as:

$$T = \begin{pmatrix} \cos\mu - \frac{1}{2}\beta' \sin\mu & \beta \sin\mu \\ -\frac{1 + \frac{1}{4}\beta'^2}{\beta} \sin\mu & \cos\mu + \frac{1}{2}\beta' \sin\mu \end{pmatrix} \tag{4.61}$$

The linear optic of an accelerator is completely determined by the knowledge of $\beta(s)$ and its derivative. Note that the complete magnet system contribute to the value of the betatron function at a given position s.

The betatron function resulting from a given magnet arrangement is readily determined using the matrix formalism discussed above. Let us assume that the machine is made of n elements. The transfer matrix for a complete turn is given by the product of n individual transfermatrices.

$$\begin{pmatrix} \cos\mu + \alpha\sin\mu & \beta\sin\mu \\ -\gamma\sin\mu & \cos\mu - \alpha\sin\mu \end{pmatrix} = \begin{pmatrix} C & S \\ C' & S' \end{pmatrix} = \prod_{j=0}^{n} M \begin{pmatrix} C & S \\ C' & S' \end{pmatrix}_j \tag{4.62}$$

Equating the elements m_{12} on both sides of the equation yields:

$$\beta(s + L, s) = \frac{S(s + L, s)}{\sin 2\pi Q} \quad . \tag{4.63}$$

The value of the betatron function at the position s is proportional to the value of the sine like function after one revolution. The

value of sin 2π Q is given by the trace of the transfermatrix for one turn:

$$\cos 2\pi Q = \frac{1}{2} \mathrm{Tr}\,(C(s + L, s) + S'(s + L, s)). \tag{4.64}$$

4.5 Off Energy Particles

The particle energy will in general differ from the design energy. A finite energy deviation will to first order only affect the radial motion which is now described by the solution to eq. 4.18

$$\begin{aligned} x''(s) + K_x(s)\, x(s) &= G(s) \frac{\Delta p}{p} \\ K_x(s) &= G^2(s) + K(s) \end{aligned} \tag{4.18}$$

The solution to eq. 4.18 can be written as the sum of two functions

$$x(s) = x_p(s) + x_\beta(s) \tag{4.65}$$

$x_\beta(s)$ is the solution to the homogeneous equation and describe the betatron oscillations around the closed orbit given by $x_p(s) = D(s) \frac{\Delta p}{p}$, where D(s) is the unique particular solution to the inhomogeneous equation

$$D''(s) + K_x(s)\, D(s) = G(s) \tag{4.66}$$

satisfying the boundary condition

$$\begin{aligned} D(L) &= D(0) \\ D'(L) &= D'(0) \end{aligned} \tag{4.67}$$

The solution can be written as (see chapter 5.2.2 with the substitution $x_c \to D$ and $\delta G \to G$):

$$D(s) = \frac{\sqrt{\beta(s)}}{2\sin\pi\nu} \oint G(s')\ \sqrt{\beta(s')}\cos(\mu(s) - \mu(s')) - \pi Q)ds' \qquad (4.68)$$

Thus with the knowledge of the betatron function one can compute the off energy function. The variation of D(s) over a FODO cell is plotted in Fig. 4.2.

We can also write the solution in matrix form for the various elements which make up an accelerator.

D(s) must satisfy eq. 4.18 with constant values of K(s) and G(s). The solution shall satisfy the boundary condition

$$D(0) = D'(0) = 0 \qquad (4.69)$$

Inspection of equation 4.62 suggest the following Ansatz

$$D(s) = (a + b\cos\sqrt{K}\,L) \qquad (4.70)$$

Inserting this Ansatz into eq. 4.62 yields

$$a = \frac{1}{K\rho} \qquad (4.71)$$

and the boundary condition in eq. 4.65 yields

$$b = \frac{-1}{K\rho} \quad . \qquad (4.72)$$

The particular solution of the inhomogenous equation for a focusing element is thus given by:

$$D(s) = \frac{(1 - \cos\sqrt{K}\,L)}{K\rho} \qquad K \quad 0 \qquad (4.73)$$

Correspondingly the particular solution of eq. 4.62 for a defocusing element is given by

$$D(s) = \frac{(1 - \cosh\sqrt{|K|}\,L)}{|K|\rho} \qquad (4.74)$$

The matrix formalism discussed in chapter 4.3 can be extended to include off momentum particles

$$\begin{pmatrix} x \\ x' \\ \frac{\Delta p}{p} \end{pmatrix}_{s_1} = M \begin{pmatrix} x \\ x' \\ \frac{\Delta p}{p} \end{pmatrix}_{s_0} \qquad (4.75)$$

with

$$M(s|s_0) = \begin{pmatrix} C & S & D \\ C' & S' & D' \\ 0 & 0 & 1 \end{pmatrix}_s$$

The values for C, S and D are given above. The values of D and D' can be computed from eq. 4.73 for a focusing element and from eq. 4.74 for a defocusing element.

4.5 The FODO Cell

The commonly used FODO cell, shown in Fig. 4.2 is made of a horizontally focusing and defocusing quadrupole doublet spaced by dipole magnets. In this chapter we will evaluate the optical properties of such a cell in the thin lens approximation. In this approximation the length of a lens l approaches zero with

$K\,l \to \frac{1}{f}$ = constant i.e. $\sqrt{K}\,l \to 0$. The transfer matrix for the FODO cell shown in Fig. 4.2 is given by the product of matrices for the individual elements. The transfer matrix at the entrance of a focusing quadrupole is given by

$$M = M_o\, M_D\, M_o\, M_F$$

$$= \begin{pmatrix} 1 & \frac{L}{2} \\ 0 & 1 \end{pmatrix} \begin{pmatrix} 1 & 0 \\ \frac{1}{f} & 1 \end{pmatrix} \begin{pmatrix} 1 & \frac{L}{2} \\ 0 & 1 \end{pmatrix} \begin{pmatrix} 1 & 0 \\ \frac{-L}{f} & 1 \end{pmatrix}$$

$$= \begin{pmatrix} 1 - \frac{L}{2f} - \frac{L^2}{4f^2} & L + \frac{L^2}{4f} \\ \frac{-L}{2f^2} & 1 + \frac{L}{2f} \end{pmatrix} \qquad (4.77)$$

f is the focal length of the lens and L the cell length. This matrix must equal the Twiss matrix T - i.e. $M_{ih} = T_{ih}$

$$T = \begin{pmatrix} \cos\mu + \alpha\sin\mu & \beta\sin\mu \\ -\gamma\sin\mu & \cos\mu - \alpha\sin\mu \end{pmatrix} \qquad (4.78)$$

The Twiss parameters can then easily be expressed in terms of the focusing strength f and the cell length L using the relationship above.

The phase advance μ across the cell is obtained from:

$$\begin{aligned} \mathrm{Tr}\, T &= \mathrm{Tr}\, M \\ 2\cos\mu &= 2 - \frac{L^2}{4f^2} \\ \sin\frac{\mu}{2} &= \frac{L}{4f} \end{aligned} \qquad (4.79)$$

The value of the β-function at a position of a focusing quadrupole is given by:

$$T_{12} = M_{12}$$

$$\beta_F \sin\mu = L\,(1 + \frac{1}{4}\frac{L}{f})$$

$$\beta_F = \frac{L}{\sin\mu}(1 + \sin\tfrac{\mu}{2}) = 2f\,\left(\frac{1 + \frac{1}{4}\frac{L}{f}}{1 - \frac{1}{4}\frac{L}{f}}\right)^{1/2} \qquad (4.80)$$

The β function at the position of a defocusing quadrupole is obtained by interchanging the position of M_D and M_F in eq. 4.77. This yields:

$$\begin{aligned} \beta_D &= \frac{L}{\sin\mu}\,(1 - \sin\tfrac{\mu}{2}) \\ \beta_D &= 2f\,\left(\frac{1 - \frac{1}{4}\frac{L}{f}}{1 + \frac{1}{4}\frac{L}{f}}\right)^2 \end{aligned} \qquad (4.81)$$

The values of the β-functions normalized to the cell length L is plotted in Fig. 4.6a versus the phase advance μ. Note that the difference:

$$\beta_F - \beta_D = 4f\,\mathrm{tg}\tfrac{\mu}{2} \qquad (4.82)$$

increases monotonically with the phase advance.

The value of α_F is extracted from the relation

$$T_{11} - T_{22} = M_{11} - M_{22}$$

$$\alpha_F = -\frac{1 + \sin\frac{\mu}{2}}{\cos\frac{\mu}{2}} \qquad (4.83)$$

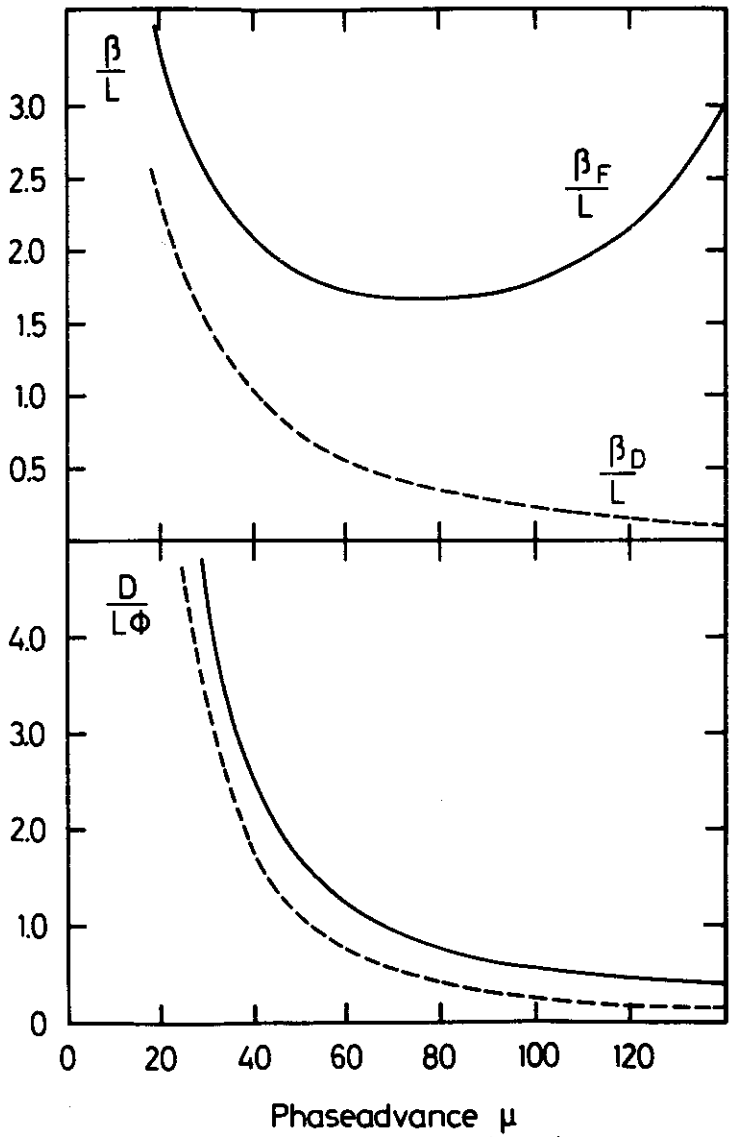

Fig. 4.6 - The extreme values of the β-function and the off energy function as a function of the phase advance μ per cell.

The value of γ_F is determined from:

$$\begin{aligned} T_{21} &= M_{21} \\ -\gamma_F \sin\mu &= \frac{-L}{2f^2} \\ \gamma_F &= \frac{1}{f \cos\frac{\mu}{2}} \end{aligned} \tag{4.84}$$

The values of α_D and γ_D at the position of a defocusing quadrupole are given by interchanging M_D and M_F in eq. 4.77. This yields:

$$\alpha_D = \frac{1 - \sin(\frac{\mu}{2})}{\cos\frac{\mu}{2}} \tag{4.85}$$

$$\gamma_D = \frac{1}{f \cos\frac{\mu}{2}} \tag{4.86}$$

To determine the dispersion function D(s) we must make use of the 3 x 3 matrices defined in eq. 4.76. The computational effort can be reduced by making use of the fact that the slopes of the dispersion functions disappear in the middle of the quadrupoles:

$$\begin{pmatrix} D_D \\ 0 \\ 1 \end{pmatrix} = M \begin{pmatrix} D_F \\ 0 \\ 1 \end{pmatrix} \tag{4.87}$$

with $M = M_D(\frac{1}{2}f)\, M_O(\frac{1}{2}L) M_F(\frac{1}{2}f)$

$$\begin{pmatrix} 1 & 0 & 0 \\ \frac{1}{2}f & 1 & 0 \\ 0 & 0 & 1 \end{pmatrix} \begin{pmatrix} 1 & \frac{1}{2} & \frac{L\phi}{8} \\ 0 & 1 & \frac{\phi}{2} \\ 0 & 0 & 1 \end{pmatrix} \begin{pmatrix} 1 & 0 & 0 \\ \frac{1}{2f} & 1 & 0 \\ 0 & 0 & 1 \end{pmatrix} \tag{4.88}$$

$$\begin{pmatrix} 1 - \frac{1}{4}\frac{L}{f} & \frac{L}{2} & \frac{L\phi}{8} \\ -\frac{L}{8f^2} & 1 + \frac{L}{4f} & (1 + \frac{L}{8f})\frac{\phi}{2} \\ 0 & 0 & 1 \end{pmatrix} \qquad (4.89)$$

L and ϕ are respectively the length and the bending angle of the cell. This yields the equations:

$$\begin{aligned} D_D &= (1 - \frac{L}{4f})\, D_F + L\frac{\phi}{8} \\ 0 &= -(\frac{L}{8f^2})\, D_F + (1 + \frac{L}{8f})\frac{\phi}{2} \end{aligned} \qquad (4.90)$$

Solving eq. 4.90 for the dispersion functions yield:

$$\begin{aligned} D_F &= \frac{1}{\sin^2\frac{\mu}{2}} \quad \frac{L\phi}{4}(1 + \tfrac{1}{2}\sin\tfrac{\mu}{2}) \\ &= (\frac{4f^2}{\rho})(1 + \frac{L}{8f}) \end{aligned} \qquad (4.91)$$

$$\begin{aligned} D_D &= \frac{1}{\sin^2(\frac{\mu}{2})} \quad \frac{L\phi}{4}(1 - \tfrac{1}{2}\sin\tfrac{\mu}{2}) \\ &= (\frac{4f^2}{\rho})(1 - \frac{L}{8f}) \end{aligned} \qquad (4.92)$$

The normalized dispersions $\frac{D}{L\phi}$ are plotted in Fig. 4.6b versus phase advance.

The average value of the dispersion function is given by:

$$\langle D \rangle = \frac{4f^2}{\rho} \quad . \qquad (4.93)$$

4.6 The Courant-Snyder Invariant

The transverse motion of a charged particle in a magnetic field including synchrotron radiation (see chapter 7) is described by the solutions to the equation

$$u'' + J(s)\, u' + K(s)\, u = 0 \; . \qquad (4.94)$$

At present energies the synchrotron radiation from a proton can be neglected, i.e. J(s) = 0 and eq. 4.94 is reduced to the familiar Hill's equation.

The Wronskian determimant is defined as:

$$W(s) = \begin{pmatrix} u_1 & u_2 \\ u_1' & u_2' \end{pmatrix} \qquad (4.95)$$

u_1 and u_2 are solutions of the differential equation, i.e. they satisfy:

$$\begin{aligned} u_1'' + J(s)\, u_1' + K(s)\, u_1 &= 0 \\ u_2'' + J(s)\, u_2' + K(s)\, u_2 &= 0 \end{aligned} \qquad (4.96)$$

Multiplying the first equation with u_2, the second with u_1 and subtract the two equations yield:

$$\frac{dW}{ds} + J\, W = 0 \qquad (4.97)$$

with $W = u_1 u_2' - u_1' u_2$.

The solution of this equation is given by

$$W(s) = W_0\, e^{\int_{s_1}^{s_2} J\, ds} \; . \qquad (4.98)$$

Thus in the case of an electron the Wronskian depends on s whereas for a proton $W(s) = W_0$ is a constant of motion.

To determine the invariant W_0 we take $u_1 = \sqrt{\beta}\, e^{i\mu(s)}$ and set $u_2 = u$, i.e. u_2 is an arbitrary real solution of Hill's equation.

$$W_0 = (u\, u_1' - u'\, u_1) = u_1 \left(u \frac{u_1'}{u_1} - u'\right) \tag{4.99}$$

$$= u_1 \left(u \frac{i - \alpha}{\beta} - u\right)$$

where eq. 4.51 has been used to substitute

$$\frac{u_1'}{u_1} = \frac{i - \alpha}{\beta}$$

$$W_0 W_0^* = u_1 u_1^* \left(u \frac{i - \alpha}{\beta} - u'\right)\left(u \frac{[-i - \alpha]}{\beta} - u'\right) \tag{4.100}$$

With $u_1 u_1^* = \beta$ the equation above simplifies to:

$$WW^* = \frac{u^2 + (\alpha u + \beta u')^2}{\beta} = \frac{\varepsilon}{\pi} \ . \tag{4.101}$$

We consider the value of WW^* at a fixed azimuth s_0, i.e. α_0 and β_0 are constants. On each succesive turn the particles will arrive at $s = s_0$ with different values of u and u' however the values must satisfy eq. 4.101. Thus on successive turns the particles traces an ellipse in u u' space as indicated in Fig. 4.7. The area of the ellipse is given by

$$A = \pi\, u_{max}\, u_0' \tag{4.102}$$

with u_{max} and u_0' defined in Fig. 4.7.
It follows from eq. 4.101:

$$u_{max} = \sqrt{\frac{\varepsilon\beta}{\pi}} \quad \text{and} \quad u_0 = \sqrt{\frac{\varepsilon}{\pi\beta}} \tag{4.103}$$

Substitute these values into eq. 4.102 yields:

$$A = \varepsilon \ .$$

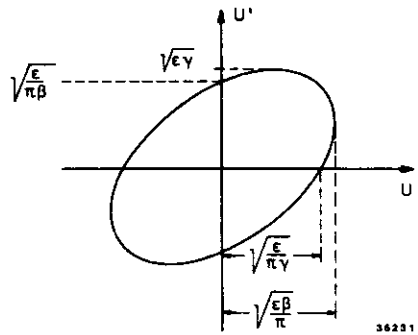

Fig. 4.7
The phase ellipse.

The quantity uu' is by definition the beam emittance - i.e. the product of beam size and angular divergence. The Wronskian can thus be identified with the beam emittance and it follows that the beam emittance is a constant of motion for a proton beam, but not for an electron beam because of the synchrotron radiation.

The betatron motion is thus completely defined

$$u = \sqrt{\frac{\varepsilon}{\pi}}\ \sqrt{\beta}\ \cos(\mu(s) - \mu_0)) \tag{4.104}$$

Note that for a proton beam the emittance ε and hence the betatron amplitude decreases with increasing energy as:

$$\varepsilon = \pi\,(u\, u') = u \frac{p_\perp}{p} = u \frac{p_\perp}{\beta\gamma} \tag{4.105}$$

where β is the normalized particle velocity $\beta = \frac{p}{E}$ and $\gamma = \frac{E}{m_0 c^2}$. Usually the invariant emittance $(\varepsilon\ \beta\ \gamma)$ is quoted.

5. Magnet Imperfections and Resonances[10,30,31)]

5.1 Introduction

In the previous discussion we assumed that the guide field is made of ideal dipole and quadrupole magnets. However, a real magnet has imperfections, magnets are not exactly reproducible and they can only be installed with a certain precision. The resulting deviations from the ideal guide field are grouped into linear and nonlinear errors.

The linear errors are caused by imperfections in the dipole and the quadrupole components of the field and these errors cause closed orbit deviations and tune changes. The magnitude of the linear effects are independent of the particle amplitude.

The nonlinear errors are caused by higher multipole fields and their effects depend on the particle amplitude. Nonlinear effects are particular important in machines made of superconducting magnets. Superconducting magnets are rich in higher multipoles since the field is produced directly by the current distribution and not shaped by the iron yoke. An ideal $\cos\theta$ current distribution would produce a perfect dipole field. However, the $\cos\theta$ distribution in a real magnet is only approximate and it is only possible to position the wires with a certain precision. The relative strength of these errors are independent of the induction. The persistent currents, caused by flux trapped in the conductor, leads to higher multipole fields. The strength of these multipoles are independent of excitation and they are therefore particularly important at low fields - i.e. at injection.

5.2 Linear Field Errors

Dipole and quadrupole field errors raises the obvious question whether a closed orbit still exists, and if so, how is the betatron function and the tune changed in their presence. We will address these questions in this section.

5.2.1 Dipole Errors

The ideal equilibrium orbit is no longer a possible trajectory, however, in the case of small field errors we expect to find a neighbouring trajectory which will close on itself. This new orbit, depicted in Fig. 5.1 is called the disturbed closed orbit and the particles now make betatron oscillations around this orbit.

$$\Delta x = 0$$

$$\Delta x' = \Delta G \cdot \Delta s$$

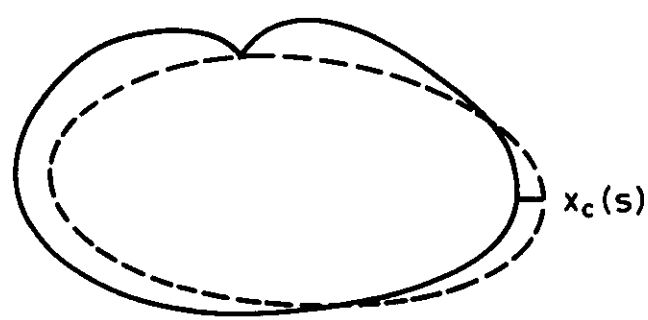

Fig. 5.1 - The change in closed orbit due to an dipole error $\Delta G \Delta s$.

The amplitude x(s) of an arbitrary particle with respect to the ideal equilibrium orbit is the sum of the disturbed closed orbit amplitude $x_c(s)$ and the betatron amplitude $x_\beta(s)$.

$$x(s) = x_c(s) + x_\beta(s) \tag{5.1}$$

Assume that there is a disturbance $\Delta B \Delta s$ located at s = 0. This disturbance will change the slope of the trajectory at this point but not its displacement.

$$\Delta x' = \frac{\Delta B \Delta s}{B\rho} \tag{5.2}$$

or $$\Delta x'' = \frac{\Delta x'}{\Delta s} = \frac{\Delta B}{B\rho} = \Delta G$$

Thus the equation for the disturbed closed orbit is given by

$$x_c'' + K_x x_c = \Delta G \tag{5.3}$$

The general solution of eq. 5.3 can be written as:

$$x_c(s) = a \sqrt{\beta(s)} \cos(\mu(s) - \mu_0) \tag{5.4}$$

The constants a and μ_0 are determined from the condition that the orbit must close on itself after one turn:

$$x_c(L) = x_c(0) \tag{5.5a}$$

$$x_c'(L) + \Delta G \, \Delta s = x_c'(0) \tag{5.5b}$$

By substituting the solution eq. 5.4 into eqs. 5.5a and 5.5b we find:

$$\mu_0 = \pi Q_x \tag{5.6}$$

$$a = \frac{\Delta G \Delta s}{2 \sin \pi Q_x} \sqrt{\beta(0)} \tag{5.7}$$

The disturbed closed orbit is thus given by:

$$x_c(s) = \frac{\Delta G \Delta s \sqrt{\beta(0)}}{2 \sin \pi Q} \sqrt{\beta(s)} \cos(\mu - \pi Q_x) \tag{5.8}$$

Assuming that the dipole errors are distributed according to $\delta G(s')$ around the ring eq. 5.8 can be generalized:

$$x_c(s) = \frac{\sqrt{\beta(s)}}{2 \sin \pi Q_x} \oint \delta G(s') \sqrt{\beta(s')} \cos(\mu(s) - \mu(s') - \pi Q_x) \, ds' \tag{5.9}$$

The salient features of eq. 5.9 can be summarized as follows:

- The displacement of the closed orbit is everywhere proportional to the strength of the disturbance $\Delta B \Delta s$ and to the square root of the beta function at the position of the disturbance. It is also proportional to the square root of the beta function at the point of observation.

- In order for the closed orbit distortion to remain finite $Q_x (Q_y)$ must not be an integer. For integer Q values the particles will cross the disturbance with the same phase on every turn - i.e. the particles will receive a kick in the same direction on every turn leading to an divergent amplitude.

Correction dipole magnets are installed in all machines to minimize the closed orbit deviations. This is done by observing the beam position with monitors at say 4 positions per betatron wavelength and adjusting the correction dipoles to minimize the closed orbit amplitude. Typically disturbed closed orbit amplitudes on the order of 1 mm rms are obtained after corrections.

5.2.2 Gradient Errors

A gradient error located at s = 0 can be represented by a thin lens of focal strength $\delta = 1/f$. Such an error will obviously modify the betatron function of the undisturbed lattice and shift the tune from its undisturbed value. These effects can be evaluated using the Twiss matrix T. The Twiss matrix for a complete turn is given by the product of a quadrupole matrix Q - representing the disturbance - and the undisturbed Twiss matrix T_0

$$T = Q\,T_0 \tag{5.10}$$

$$T = \begin{pmatrix} \cos\mu+\alpha\sin\mu & \beta\sin\mu \\ -\gamma\sin\mu & \cos\mu-\alpha\sin\mu \end{pmatrix} = \begin{pmatrix} 1 & 0 \\ -\delta & 1 \end{pmatrix} \begin{pmatrix} \cos\mu_0+\alpha_0\sin\mu_0 & \beta_0\sin\mu_0 \\ -\gamma_0\sin\mu_0 & \cos\mu_0-\alpha_0\sin\mu_0 \end{pmatrix}$$

The index refers to the undisturbed orbit. Multiplying the matrices on the right hand side and taking the trace yields:

$$\frac{1}{2}\,\mathrm{Tr}\,(T) = \cos\mu = \cos\mu_0 - \frac{\delta\,\beta_0}{2}\sin\mu_0 \tag{5.11}$$

This expression can be simplified for small tune changes - i.e. $\mu = \mu_0 + \Delta\mu$:

$$\Delta\mu = -\frac{\delta\,\beta_0}{2} \tag{5.12}$$

or since $\Delta Q = 2\pi\Delta\mu$:

$$\Delta Q = -\frac{\delta\,\beta_0}{4\pi} \tag{5.13}$$

Thus the tune change ΔQ is directly proportional to the strength of the disturbance and to the value of the betatron function at the position of the disturbance.

Next we evaluate the change in the betatron function at $s = s_2$ caused by a gradient error at $s = s_1$.

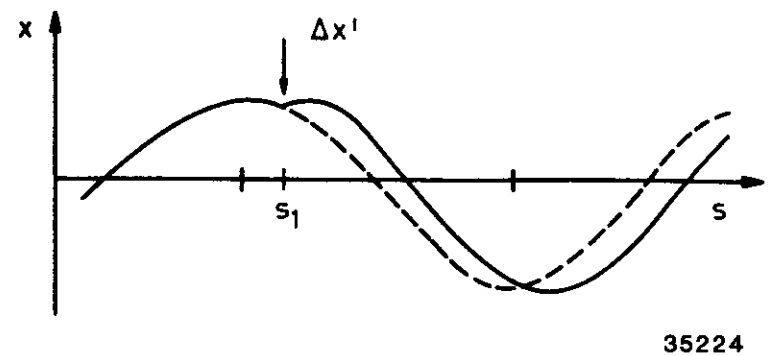

Fig. 5.2 - Change in the betatron function due to a gradient error at $s = s_1$.

The unperturbed Twiss matrix for a single turn can be written as:

$$T^0 = A(s_1 \to s_2)\,B(s_2 \to s_1) = \begin{pmatrix} a_{11} & a_{12} \\ a_{22} & a_{22} \end{pmatrix} \begin{pmatrix} b_{11} & b_{12} \\ b_{21} & b_{22} \end{pmatrix} \tag{5.14}$$

Including the disturbance at $s = s_1$ yields a Twiss matrix T:

$$T = \begin{pmatrix} a_{11} & a_{12} \\ a_{21} & a_{22} \end{pmatrix} \begin{pmatrix} 1 & 0 \\ \delta & 1 \end{pmatrix} \begin{pmatrix} b_{11} & b_{12} \\ b_{21} & b_{22} \end{pmatrix} \tag{5.15}$$

Hence

$$\Delta T = T_{12} - T^0_{12} = \delta a_{12}\,b_{12} = \delta\sin(\mu_0 - \mu_2 + \mu_1)\,\sin(\mu_2 - \mu_1)\beta_1\beta_2 \tag{5.16}$$

The change in T_{12} can also be expressed as a total differential:

$$T_{12} = \Delta(\beta_2 \sin\mu) = \Delta\beta_2 \sin\mu_0 + \beta_2 \Delta\mu \cos\mu_0 \qquad (5.17)$$

Equating eq. 5.16 and eq. 5.17 with the substitution $\Delta\mu = -\frac{\delta\beta_1}{2}$ yields the change in betatron amplitude at $s = s_2$ due to a gradient error δ at $s = s_1$:

$$\Delta\beta_2(s_2) = \frac{\delta\beta_1\beta_2 \cos[2\pi Q_x - 2(\mu_2 - \mu_1)]}{2\sin 2\pi Q_x} \qquad (5.18)$$

The change in the betatron function is directly proportional to the strength of the disturbance and the product of the betatron function at the position of the disturbance and the position of the observation.

The beam becomes unstable if the tune approaches a half integer - i.e. $Q_x \neq \frac{(2n+1)}{2}$.

The beat frequency introduced by an gradient error is twice the beat frequency caused by an dipole error.

With a gradient error k(s) distributed around the ring the tune shift and the change in betatron function can be written as:

$$\Delta Q = -\frac{1}{4\pi} \oint k(s)\, \beta(s)\, ds \qquad (5.19)$$

$$\Delta\beta(s) = \frac{\beta(s)}{2\sin 2\pi Q} \oint k(s')\, \beta(s') \cos 2[\pi Q + \mu(s') - \mu(s)]\, ds' \qquad (5.20)$$

5.3 Non Linear Errors

We have seen above that the betatron oscillations became unstable for integer and half integer tune values in the presence of dipole and quadrupole errors. Higher order multipole errors will drive higher order resonances[31] - i.e. the particle motion will now become unstable for fractional tune values 1/n = 1/3, 1/4, ... In general Q values satisfying the relation

$$\ell Q_x + m Q_z = s \qquad (5.21)$$

with $|\ell| + |m| = n$, and ℓ, m, s and n integers will be unstable. The ensuing resonance pattern is shown in Fig. 5.3 and the corresponding driving terms for the lowest order multipoles are listed in Table 5.1.

Table 5.1 - Resonance driving terms

Multipole	Order n	regular	skew
Quadrupole	2	$x^2 - y^2$	$2xy$
Sextupole	3	$x^3 - 3xy^2$	$y^3 - 3x^2y$
Octupole	4	$x^4 - 6x^2y^2 + y^4$	$4xy^3 - 4x^3y$
Decapole	5	$x^5 - 10x^3y^2 + 5xy^4$	$10x^2y^3 - 5x^4y - y^5$

For example a third order resonance will yield four forbidden lines in the resonance diagram shown above, namely $3Q_x = s$, $3Q_y = s$ and the coupling resonances $Q_x + 2Q_y = s$ and $2Q_x + Q_y = s$.

Indeed the order of a resonance is identical to the order of the driving term for an ideal closed orbit. However, in the presence of closed orbit errors a multipole of order n may excite lower orders.

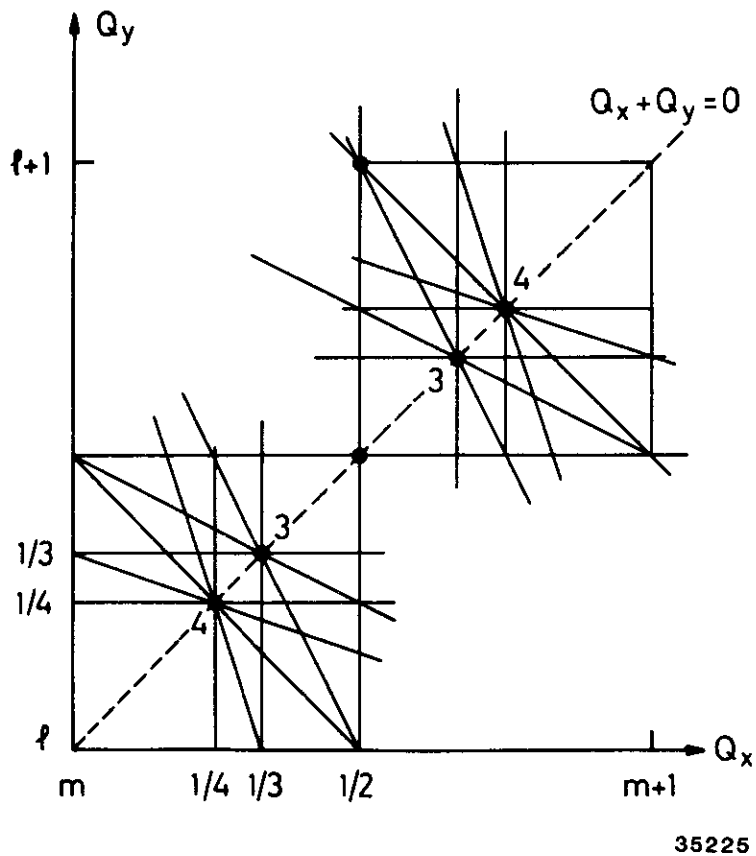

Fig. 5.3 - The pattern of forbidden tune values caused by low order resonances.

The width of resonance lines depends not only on the strength and the azimuthal distribution of the driving terms but also on the betatron amplitude in the case of non linear errors - i.e. sextupole and higher.

Multipole errors may therefore limit the usuable aperture to values which are smaller than the geometric aperture given by the vacuum chamber.

5.3.1 The Resonance Mechanism

The phase space coordinates p and x of a particle can be represented in the circle diagram (Fig. 4) as:

$$\begin{aligned} p &= \beta x' = a \sin Q\theta \\ x &= x = a \cos Q\theta \end{aligned} \qquad (5.22)$$

$a = \sqrt{(\beta x')^2 + x^2}$ is the amplitude and θ the azimuthal angle of the particle in the machine - i.e. the particle makes Q turns in the phase space diagram per revolution. This representation is well suited to demonstrate the basic resonance mechanism..

A field error $\Delta B \Delta s$ change the momentum of a particle by:

$$\Delta p = \beta \frac{\Delta B \Delta s}{B\rho} \qquad (5.23)$$

The momentum kick, shown in Fig. 5.4 advance the phase by

$$\Delta\mu = \Delta p \frac{\cos Q\theta}{a} \qquad (5.24)$$

and increase the amplitude by:

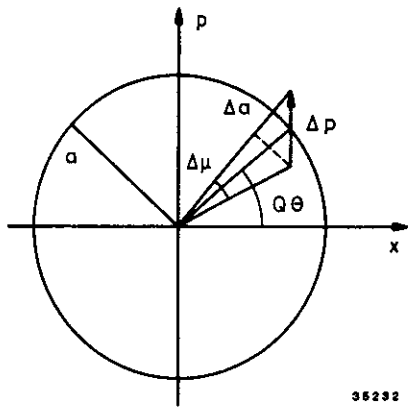

Fig. 5.4 - The circle diagram in normalized phase space.

$$\frac{\Delta a}{a} = \Delta p \frac{\sin Q\theta}{a} \tag{5.25}$$

As an example we will consider the particle motion in the plane in the presence of a sextupole of strength B'' and length l. The magnetic induction resulting from this sextupole is given by:

$$\Delta B = \frac{B''}{2} x^2 \tag{5.26}$$

The sextupole produces a momentum kick:

$$\Delta p = \beta x' = \beta\left(\frac{B'' l x^2}{2B\rho}\right) = \beta \frac{B'' l}{2B\rho} a^2 \cos^2 Q\theta \tag{5.27}$$

The resulting change in phase (eq. 5.24) and amplitude (eq. 5.25) is given by

$$\Delta\mu = \beta \frac{B'' l}{2B\rho} a \cos^2 Q\theta = \beta \frac{B'' l}{8B\rho} (3\cos Q\theta + \cos 3Q\theta) \tag{5.28}$$

$$\frac{\Delta a}{a} = \frac{\beta B'' l}{2B\rho} a \cos^2 Q\theta \sin Q\theta \tag{5.29}$$

We are now in a position to evaluate the width of the third integer stopband.

Let us assume that the radial tune Q_x is close to an 1/3 integer. In this case $\cos Q\theta$ averages to zero and we are left with the term proportional to $\cos 3Q\theta$. This term varies slowly from turn to turn modulating the unperturbed tune Q_x^o with an amplitude ΔQ_x given by:

$$\Delta Q_x = \frac{\Delta\mu}{2\pi} = \frac{\beta B'' l \cos 3Q\theta}{16\pi B\rho} \tag{5.30}$$

During the lifetime of the beam the tune will take all values within the limits:

$$Q_x^o - \frac{\beta B'' l a}{16\pi B\rho} \leq Q_x \leq Q_x^o + \frac{\beta B'' l a}{16\pi B\rho} \tag{5.31}$$

If 3 Q_x = s = integer is inside this band, the perturbed value of Q_x will become equal to the integer s after several turns. From then on the particle will lock on to the resonance and advance in phase by $2\pi s$ per turn. The resonance thus appears to have a finite width given by the strength of the disturbance B''l, the amplitude a and the value of the betatron function β at the position of the disturbance.

The change in amplitude is given by:

$$\frac{\Delta a}{a} = \frac{\beta\, B''\, l\, a}{8\, B\, \rho} \sin 3Q\theta \qquad (5.32)$$

Thus on every turn the particle receives a kick in the same direction resulting in a monotinically growing amplitude.

It is clear from the discussion above that the motion of a particle will be stable if the amplitude a satisfies the condition:

$$a < \frac{16\pi\, (B\rho)\, \Delta Q_x}{l\, \beta\, B''} \qquad (5.33)$$

where ΔQ_x is the distance between the working point and the third integer resonance. Similar relationships can be obtained for higher resonance. Thus non linear fields may limit the machine acceptance to values less than the geometric acceptance.

Such fields may be caused by the magnets or they may be due to higher order correcting fields. For example the sextupoles needed to correct the chromaticity introduce strong non linearities.

5.4 The Chromaticity

The focal length of a lens is inversely proportional to the particle momentum causing particles of different momenta to have different tune values. A single lens of length Δs leads to tune spread ΔQ of:

$$\Delta Q = \frac{1}{4\pi}\, \beta(s)\, \Delta k(s)\, \Delta s \qquad (5.34)$$

The total tune spread is obtained by substituting $\Delta k = -k(s)\, \Delta p/p$ and integrating over one revolution. This results in an expression for the natural chromaticity

$$\xi = \left(\frac{\Delta Q}{\frac{\Delta p}{p}} \right) = -\frac{1}{4\pi} \oint \beta(s)\, k(s)\, ds \qquad (5.35)$$

The natural chromaticity is negativ and large. For example the natural chromaticity of the HERA proton ring in $\xi_x = -62$ and $\xi_y = -88$ with roughly equal contributions from the arcs and the straight section. This corresponds to a tune spread of $Q_x = \pm 0.07$ and $Q_y = \pm 0.09$ for a typical momentum spread of $\pm 10^{-3}$. Thus - if left uncorrected - the beam will cross low order resonances and be lost.

However, the chromaticity can be corrected by sextupoles located adjacent to the focusing quadrupoles. At least two families of sextupoles are needed to correct for the chromaticity in both planes. Let us consider the motion in the horizontal plane. The sextupole field is given by

$$B_z = \frac{1}{2} \left(\frac{\partial^2 B_z}{\partial x^2} \right) x^2 = \frac{1}{2}\, B''\, x^2 \qquad (5.36)$$

The sextupole field can be written as an amplitude dependent gra-

dient field with

$$k = \left(\frac{B''}{2B\rho}\right) x = mx \,. \qquad (5.37)$$

The resulting tune change is given by:

$$\begin{aligned} \Delta Q &= \frac{1}{4\pi} \oint m\,\beta(s)\, x(s)\, ds \\ &= \frac{1}{4\pi} \oint m\,\beta(s)\, \left(x_\beta(x) + D(s)\,\frac{\Delta p}{p}\right) \qquad (5.38) \\ &= \frac{1}{4\pi} \oint m\,\beta(s)\, D(s)\,\frac{\Delta p}{p} \end{aligned}$$

The total chromaticity ξ of the ring is the sum of the natural chromaticity caused by the momentum spread of the particles and chromaticity produced by the correcting sextupole magnets.

$$\xi = \left(\frac{\frac{\Delta Q}{\Delta p}}{p}\right) = -\frac{1}{4\pi} \oint \beta(s)\, (k(s) - m\, D(s))\, ds \qquad (5.39)$$

6. The Synchrotron Motion [10,32]

6.1 Introduction

Energy is transferred to the particles by means of an accelerating system made of a power source and resonating cavities. The r.f. power P is fed to the cavity and excites an longitudinally electric field with a peak voltage $\hat{V}$ oscillating at a frequency ω. The required power is given by:

$$P = \frac{\hat{V}^2}{2R} \qquad (6.1)$$

R is the total shunt impedance of the cavities. As an example the PETRA cavities operating at a fixed frequency of 500 Mhz have a shunt impedance of $12\frac{M\Omega}{m}$. Ferrite loaded cavities designed to work over a large range in frequencies have much lower shunt impedances.

The average energy gain per turn for the reference particle is given by:

$$e\,U = e\,\hat{V} \sin(\omega T_0 + \phi_0) \qquad (6.2)$$

For the reference particle to remain in phase on sucessive turns ω must be an integral multiple h of the revolution frequency $\Omega_0 = \frac{2\pi}{T_0}$

$$\omega = h\,\Omega_0 \,. \qquad (6.3)$$

The harmonic number h is the maximum number of bunches which can be accelerated simultanously. Particles with energies and r.f. phases different from those of the synchronous particles will execute oscillations in energy and phase with respect to the synchronous particle.

The relative change in revolution time $\eta(p)$ for a particle with momentum different from that of the synchronous particle is given by:

$$\eta(p) = \frac{dT}{T} = -\frac{d\Omega}{\Omega} = \left(\frac{dL}{L} - \frac{d\beta}{\beta}\right) \qquad (6.4)$$

where L denotes the machine circumference and βc the particle velocity. The first term results from the change in orbit length with momentum and the second term from the change in velocity.

The time dilatation function $\eta(p)$ is in general written as:

$$\eta(p) = \left(\frac{1}{\gamma_{tr}^2} - \frac{1}{\gamma^2}\right) \frac{dp}{p} \qquad (6.5)$$

with:

$$\frac{d\beta}{\beta} = \frac{1}{\gamma^2}\,\frac{dp}{p}$$

$$\frac{1}{\gamma_{tr}^2} = \left(\frac{dL}{L}\right)\left(\frac{dp}{p}\right)^{-1} \qquad (6.6)$$

Note that for particles with the transition energy $\gamma = \gamma_{tr}$ the revolution time is independent of momentum.

The transition energy γ_{tr} can be expressed using the optical parameters. The incremental change in orbit length for a particle travelling a distance ds with a radial amplitude x, is given by:

$$dL = (1 + G(s)\,x(s))\,ds \qquad (6.7)$$

$$L = \oint dL = \oint (1 + G(s)\,x(s))\,ds \qquad (6.8)$$

$$dL = L - L_0 = \oint G(s)\,D(s)\,\frac{dp}{p}\,ds$$

The first term in eq. 6.5 is given by:

$$\frac{1}{\gamma_{tr}^2} = \alpha = \left(\frac{dL}{L}\right)\left(\frac{dp}{p}\right)^{-1} = \frac{1}{L}\oint G(s)\,D(s)\,ds \qquad (6.9)$$

The quantity α is usually called the momentum compaction. In the case of a separate function machine only the bending magnets contribute to α:

$$\alpha = \frac{G_0}{L}\oint D(s)\,ds \qquad (6.10)$$

As a rough approximation

$$\alpha = \frac{1}{Q^2} \qquad (6.11)$$

For electrons usually $\gamma >> \gamma_{tr}$ and an electron with a positive Δp has longer revolution time than the synchronous particle. This is also true for protons above the transition energy. However, below the transition energy a particle with positive ΔE has a shorter revolution time. At $\gamma = \gamma_{tr}$ the revolution time is independent of momentum and there is no phase focusing.

The synchrotron motion is illustrated in Fig. 6.1 for a particle above the transition energy. Plotted is the energy deviation ΔE versus the phase deviation $\Delta\phi$ both counted with respect to the synchronous particle. Consider a particle with positive ΔE which traverses the r.f. cavity at the synchronous phase ϕ_0. After one revolution the particle will traverse the r.f. cavity with the phase $\phi_0 + \Delta\phi$. Thus it will gain less energy than the synchronous particle. The particle will continue to move away in phase until $\Delta E = 0$. It will then start to move towards ϕ_0 and arrive at ϕ_0 with an energy less than that of the synchronous particle. From then on it will gain more energy than the synchronous particle but continue to move away in phase until its energy equals that of the synchronous particle. As soon as the energy is higher than that of the synchronous particle it will start to move towards ϕ_0 and arrive at ϕ_0 with an energy higher than that of the synchronous particle. This completes one period. The aim of this chapter is to derive and solve the equations for the synchrotron oscillations and to determine the stable boundaries in $\Delta\phi$ and ΔE in terms of the r.f. parameters. The effects of the synchrotron radiation on the synchrotron motion will be discussed in chapter 7.

6.2 The Equation of Motion

The synchronous particle is accelerated at a constant radius R_0 and the magnetic induction must therefore be increased proportional to the gain in momentum:

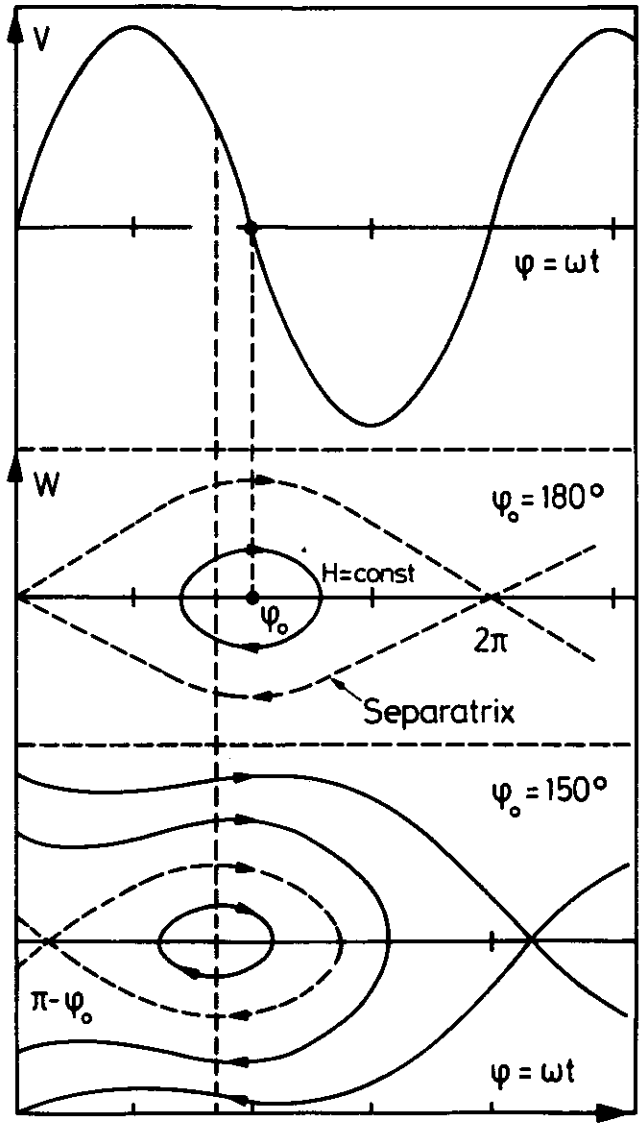

Fig. 6.1 - Longitudinal trajectories in $W = \frac{\Delta E}{\Omega_0}, \phi$ space for a stationary bucket $\phi_0 = 180^0$ and a moving bucket $\phi = 150^0$.

$$dp = eR_0 \frac{dB}{dt} T_0 \qquad (6.12)$$

T_0 is the revolution time $T_0 = \frac{2\pi R_0}{\beta c}$.

The relationship between energy gain and ramping speed is given by:

$$dE_0 = 2\pi e R_0^2 \frac{dB}{dt} = e \hat{V} \sin\phi_0 \qquad (6.13)$$

We will now consider the synchrotron motion of particles with small energy and phase deviations with respect to the synchronous particle.

$$\Delta\phi = \phi - \phi_0 , \quad dE = E - E_0 \text{ and } d\Omega = \Omega - \Omega_0 \qquad (6.14)$$

The change in revolution frequency for a particle with an energy deviation ΔE was derived above.

$$- \frac{d\Omega}{\Omega} = \eta \frac{dp}{p} = \eta \frac{dE}{R \Omega p} \qquad (6.15)$$

The corresponding change in phase angle is given by:

$$d\phi = - h \, d\theta = - h \Omega \, dt \qquad (6.16)$$

Combining eqs. 6.15 and 6.16 yields:

$$\frac{dE}{\Omega} = \left(\frac{p R}{h \eta \Omega} \right) \frac{d\phi}{dt} \qquad (6.17)$$

The energy gain of a particle arriving at a different phase will differ from that of the synchronous particle

$$\Delta p = \frac{\Delta E}{R\Omega} = \frac{e \hat{V}}{R \Omega} \sin\phi = \frac{T e \hat{V}}{2\pi R} \sin\phi \qquad (6.18)$$

$$\dot{p}R = \frac{e\hat{V}}{2\pi} \sin\phi \qquad [6.19)$$

The energy gain relative to that of the synchronous particle is given by:

$$R\dot{p} - R_o\dot{p}_o = \frac{e\hat{V}}{2\pi}(\sin\phi - \sin\phi_o) \qquad (6.20)$$

Expanding R and p to first order yield:

$$\frac{d}{dt}(R_o\,\Delta p) = \frac{e\hat{V}}{2\pi}(\sin\phi - \sin\phi_o) \qquad (6.21)$$

Substituting $p = \frac{dE}{R\Omega}$ in the equation above and consider only small amplitude phase oscillation yields:

$$\frac{d}{dt}\left(\frac{\Delta E}{\Omega_o}\right) = \frac{e\hat{V}}{2\pi}(\sin\phi - \sin\phi_o) = \frac{e\hat{V}}{2\pi}\cos\phi\,\Delta\phi \qquad (6.22)$$

Combining eqs. 6.17 and 6.21 yield the equations for small amplitude phase oscillations:

$$\frac{d}{dt^2}(\Delta\phi) + \omega_s^2 = 0 \qquad (6.23a)$$

$$\omega_s = \left(\frac{-\eta_o\, h\, e\hat{V}\cos\phi_o\Omega_o}{2\pi\, p_o\, R_o}\right)^{1/2} \qquad (6.23b)$$

The solution for $\eta_o\cos\phi_o < 0$ is a sinusoidal oscillation with frequency ω_s:

$$\Delta\phi = A\sin(\omega_s t + \phi_o) \qquad (6.24)$$

We may now distinguish two cases:

Below transition energy $\eta_o < 0$ and the phase ϕ_o must be choosen between 0 and $\pi/2$ for stable acceleration and between $3/2\pi$ and 2π for stable deacceleration. Above transition energy $\phi_o > 0$,and ϕ_o must be between $\pi/2$ and π for stable acceleration and between π and $3/2\pi$ for stable deacceleration.

6.3 Phase Space Boundary and small Amplitude Oscillations

The limiting values in phase and energy for an assembly of particles traversing a given r.f. system can be determined using the Hamiltonian formalism.

The phase angle ϕ and the normalized energy

$$W = \frac{E}{\Omega_o} \qquad (6.25)$$

are used as conjugate variables. The Hamiltonian equations expressed in terms of these variables:

$$\frac{d\phi}{dt} = \frac{\partial H}{\partial t} = \frac{h\,\eta_o\Omega_o}{p_o\,R_o}W \qquad (6.26)$$

$$\frac{dW}{dt} = -\frac{\partial H}{\partial \phi} = \frac{e\hat{V}}{2\pi}(\sin\phi - \sin\phi_o) \qquad (6.27)$$

The equations above were obtained by inserting eqs. 6.17 and 6.22 into the Hamiltonian equations of motion.

The synchrotron motion is thus described by the following Hamiltonian:

$$H = \frac{h\,\eta_o\Omega_o}{2p_o\,R_o}W^2 + \frac{e\hat{V}}{2\pi}(\cos\phi - \cos\phi_o + (\phi-\phi_o)\sin\phi_o) \qquad (6.28)$$

The longitudinal motion of the particles are represented in the W-ϕ plane by trajectories of constant H. Note that the synchrotron motion repeat itself every 2π in phase, i.e. h times around the ring. Within each period of 2π the motion has two fix points given by $\dot{\phi} = \dot{W} = 0$. From eqs. 6.26 and 6.27 these fix points occur at:

$$W = 0\ ,\quad \phi = \phi_o \quad \text{or} \quad \phi = \pi - \phi_o \qquad (6.29)$$

The fix point $W = 0$ and $\phi = \phi_o$ are inside the stable region and correspond to the synchronous particle. The separatrix - i.e. the limiting curve which separates the stable and the unstable region passes through the second fix point at $W = 0$ and $\phi = \pi - \phi_o$. Note that the particle motion in ϕ and W becomes slow as particles approaches the fix point - i.e. the synchrotron frequency ω_s slows down as the particles approach the limit of stability.

The separatrix can be evaluated by inserting the coordinates of the unstable fix point into the Hamiltonian eq. 6.28. The maximum energy deviation is given by

$$(\hat{W})^2_{sep} = \frac{e\hat{V}p_o R_o}{\pi h \eta_o \Omega_o} \left((\pi - 2\phi_o) \sin\phi_o - 2\cos\phi_o \right) \qquad (6.30)$$

To obtain the extreme in phase we equate:

$$H = \frac{h\eta_o\Omega_o}{2p_o R_o} \hat{W}^2_{sep} = \frac{h\eta_o\Omega_o}{2p_o R_o} W^2 + \frac{e\hat{V}}{2\pi} (\cos\phi - \cos\phi_o + (\phi - \phi_o)\sin\phi_o) \qquad (6.31)$$

Substituting $\hat{W}^2_{sep}$ according to eq. 6.30 on the left hand side and introducing the coordinates ϕ_{max} and $W = 0$ on the right hand side of eq. 6.31 yield the following transcendental equation for the maximum phase:

$$(\pi - 2\phi_o) \sin\phi_o - 2\cos\phi_o = \cos\phi_{max} - \cos\phi_o + (\phi_{max} - \phi_o)\sin\phi_o \qquad (6.32)$$

The phase space trajectories for $\phi_o = 180^o$ and $\phi_o = 150^o$ are shown in Fig. 6.1. These trajectories correspond respectively to a stored

and an accelerated beam above the transition energy.

The amplitude of the longitudinal oscillation is determined by the initial conditions of the injected particle. Let us consider a particle which is injected at the correct r.f. phase $\phi = \phi_o$ but with a normalized energy deviation $\hat{W} = \frac{\Delta E}{\Omega_o}$. If $\hat{W}$, ϕ_o is within the separatrix then the particle will travel on a closed trajectory in ϕ,W space with a maximum energy deviation $\hat{W}$. The maximum excursion in phase can be evaluated from the Hamiltonian:

$$H(\phi,W) = \frac{h\eta_o\Omega_o}{2p_o R_o} \hat{W}^2 = \frac{h\eta_o\Omega_o}{2p_o R_o} W^2 + \frac{e\hat{V}}{2\pi} (\cos\phi - \cos\phi_o + (\phi - \phi_o)\sin\phi_o) \qquad (6.33)$$

Let us consider three special cases:

a) Storage of particles with energies below the transition energy. In this case $\phi_o = 0$ and the resulting value of ϕ_{max} is obtained from eq. 6.33 for $W = 0$

$$\left(\frac{h\eta_o\Omega_o}{2p_o R_o} \right) \hat{W}^2 = \frac{e\hat{V}}{2\pi} (\cos\phi_{max} - 1)$$

$$\phi_{max} = \pm 2 \arcsin \left(\frac{\pi h (-\eta_o) \Omega_o}{2p_o R_o e \hat{V}} \right)^{1/2} \hat{W} \qquad (6.34)$$

b) Storage of particles with energies above the transiton energy. In this case $\phi_o = \pi$ and ϕ_{max} is again obtained from eq. 6.32 with $W = 0$.

$$\phi_{max} = \pm \arccos \left(\frac{\pi h \eta_o \Omega_o}{2p_o R_o e \hat{V}} \right)^{1/2} \hat{W} \qquad (6.35)$$

c) A particle with $\gamma > \gamma_{tr}$ is accelerated and we consider small amplitude oscillations $\Delta\phi = \phi - \phi_o$. The Hamiltonian in eq. 6.33 can then be simplified to:

$$\frac{h\eta\Omega_o}{ep_oR_o}\,\tilde{W}^2 = \frac{h\eta_o\Omega_o}{2p_oR_o}\,W^2 - \frac{e\hat{V}}{2\pi}\left(\frac{\Delta\phi}{2}\right)^2\cos\phi_o \qquad (6.36)$$

The extreme amplitudes in phase for a particle with $W_{max} = W$ is given by

$$\Delta\phi = \pm\left[\frac{-2\pi h\,\eta\,\Omega_o}{e\,\hat{V}\,p_oR_o\cos\phi_o}\right]^{1/2}\hat{W}\,. \qquad (6.37)$$

6.4 Adiabatic Damping

The equation for the synchrotron oscillation was derived assuming time independent parameters for the synchronous particle. This is permitted since the timescale for an accelerating cycle is very long compared to the synchrotron oscillation period T_s. The change in W and ϕ during the accelerating cycle can be evaluated using the Bolzmann-Ehrenfest theorem. If a non-dissipative oscillatory system is described by the cannonical variables p and q, then, according to the Bolzmann-Ehrenfest theorem, these parameters will change during the cycle such that

$$I = \oint p\,dq = \text{constant.} \qquad (6.38)$$

where the integral extends over one period of oscillation.

We now use this theorem to investigate the time behaviour of W and ϕ for small amplitude oscillations.

$$I = \oint W\,d\phi = \oint W\frac{d\phi}{dt} = \left(W\frac{d\phi}{dt}\right)\frac{2\pi}{\omega_s} \qquad (6.39)$$

Replacing $\frac{d\phi}{dt}$ according to eq. 6.26 and ω_s according to eq. 6.23b yields:

$$I = W^2\left[\frac{-(2\pi)^2\,h\,\eta_o\Omega_o}{p_oR_o\,e\,\hat{V}\cos\phi_o}\right]^{1/2} \qquad (6.40)$$

The normalized energy makes sinusoidal oscillations. Averaged over one turn $W^2 = \frac{1}{2}\hat{W}^2$ where $\hat{W}$ is the peak amplitude. Then adiabatically $\hat{W}$ will change as:

$$\hat{W} \sim \left[\frac{-p_oR_o\,\hat{V}\cos\phi_o}{\eta_o\,\Omega_o}\right]^{1/4} \qquad (6.41)$$

i.e. $\hat{W}$ will grow proportional to $p_o^{1/4}$.

We can write down a similar equation for the phase oscillations:

$$I = \oint \Delta\phi\,dW = (\Delta\phi\,\frac{dW}{dt})\,\frac{2\pi}{\omega_s} \qquad (6.42)$$

Replacing $\frac{dW}{dt}$ according to eq. 6.27 and ω_s according to eq. 6.28b lead to

$$\hat{\Delta\phi} \sim \left[\frac{\eta_o\,\Omega_o}{p_oR_o\cos\phi_o}\right]^{1/4} \qquad (6.43)$$

Thus the maximum value of the pase amplitude $\hat{\Delta\phi}$ decreases with momentum as:

$$\hat{\Delta\phi} \sim p_o^{-1/4} \qquad (6.44)$$

Note that $W\,\Delta\phi$ is an invariant.

7. Effects of the Synchrotron Radiation on the Single Particle Motion [9]

7.1 Introduction

The instantaneous power P_γ radiated by a relativistic particle of energy E deflected in a magnetic field of induction B is given by:

$$P_\gamma = \frac{e^2 c^3}{2} C_\gamma E^2 B^2 \qquad (7.1)$$

where

$$C_\gamma = \frac{4}{3} \left(\frac{e^2}{mc^2} \right) \frac{1}{(mc^2)^2} .$$

The instantaneous radiated power is proportional to the product of beam energy and magnetic induction squared and inversely proportional to the fourth power of particle mass. For given values of E and B an electron will loose 10^{13} times more energy than a proton per turn. The motion of the protons is thus not influenced by synchrotron radiation at present energies and the equations discussed above remain valid. On the other hand the design of an electron machine is governed by synchrotron radiation and the single particle motion is strongly influenced by the emission of photons.

The average energy loss (eU_0) of an electron of energy E_0 moving on the design orbit is obtained by integrating P_γ over one turn.

$$(e\,U_0) = \frac{1}{2} \oint P_\gamma \, ds \qquad (7.2)$$

$$(e\,U_0) = \frac{C_\gamma E_0^4}{2\pi} \oint G^2(s) \, ds$$

For a seperate function machine with $G = \frac{1}{\rho_0}$ in the dipoles and zero elsewhere:

$$(e\,U_0) = \frac{88.5 \text{ keV } E_0^4 \text{ (GeV)}}{\rho_0 (m)} \qquad (7.3)$$

The synchrotron radiation is focused within a cone of opening angle $\frac{1}{2\gamma}$ along the direction of particle motion. The electrons do not radiate continously but emit discrete quanta with an energy distribution shown schematically in Fig. 7.1. A half of the total radiated power is

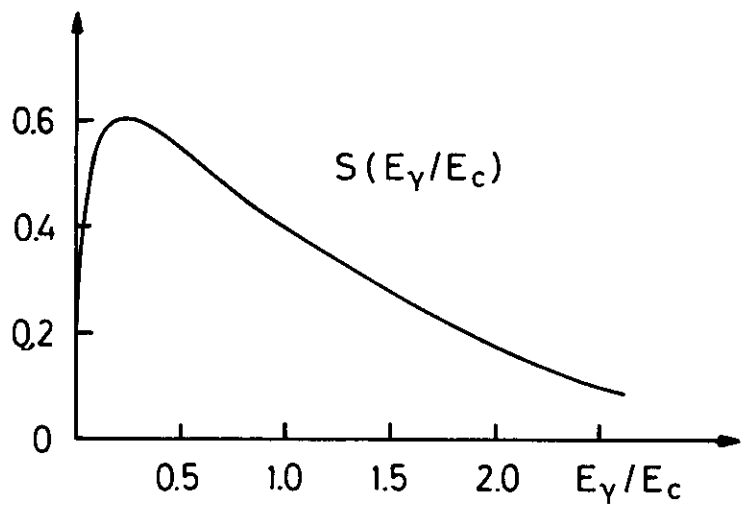

Fig. 7.1 - The energy distribution of the synchrotron radiation measured in units of the critical energy.

carried by photons with energies above the critical energy E_c:

$$E = \frac{2.23\ \text{keV}\ E_0^3\ (\text{GeV})}{\rho_0(\text{m})}$$

The mean photon energy is proportional to the critical energy

$$\langle E_\gamma \rangle = \frac{8}{15\sqrt{3}}\ E_c \qquad (7.5)$$

The average energy loss suffered by the electrons per turn must be replenished by the r.f. system. However, both the number and the energy of the emitted photons fluctuate from turn to turn and this represents a source of noise which excites oscillations.

Both the betatron oscillations and the synchrotron oscillation are damped by the average effects of the synchrotron radiation and excited by its quantum fluctuations. The final beam dimensions result from the equilibrium between the two effects.

The synchrotron radiation also governs the design of the technical components for HERA's electron ring.

The total power radiated by the beam is given by $P_b = (e\ U_0)\ n_e$. At 30 GeV the nominal current of 56 mA radiates a total power of 7.5 MW. This radiation will strike the outer walls of the vacuum chamber with a linear power density of max. 2.1 kW/m.

Furthermore a certain percentage of the photons will Compton scatter and to avoid radiation damage to equipment in the tunel the majority of these photons must be confined within the vacuum chamber, respectively with the magnet system. A photon striking the wall of the vacuum chamber will lead to gas desorption. In order to achieve the vacuum needed one must use either a distributed pumping system or closely spaced discrete pumps.

Below we will discuss the effects of the synchrotron radiation on the single particle motion. This discussion will follow the excellent account given by M.Sands in reference 9.

7.2 Radiative Damping

7.2.1 The longitudinal motion

The instantaneous power radiated by an off energy electron differs from that radiated by the synchronous electron since the particles have different energies and travel through different regions of the guide field. The average energy loss per turn (eU) for an off energy particle is given by:

$$eU = e\,U_0 + 0\,\Delta E \qquad (7.6)$$

where $0 = e(\frac{dU}{dE})_{E_0}$. The equation of synchrotron motion (eq. 6.20) must be modified to include the energy loss due to synchrotron radiation:

$$\frac{d}{dt}\left(\frac{\Delta E}{\Omega_0}\right) = \frac{e\,\hat{V}}{2\pi}\cos\phi_0\,\Delta\phi - 0\,\Delta E \qquad (7.7)$$

Combining eq. 7.7 with eq. 6.15 yields the phase oscillation equation in the presence of synchrotron radiation.

$$\frac{d^2\Delta\phi}{dt^2} + 2\alpha_\varepsilon \frac{d\Delta\phi}{dt} + \omega_s^2 \Delta\phi = 0 \qquad (7.8)$$

with $\alpha_\varepsilon = \frac{0}{2T_0}$.

For damping times $\tau_\varepsilon = \frac{1}{\alpha_\varepsilon}$ which are long compared to the revolution time eq. 7.8 has the solution.

$$\Delta\phi = A\, e^{-\alpha_\varepsilon \cdot t} \cos(\omega_s t) \qquad (7.9)$$

Thus, neglecting quantum fluctuations, the amplitude of the longitudinal oscillation decreases expeonentially with a time constant τ_ε.

α_ε can be expressed in terms of the lattice parameters. To this end we integrate the energy loss over one turn:

$$(e\,U) = \oint P_\gamma dt = \frac{1}{c} \oint P_\gamma \left(1 + \frac{x}{\rho}\right) ds \qquad (7.10)$$

Since we are interested in the energy loss of an off energy electron $x = D \frac{\Delta E}{E_0}$.

Differentiation of eq. 7.10 yields:

$$\left(\frac{e\,dU}{dE}\right)_{E=E_0} = \frac{1}{2} \oint \left(\frac{dP_\gamma}{dE} + \frac{D}{\rho} \frac{P_\gamma}{E_0}\right) ds \qquad (7.11)$$

The first term evaluated according to eq. 7.1 and with the substitution: $\frac{dB}{dE} = \frac{dB}{dx} \frac{dx}{dE} = \frac{D}{E_0} \frac{dB}{dx}$ yields:

$$\frac{dP_\gamma}{dE} = 2 \frac{P_\gamma}{E_0} + 2 \frac{DP_\gamma}{E_0 B_0} \frac{dB}{dx} \qquad (7.12)$$

Eq. 7.11 is written as:

$$\frac{edU}{dE} = \frac{e\,U_0}{E_0} (2 + \Delta J) \qquad (7.13)$$

with

$$\Delta J = \frac{1}{c\,U_0} \oint \left(DP_\gamma \left(\frac{1}{\rho} + \frac{2}{B_0} \frac{dB}{dx}\right)\right) ds \qquad (7.14)$$

The expression for ΔJ can be simplified using eq. 7.2 and the definition $K_1(s) = \frac{1}{B_\rho} \left(\frac{dB}{dx}\right)$

$$\Delta J = \frac{\oint D(s)\,G(s)\,(G^2(s) + 2K_1(s))\,ds}{\oint G^2(s)\,ds} \qquad (7.15)$$

Eq. 7.15 evaluated for a separate function machine yields

$$\Delta J = \frac{1}{2\pi} G_0^2 \int_{\text{magnets}} D(s)\,ds = \frac{\alpha R}{\rho_0} \qquad (7.16)$$

where R is the average machine radius. Note that for a separate function machine ΔJ is small whereas it is large for a combined function machine,i.e. an accelerator satisfying $G(s)\,K(s) \neq 0$.

The inverse damping time α_ε - evaluated for a separate function machine - is given by:

$$\alpha_\varepsilon = \frac{e\,U_0}{2E_0 T_0} \left(2 + \frac{\alpha R}{\rho_0}\right) \approx \frac{e\,U_0}{E_0 T_0} \qquad (7.17)$$

The characteristic damping time for longitudinal oscillations is simply the time it takes the electron to radiate away all its energy. Evaluated for the electron ring of HERA gives $\frac{1}{\alpha_\varepsilon} = 4.5$ msec at 30 GeV. Note that the damping time is inversely proportional to E_0^3.

7.2.2 The vertical betatron oscillations

The radiative damping mechanism for the vertical betatron motion is illustrated in Fig. 7.2. The electron emitts a photon along its direction of motion - i.e. the electron suffers only a loss of energy without a change of position or slope. However, in traversing the r.f. cavities the electron receives a longitudinal kick compensating the average energy loss - i.e. $\Delta E = e\,U_0$. Thus the slope of the particle is slightly reduced after traversing the cavity:

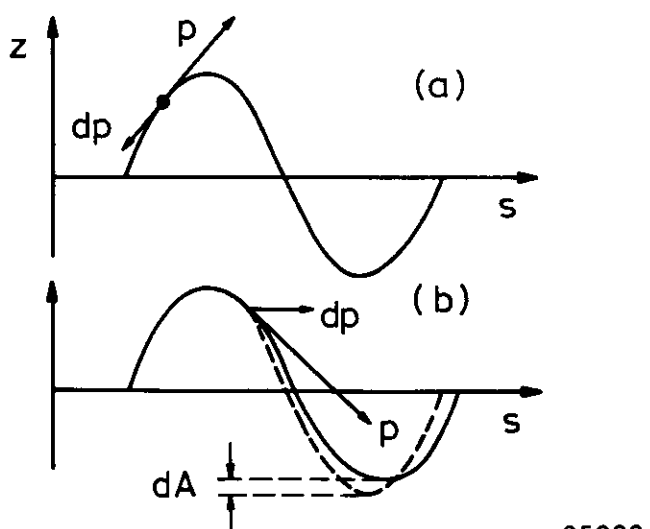

Fig. 7.2 - The vertical motion of a particle in the arcs (a) and in the r.f. cavities (b).

$$z' + dz' = \frac{p}{p_0 + \delta p} = z'\,(1 - \frac{\delta p}{p_0}) \qquad (7.18)$$

$$dz' \approx -z'\,\frac{dE}{E_0} = -z'\,(\frac{e\,U_0}{E_0})$$

The position z and the slope z' of the electron is given by

$$z = A\cos\mu \quad \text{respectively} \quad z' = \frac{A}{\beta}\sin\mu. \qquad (7.19)$$

The amplitude A can be written as:

$$A^2 = z^2 + (\beta z')^2 \qquad (7.20)$$

The change in amplitude caused by the energy loss due to synchrotron radiation and its replenishment by the r.f. cavities is given by:

$$AdA = -\beta^2 z'\,dz' = -(\beta z')^2\,(\frac{e\,U_0}{E_0}) \qquad (7.21)$$

The electron emits photons with equal probability along the orbit. Averaging $\beta z'$ over all phase angles μ yields:

$$\langle \beta z' \rangle^2 = \frac{A^2}{2} \qquad (7.22)$$

Inserting eq. 7.22 into eq. 7.21 and integrating over t yields

$$A = A_0\,e^{-\alpha_z t} \qquad (7.23)$$

with $\alpha_z = \dfrac{(eU_0)}{2E_0T_0}$.

The amplitude of the transverse motion is thus exponentially damped with a damping time twice the longitudinal damping time.

7.2.3 Damping of the radial betatron motion

The damping mechanism outlined above is also effective for the radial betatron motion. However, the photon is radiated in a region

with radial dispersion and this yields a term which is antidamping. The basic mechanism is outlined in Fig. 7.3. The total radial diplacement is a sum of the closed orbit displacement x_ε and the betatron displacement with respect to this closed orbit

$$x = x_\beta + x_\varepsilon \tag{7.24}$$

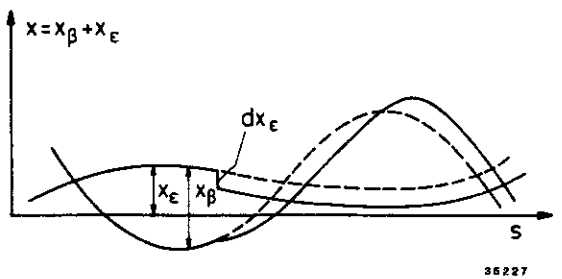

Fig. 7.3 - Radial amplitude growth due to the emission of synchrotron radiation at a position with dispersion.

When the electron radiates a photon the closed orbit will suddenly jump by $dx_\varepsilon = D\frac{dE}{E_o}$. However, the spatial position of the electron remains unchanged such that a change in the closed orbit must be compensated by a change in betatron amplitude:

$$dx_\beta = -D\frac{dE}{E_o} \tag{7.25}$$

The change in slope due to D' is neglected.

The radial position and slope of the electron can be written as:

$$x_\beta = A\cos\mu,\ x'_\beta = \frac{A}{\beta}\sin\mu\ . \tag{7.26}$$

This yields:

$$AdA = x_\beta\, dx_\beta = -D\, x_\beta \frac{dE}{E_o} \tag{7.27}$$

The energy loss in a path length $d\ell$ is given by:

$$dE = -\frac{P_\gamma}{c}d\ell = -\left(1+\frac{x_\gamma}{\rho_o}\right)\frac{P_\gamma}{c}ds \tag{7.28}$$

The resulting change in amplitude

$$AdA = D\, x_\beta \left(1+\frac{x_\beta}{\rho_o}\right)\frac{P_\gamma}{c}\frac{ds}{E_o} \tag{7.29}$$

The expectation value of dA is obtained by averaging eq. 7.29 over all phase angles

$$\frac{\langle dA\rangle}{A} = \frac{D}{2\rho_o}\frac{P_\gamma}{E_o}\frac{ds}{c} \tag{7.30}$$

For a separate function machine, $e\,U_o$, the total energy loss per turn, is equal to $P_\gamma\frac{ds}{c}$ summed over all the dipole magnets. The resulting change in the amplitude is

$$\frac{dA}{A} = \frac{\langle D\rangle}{2\rho_o}\frac{e\,U_o}{E_o} \tag{7.31}$$

Thus the finite dispersion leads to an exponentially growing radial amplitude with a time constant given by:

$$\frac{\langle D \rangle}{\rho_o} \frac{e\,U_o}{2E_oT_o} \tag{7.32}$$

The total change in amplitude is simply the sum of the dispersion effect and the r.f. acceleration effect derived in chapter 7.2.2.

$$\frac{1}{A}\frac{dA}{dt} = \alpha_x = -\left(1 - \frac{\langle D \rangle}{\rho_o}\right)\frac{e\,U_o}{2E_oT_o} \tag{7.33}$$

Substituting $\langle D \rangle = \alpha R$ and comparing with eq. 7.16 yields:

$$\alpha_x = -(1 - \Delta J)\frac{U_o}{2E_oT_o} \tag{7.34}$$

For a separate function machine ΔJ is less than one and the radial motion is damped.

7.2.4 Robinson's Theorem

We have evaluated the damping times for all three degrees of freedom. The damping coefficients can be written as:

$$\alpha_i = J_i \frac{\langle P_\gamma \rangle}{2E_o} = J_i \frac{e\,U_o}{2E_oT_o} \tag{7.35}$$

with $J_x = 1 - \Delta J$, $J_z = 1$ and $J_\varepsilon = 2 + \Delta J$.

Note that the sum of the damping partition number is a constant:

$$\Sigma\, J_i = 4 \tag{7.36}$$

This has been shown by Robinson[33] to be true on general grounds as long as effects of the fields induced by the circulating electron beams can be neglected. ΔJ is a property of the detailed layout of the

ring. Note that for a separate function machine $\Delta J << 1$ leading to damping in all three degrees of freedom. In a combined function machine ΔJ will be larger than one causing the radial beam size to grow exponentially.

7.3 Radiation excitation and beam dimensions

In the preceeding section we have shown that the single particle motion is damped by the interplay between the average energy loss due to synchrotron radiation and its replenishment by the r.f. system. However, the emission of synchrotron radiation is a quantum process - the radiation is emitted in discrete quanta and both the energy and the number of the photons fluctuate. These fluctuations are a source of noise and excite single particle oscillations. The final beam dimensions result from the equilibrium between the damping caused by the average energy loss and the noise introduced by its fluctuations.

The electrons in a r.f. bucket of width ΔE have a Gaußian energy distribution with a rms value of

$$\sigma_\varepsilon = \left(\frac{C_q}{\rho J_E}\right)^{1/2} \frac{E^2}{m_oc^2} \tag{7.37}$$

with $C_q = \frac{55\,\hbar}{32\sqrt{3}\,mc} = 3.84\ 10^{-13}$ cm.

This results in a rms bunch length:

$$\sigma_\ell = \left(\frac{R\,\alpha\,\Omega_o}{\omega_s}\right)\frac{\sigma_E}{E} \tag{7.38}$$

Thus the bunch length of the electron beam is rather short, the rms bunch length in HERA is of the order of a cm at 30 GeV and

scales with energy and tune as $\sigma_\ell \sim E/Q$.

The final emittance is the equilibrium between the damping caused by the r.f. system, compensating the average radiation loss and the growth caused by the quantum fluctuations.

$$\varepsilon_x = \left(\frac{J_\varepsilon}{J_x}\right)\left(\frac{\sigma_\varepsilon}{E}\right)^2\left(\frac{\langle D_x\rangle}{\langle\beta_x\rangle}\right) \approx \left(\frac{J_\varepsilon}{J_x}\right)\left(\frac{\sigma_E}{E}\right)^2\left(\frac{R_{arc}}{8Q_{arc}^3}\right)\frac{\mu^3}{tg\left(\frac{\mu}{2}\right)\sin^2\left(\frac{\mu}{2}\right)} \qquad (7.39)$$

R_{arc} is the average radius in the arcs and Q_{arc} is the contribution to the tune from the arcs. Note that the factor

$$\frac{\mu^3}{tg\left(\frac{\mu}{2}\right)\sin^2\left(\frac{\mu}{2}\right)}$$

is 8 at $\mu_0 = 0$ and varies little with the phase advance μ for μ less than 90^0 per cell.

The emittance of an electron beam is not a constant of motion but varies with the tune. Strong focusing, i.e. short cell length and large phase advance per cell will lead to a small radial emittance.

Since the vertical dispersion is rather small the vertical emittance is mainly due to the coupling of vertical and radial motion. In general the coupling may be as small as a few percent for a well aligned machine.

This results in a ribbon type beam for the electrons as compared to a round proton beam. However, it is of course in principle possible to deliberately increase the coupling between the radial and the vertical motion by installing skewed quadrupoles.

8. Polarisation [34]

The importance of colliding electrons or positrons of well defined helicity with protons is discussed in section 2.

Beams with a high degree of polarisation has been observed[35] at PETRA and the beams have been collided without destroying the initial polarisation. Scaling from these results it seems reasonable to expect transversely polarized $e^{\pm}$ beams in HERA.

8.1 Transverse polarisation

The spin of electrons (positrons) injected into an accelerator will align along the direction of its vertical guide field. The spin sum along the vertical direction is zero for an unpolarized beam, i.e. there is the same number of electrons with spin pointing upwards as downwards. As the electrons are deflected in the magnetic guide field they emit synchrotron radiation which in part is due to a spin flip transition. The probability of magnetic dipole emission depends on the orientation of the initial spin. These probabilities are given by:

$$\begin{aligned} W(\uparrow\downarrow) &= \frac{5\sqrt{3}}{16}\frac{e^2\gamma^5\hbar}{m^2c^2\rho^3}\left(1+\frac{8}{5\sqrt{3}}\right) \\ W(\downarrow\downarrow) &= \frac{5\sqrt{3}}{16}\frac{e^2\gamma^5\hbar}{m^2c^2\rho^3}\left(1-\frac{8}{5\sqrt{3}}\right) \end{aligned} \qquad (8.1)$$

where the arrows $(\uparrow\downarrow)$ indicate the initial and the final spin directions either parallel or antiparallel to the direction of the magnetic induction. The circulating beam will gradually become polarized with

the spins aligned antiparallel to direction of the guide field. The beam polarisation builds up exponentially:

$$P(t) = P_0 (1 - e^{-t/\tau_\rho}) \qquad (8.2)$$

In the absence of populations effects P_0, the maximum degree of polarisation, is given by:

$$P_0 = \frac{n(\downarrow) - n(\uparrow)}{n(\downarrow) + n(\uparrow)} \qquad (8.3)$$

where the final polarisation $n(\downarrow)$ and $n(\uparrow)$ are determined by detailed balance:

$$n(\uparrow)\, W(\uparrow\downarrow) = n(\downarrow)\, W(\downarrow\uparrow) \qquad (8.4)$$

Combining eqs. 8.3 and 8.4 yields:

$$P_0 = \frac{W(\uparrow\downarrow) - W(\downarrow\uparrow)}{W(\uparrow\downarrow) + W(\downarrow\uparrow)} = \frac{8}{5\sqrt{3}} = 0.92 \qquad (8.5)$$

τ_p, the build up time of polarisation is given by

$$\tau_p = (W(\uparrow\downarrow) + W(\downarrow\uparrow))^{-1} \qquad (8.6a)$$

Using eq. 8.1 and inserting the numerical values yields:

$$\tau_p = \frac{98(s)\, \rho^2(m)\, R(m)}{E^5(GeV)} \qquad (8.86b)$$

where ρ is the bending and R the average radius of the machine.

The requirement that τ_p must be short compared to the storage time of several hrs determines the minimum electron energy. The polarisation time for a 30 GeV electron beam in HERA is of about 20 min.

Bargman, Michel and Telegdi [36] have written down the general equation

for spin motion in electric and magnetic fields. For the spin motion in a circular accelerator this expression can be simplified to:

$$\frac{d\vec{n}}{ds} = -\left(\frac{e\, B_0}{m\, c^2}\right)\left(a + \frac{1}{\gamma}\right) \hat{z} \times \vec{n}$$

The coordinate system, moves with the beam. $\vec{n}$ is the direction of the spin in space and B_0 is pointing along the vertical direction $\hat{z}$ and $a = \frac{(g-2)}{2} = 0.0011597$.

It follows immediately from eq. 8.7 that the spin component along the $\hat{z}$ direction is conserved whereas the radial spin component S_x or the spin component directed along the direction of particle motion S_s precesses an angle

$$\frac{e\, B_0}{m\, c^2}\, a\, 2\pi\, \rho = 2\pi\, \gamma a \text{ per turn} \qquad (8.8)$$

$$= (2\pi)\, \frac{E}{0.44065}$$

The electrons in a bunch have different energies corresponding to different precision frequencies γa. This destroys the polarisation along the $\hat{x}$ and the $\hat{s}$ direction.

The radiative polarisation generates a vertical spin alignment in the arcs while the experiments require a longitudinal polarisation at the interaction point, preferable with the option to change from one helicity to the other. A possible spin rotator is be discussed in chapter 10.

8.2 Depolarisation Mechanisms[34,37]

The discussion above is valid for an ideal machine. The guide field of a real machine, however, is not perfect and these imperfections may depolarize the beam.

If the beams are polarized along the vertical direction then errors in the vertical field will not affect the spin. The particles must still turn 2π and their spin precess by $2\pi a\gamma$.

A non vanishing radial field, however, will cause the electron spin to precess around the $\bar{x}$ axis leading to depolarisation. Let us assume that a quadrupole is misaligned by 1 mm in the vertical direction. Using HERA parameters this corresponds to a vertical deflection:

$$\Delta\theta = \frac{(\Delta B_x \ell)}{B\rho} = \frac{12.5\ \text{T/m}\ (10^{-3}\ \text{m})\ 1\text{m}}{3.33 \cdot 30} = 0.125\ \text{mrad}$$

equivalent to a precision angle ϕ_x:

$$\phi_x = (a\,\gamma)\,\Delta\theta = 8.6\ \text{mrad at 30 GeV.}$$

This is a rather small angle, however, if $a\gamma = n$ = integer then the effect add on successive turns leading to complete depolarization. The depolarizing resonances $\gamma a = n$ are spaced 440 MeV apart and the beam energy must be choosen such that the spin tune does not equal an integer number. However, the electrons have a finite energy spread with a rms width σ_ε growing proportional to E^2. At 27.5 GeV at HERA the computed energy spread is 28 MeV - i.e. the spacing between adjacent resonance is 16 σ_ε and this should be sufficient. Note that this effect may make it difficult to achieve transverse polarisation in larger machines like LEP.

The spin motion is also modulated by the synchrotron and betatron motion such that the general resonance condition can be written as:

$$\gamma a \pm k_x Q_x \pm k_z Q_z \pm k_s Q_s = n. \qquad (8.9)$$

where k and n are integers and $Q_{x,z,s}$ the tune shifts.

The importance of these side band resonances will be enhanced by the synchrotron radiation. To illustrate the effect let us consider a planar machine. The electron emits a photon at a position of non-vanishing vertical dispersion. The vertical closed orbit will jump and the particle starts to make vertical oscillations which takes it through regions of space with non vanishing radial field components. The spin will thus precess around the radial axis away from the vertical spin direction. The vertical oscillations damps out after a few msec but the spin is now pointing in a different direction. The polarising mechanism will restore the original spin direction with a time constant τ_p. However, since the electron radiates some 10^{11} times during one damping time τ_p the spin will gradually diffuse away from the vertical axis leading to an unpolarized beam.

The crucial quantity which determins the spin diffusion is the so called spin diffusion coefficient or spin chromaticity:

$$\vec{d} = \gamma \left(\frac{\partial \vec{n}}{\partial \gamma} \right) \frac{\delta E}{E} \qquad (8.10)$$

The spin rotators, unless very carefully designed and matched into the lattice, will be strong sources of beam depolarisation.

In the linear approximation, prescriptions[38] exist how to design a machine, including spin rotators, such that the spin dispersion is zero. The beam-beam interaction will also cause depolarisation and this effect is now being evaluated using spin tracking programs.

9. Current Limitations [39]

The motion of a single particle is determined by the guide field, but particles moving within an assembley of particles will experience additional forces resulting from:

- The repulsion of like sign particles moving together. In this case the electric and magnetic force subtract resulting in a space charge force which decreases inversely proportional to the energy of the particle squared. For particles moving in opposite directions the forces add and the resulting beam-beam instability is the ultimate performance limit of a colliding beam machine.

- Electric and magnetic fields associated with longitudinal and transverse oscillations of the particles interact with the surroundings (beam pipe, cavities) and induce electro-magnetic fields which in turn may act back on the beam. The resulting force can drive the beam unstable if the phase of the induced force is ahead of the oscillation and its strength is large enough to overcome the natural damping caused by the incoherence of the particle motion. If the induced fields decay rapidly then only the bunch itself is affected and we have a single bunch instability. However adjacent bunches may communicate by means of slowly decaying wake fields causing collective bunch instabilities.

In this chapter we will discuss some of the instabilities which can affect a bunched proton beam. The electron motion is in general more stable due to the strong radiative damping.

9.1. Longitudinal Instabilities

9.1.1 Introduction

As discussed below, it seems advantageous to cross the electron and the proton beam at a finite angle. The electron bunch, due to its radiative damping, is much shorter than the proton bunch and the luminosity is therefore directly proportional to the linear charge density of the protons $e\lambda(s)$ - i.e. short, intense proton bunches are needed to reach high luminosity. The longitudinal electron distribution can be approximated by a Gaußian whereas the proton line density is well represented by a parabolic function

$$\lambda(s) = \frac{6N_b}{\ell^3}\left(\frac{\ell^2}{4} - s^2\right) \qquad (9.1)$$

where ℓ is the bunch length measured at the base.

The luminosity is also directly proportional to the number of proton bunches - i.e. we would like to store a larger number of bunches in HERA.

The combination of a high line density and a large number of bunches make HERA prone to instabilities.

Let us first consider the situation shown in Fig. 9.1. A continous particle beam of radius a moves along the $\vec{s}$ direction with velocity $\vec{\beta}c$ in the center of circular beam pipe of radius b. A varying longitudinal particle density gives rise to a longitudinal space charge force and to longitudinal wake fields produced by currents induced in the walls of the beam pipe. The sum of both

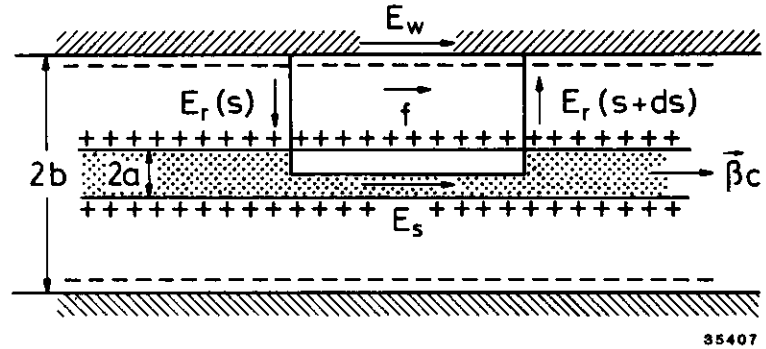

Fig. 9.1 - A uniform beam of radius a moving with β^*c along the $\vec{s}$ direction in the center of a circular beam pipe of radius b.

effects produces a longitudinal voltage which acts on the beam. We will now evaluate these effects.

The electric and the magnetic fields produced by moving charges can easily be obtained by solving Maxwell's equations.

$$\epsilon_0 \operatorname{div} \vec{E} = \rho(s) \tag{9.2a}$$

$$\frac{1}{\mu_0} \operatorname{rot} \vec{B} = \rho(s)\ (\vec{\beta} c) \tag{9.2b}$$

with $\rho = \frac{e\lambda(s)}{\pi a^2}$.

The line density $\lambda(s)$ is assumed to vary slowly as a function of s. Maxwell's equations have then the solutions:

$$E_r = \frac{e\,\lambda}{2\pi\epsilon_0}\,\frac{r}{a^2}\ ;\ B_\theta = \frac{\mu_0\, e\,\lambda\,\beta c}{2\pi}\,\frac{r}{a^2} \qquad r \le a \tag{9.3a}$$

$$E_r = \frac{e\,\lambda}{2\pi\epsilon_0}\,\frac{1}{r}\ ;\ B_\theta = \frac{\mu_0\, e\,\lambda\,\beta c}{2\pi}\,\frac{1}{r} \qquad r \ge a \tag{9.3b}$$

The longitudinal field at the center of the beam can then be determined from the relationship:

$$\oint \vec{E}\,\vec{d\ell} = -\frac{\partial}{\partial t} \int \vec{B}\,\vec{dt} \tag{9.4}$$

The integration path $\vec{\ell}$ and the enclosed area $\vec{f}$ are defined in Fig. 9.1.

Inserting the fields from eqs. 9.3a, b into eq. 9.4 and evaluating the integrals gives the following relation for the longitudinal field E_s at the center of the beam:

$$E_s = \frac{e\, g_0}{4\pi\epsilon_0}\,(1 - \beta^{*2})\,\frac{\partial\lambda}{\partial s} + E_w \tag{9.5}$$

The constant g_0 is defined as $g_0 = (1 + 2 \ln \frac{b}{a})$ and E_w is the electric field on the axis resulting from induced wall currents.

In general the particle density fluctuates over distances which are large compared to the diameter of the beam pipe. In this case the beam sees an inductive resistance:

$$E_w = -\frac{L}{2\pi R}\,\frac{dI_w}{dt} = \frac{e\,\beta^{+2}\,c^2\,L}{2\pi\,R}\,\frac{\partial\lambda}{\partial s} \tag{9.6}$$

L is the total inductance seen by the beam per turn.

The total axial electric field resulting from space charge and inductance is given by:

$$E_s = -e\left(\frac{g_0}{4\pi\,\epsilon_0\,\gamma^2} - \frac{\beta^2\,c^2\,L}{2\pi\,R}\right)\frac{\partial\lambda}{\partial s} \tag{9.7}$$

The total voltage seen by the particle per turn

$$U_s = -R\left(\frac{g_0\,Z_0}{2\beta\gamma^2} - \Omega_0\,L\right)\frac{\partial\lambda}{\partial s} \tag{9.8}$$

$Z_0 = \frac{\mu_0}{\epsilon_0} = 377$ Ohms and Ω_0 is the angular revolution frequency. Note that only the inductive term remains at large values of γ.

The fluctuations must be of the form:

$$\Lambda = \Lambda_0 + \Lambda_1\, e^{i(n\theta - \omega t)} \tag{9.9}$$

or

$$I = I_0 + I_1\, e^{i(n\theta - \omega t)}$$

for an instability to occur. Furthermore the angular frequency of the disturbance ω must be an integer multiple of the angular revolution frequency Ω_o, i.e. $\omega = n\Omega_o$. A density fluctuation of this form leads to an effective voltage per turn:

$$U_s = -i\, Z_i\, I_1\, e^{i(n\theta - \omega t)} \qquad (9.10)$$

In the case considered above the resistance is purely imaginary with

$$Z_i = R\left(\frac{n\, g_o\, Z^o}{2\beta\, \gamma^2} - \omega L\right) \qquad (9.11)$$

In general Z_i will have both a real and an imaginary part:

$$Z = Z_r + i\, Z_i \qquad (9.12)$$

The interaction between the beam and the environment shifts the frequency of the disturbance by $\Delta\omega$. Note that instabilities can only occur for certain values of $\omega = n\,\Omega_o + \Delta\omega$. The frequency shift for a general impedance Z is complex;

$$\Delta\omega = \Delta\omega_r + i\Delta\omega_i \qquad (9.13)$$

Substitute eq. 9.13 into eq. 9.9 yields:

$$I = I_o + I_1\, e^{\Delta\omega_i}\, e^{i(n\theta - (n\Omega_o + \Delta\omega_r)\, t)} \qquad (9.14)$$

An imaginary frequency shift leads to exponentially growing or decaying oscillations with a time constant $\frac{1}{\Delta\omega_i}$. Depending on initial conditions (noise etc) one or both of these solutions may be realized - i.e. the beam is unstable.

The reactive impedance $Z = i\, Z_i$ considered above yields:

$$(\Delta\omega)^2 = \frac{e\eta\Omega_o^2\, n\, I_o\, Z_i}{2\pi\, \beta^2\, E} \qquad (9.15)$$

with Z_i given by eq. 9.11.

An inspection of eq. 9.7 shows that an inductive impedance drives the beam unstable at energies below the transition energy, however, the beam is stable above the transition energy. The situation is reversed for a capacitive resistance, stable particles motion below and unstable particles motion above the transition energy. A resistive impedance always drives the beam unstable.

If all the particles in the beam have the same energy, as in the case considered above, then they remain in phase and even a minute disturbance is sufficient to cause an exponentially growing amplitude. This is no longer true if the particles in the beam have a finite energy spread. In this case the particles have different revolution frequencies and only act coherently over a time interval which is inversely proportional to the spread in revolution frequencies. As long as the frequency shift of the disturbance is smaller than the spread in revolution frequencies energy can be transferred from the instability and converted into incoherent motion. Thus the unstable motion is damped and the disturbance must exceed a certain threshold before the particle motion becomes unstable. This general mechanism is called Landau damping.

In the case of a bunched beam the damping is caused by the spread in phase oscillation frequencies S resulting from non linearities in the r.f. potential. For a bunch which is somewhat smaller than the r.f. bucket:

$$S \propto \frac{\omega_s}{16} \phi_{RF} \qquad (9.16)$$

ϕ_{RF} is the bunch length measured in RF phase angle.

The particle motion will be stable as long as:

$$S > 4\Delta\omega_i \qquad (9.17)$$

We will discuss some of the instabilities which may occur for a bunched beam in more detail.

9.1.2 The microwave instability (turbulence)

This instability involves high frequencies corresponding to wave lengths which are short compared to the bunch length and in this case the theory developed for a continous beam may be applied. Above threshold the momentum spread and the bunch length are blown up to values which are large compared to the equilibrium values determined by the r.f. parameters and the injected bucket area.

To avoid this instability the longitudinal impedance Z divided by the mode number $n = \frac{\omega}{\Omega_0}$ must satisfy the condition

$$\left|\frac{Z}{n}\right| < \frac{3 F (m_p c^2) \gamma |\eta|}{e I_0} \left(\frac{\Delta p}{p}\right)^2 \qquad (9.18)$$

For a parabolic current distribution $F \sim 0.65$. It is clear that the beampipe must be designed to minimize Z. At the SPS $\frac{Z}{n}$ is around 30Ω and we should be able to do better at HERA. Note that I_0 is the peak current i.e. about 60 amp in HERA at 820 GeV and a parabolic

current distribution. The HERA parameters demand $|\frac{Z}{n}| < 60\Omega$ at the peak energy of 820 GeV and $|\frac{Z}{n}| < 10\Omega$ at injection energy of 40 GeV to avoid this instability.

9.1.3 The inductive wall impedance

The reactive impedance seen by a bunched beam will in general be inductiv for low and medium frequencies. As shown in Fig. 9.1, the induced voltage U_s, will distort the circumferential r.f. voltage seen by the particle and hence affect the particle motion within the bunch. In particular, the induced voltage U_s will shift the incoherent phase oscillation frequency and change the bunch length. The incoherent frequency shift, for a parabolic line density distribution is given by:

$$\frac{\Delta\omega_s}{\omega_s} = \frac{3 I_0 (\Omega_0 L)}{2\pi^2 h M V \cos\phi_0} \left(\frac{2\pi R}{\ell}\right)^3 \qquad (9.19)$$

I_0 is the total current, L the inductance integrated around the ring, Ω_0 the revolution frequency i.e.

$$\Omega_0 L = \left(\frac{Z}{n}\right)_{ind},$$

h is the harmonic number, M is the number of bunches and R is the geometric radius.

The frequency shift will reduce the Landau damping - indeed the Landau damping disappears completely if the incoherent frequency distribution is shifted so far that this is outside the frequency of the disturbance. Note that the frequency shift is inversely proportional to the third power of the bunch length - i.e. the beam

can be stabilized by an increase in bunch length and a corresponding reduction in luminosity.

The bunch length is increased above the transition energy and decreased below. For protons

$$\frac{\Delta \ell}{\ell} = -\frac{1}{2}\,\frac{\Delta\omega_s}{\omega_s} \qquad (9.20)$$

The inductive impedance $|\frac{Z}{n}|_{ind}$ depends strongly on the detailed layout of the vacuum chamber and the cavities. At the ISR $|\frac{Z}{n}|_{ind} \simeq 20$ ohms was measured, at the SPS $|\frac{Z}{n}|_{ind} \approx 10$ ohms. At the peak energy of 820 GeV the estimated frequency shift in HERA is

$\frac{\Delta\omega_s}{\omega_s} = -0.04$ with an accelerating peak voltage of 100 MV and

$|\frac{Z}{n}|_{ind} = 10$ ohms.

Coupled bunch mode instabilities

A single bunch may execute different types of oscillations characterized by a mode number m - i.e. a dipole mode with frequency ω_s, a quadrupole mode with frequency $2\omega_s$, a sextupole mode with frequency $3\omega_s$ and so on. These modes are in general excited by narrow band, high Q resonators like the cavities. However, if several equidistant bunches are stored along the circumference of the machine, then these bunches may be coupled together by broad band, low Q resonators and execute additional coupled mode oscillations. The number of independent oscillation modes are equal to the numbers of bunches.

The strength of these instabilities are difficult to estimate, however, several methods are available to stabilize the beam.

a) Identify and damp the resonator which couples the bunches.

b) Increase the Landau damping either by a blow up of the bunch area ($S = \frac{\omega_s \phi_o^2}{16}$) or by operating a cavity at a harmonic of the r.f. frequency.

c) Decouple the bunch by using a cavity which operates on a sub-harmonic of the r.f. frequency. In this case different bunches have different synchrotron frequencies.

d) Use a feed back system.

9.2 RF Noise

The r.f. system contains a white noise spectrum. The part of the noise spectrum with frequencies around $n\,\omega_s$ - where n is an integer - will lead to a slow build up the rms phase oscillation amplitudes - i.e. to a dilution of longitudinal phase space density. This effect has been sucessfully compensated at the SPS collider using a very low noise feed back system.

9.3 Transverse instabilities

9.3.1 Transverse space charge effects

As discussed in chapter 4 the transverse motion of a single particle in the guide field of a circular accelerator is described by the solution to Hill's euqation:

$$u''(s) + K_0(s)\, u(s) = 0 \qquad (4.25)$$

This equation is valid for both the radial (x) and the vertical (z) motion provided $\Delta p = 0$.

The space charge force acting between non relativistic particles moving together will modify the focusing strength

$$K(s) = K_0(s) + \delta K . \qquad (9.21)$$

From eq. 5.34 a gradient change δK will lead to a spread in tune values:

$$\Delta Q = - \frac{\delta K\, \beta\, (2\pi R)}{4\pi} \qquad (5.34)$$

To avoid beam losses resulting from crossing a half integer resonances:

$$\Delta Q \lesssim 0.25 .$$

We will now estimate the limit on the current imposed by the space charge force. To this purpose we assume a uniform beam of radius a moving along the positive s direction with a uniform velocity $\vec{\beta c}$ as considered above.

The electric and the magnetic fields for $r \leq a$ produced by the moving charges are given by eq. 9.3a.
The resulting force on a particle travelling a distance x from the center of the beam is given by

$$F = e\,(\vec{E} + \vec{v} \times \vec{B})$$
$$F_r = \left(\frac{e\,\rho}{2\varepsilon_0} \right) \frac{r}{\gamma^2} \qquad (9.22)$$

i.e. the space charge force has only a radial component which disappears at relativistic energies.

The force is equivalent to an acceleration:

$$(m_0\gamma) \left(\frac{d^2x}{dt^2} \right) = (m_0\gamma)\, (\beta c)^2 \frac{d^2x}{ds^2} = \frac{e\,\rho}{2\varepsilon_0} \frac{x}{\gamma^2} \qquad (9.23)$$

The particle density $\frac{\rho}{e}$ can be expressed by the total number of particles stored along the circumference $2\pi R$ of the ring:

$$\frac{\rho}{e} = \frac{N}{(2\pi R)\, \pi a^2} \qquad (9.24)$$

This leads to the equation:

$$\delta\left(\frac{d^2x}{ds^2} \right) = r_0 \frac{N}{R\pi a^2} \frac{1}{\beta^2\gamma^3} x \qquad (9.25)$$

From a comparison with eq. 4.25 we see that the total change is focusing power per turn is given by

$$\delta K = - \frac{r_0 N}{\pi\, a^2 \beta^2 \gamma^3 R} \qquad (9,26)$$

The corresponding tune shift is obtained by combining eq. 9.26 with eq. 5.34:

$$\Delta Q = - \frac{r_0 N}{2\pi\, a^2 \beta^2 \gamma^3} \beta = \frac{r_0 N}{2\pi a^2 \beta^2 \gamma^3} \frac{R}{Q} \qquad (9.27)$$

Thus the beam is stable if:

$$N \leq \frac{2Q|\Delta Q|(\pi a^2)\, \beta^2 \gamma^3}{r_0 R} \qquad (9.28)$$

The space charge limits the amount of current which can be stored in a machine with a aperture (πa^2). This is the basic limitation at low energies.

9.3.2 Transverse head tail instability

This instability, first observed at ADONE, was explained by Pellegrini and Sands as due to the following mechanism: The particles moving in the head of a bunch makes betatron oscillations which induce strong, rapidly decaying transverse electromagnetic fields. These fields will interact with the particles in the tail of the bunch and will increase their betatron oscillations. After half a synchrotron oscillation period the particles in the head and the particles in the tail have changed place and the feed back loop is now closed if the betatron phase of the particles in the new head is ahead of the betatron phase of the particles in the new tail. This will occur if the chromaticity is negative.

To see this let us evaluate the difference in betatron phase between particles in the head and the tail of a bunch. This phase shift is obtained by integrating $\Delta\omega_\beta$ over half a synchrotron period:

$$\Delta\omega = \int_0^{T_s/2} \Delta\omega_\beta \, dt \qquad (9.29)$$

The betatron phase depends on Q and the revolution frequency Ω_o.

$$\frac{\Delta\omega_\beta}{\omega_\beta} = \left(\frac{\Delta Q}{Q} + \frac{\Delta\Omega}{\Omega} \right) \qquad (9.30)$$

The change in tune ΔQ is given by the chromaticity:

$$\Delta Q = \xi \frac{\Delta p}{p} = \frac{\xi}{\beta^2} \frac{dE}{E} \qquad (5.35)$$

The change $\Delta\Omega$ in revolution frequency is given by the time dilation factor $\eta(p)$. We consider a proton with an energy well above the transition energy

$$\frac{\Delta\Omega}{\Omega} = -\frac{\eta}{\beta^2} \frac{dE}{E} \approx -\frac{\alpha}{\beta^2} \frac{dE}{E} \qquad (6.5)$$

Combining both terms yield:

$$\Delta\omega_\beta = \frac{\omega_\beta}{\beta^2} \left(\frac{\xi}{Q} - \alpha \right) \frac{dE}{E} \qquad (9.31)$$

$$\approx \frac{\omega_\beta}{\beta^2} \frac{\xi}{Q} \frac{dE}{E} \, .$$

Substituting eq. 9.31 into the integral of eq. 9.29 yields:

$$\Delta\mu = -\frac{2}{\beta^2} \left(\frac{\omega_\beta}{\omega_s} \right) \left(\frac{\xi}{Q} \right) \frac{dE}{E} \qquad (9.32)$$

Since the uncorrected natural chromaticity is negative the betatron phase advance $\Delta\mu$ will be positive. Thus the fundamental head-tail mode is unstable.

Note that sextupoles can be used to cancel the natural chromaticity - i.e. $\xi = 0$. In this case no phase relation exists between particles in the head and in the tail of the bunch and the fundamental head-tail instability does not occur. However, it is difficult to cancel the chromaticity exactly. Furthermore higher order single bunch head tail modes can occur for positive values of the chromaticity.

If the transverse impedance has a sufficiently long memory it may also couple head tail oscillations of adjacent bunches.

Both the single and coupled head tail modes may be corrected by using an octupole magnet to induce a tune spread. However, remember that an octupole is a non linear element which drives resonance lines and may by itself limit the acceptance.

9.3.4 The beam-beam tune shift

The electric and magnetic force between interacting bunches moving in opposite direction add resulting in a strong direct space charge force which persists at higher energies. For bunches of opposite charge the forces are attractive - i.e. one bunch acts as a focusing lens in both planes. For like sign bunches the force is repulsive and equivalent to a defocusing lens. For particles travelling close to the axis the lens will be nearly linear while it is strongly non linear for particles with a large displacement.

This interaction affects the particle motion in several ways:

- it excites coherent transverse oscillations
- it introduces a non linear coupling of vertical and horizontal motion
- it excites higher order resonances.

Although the beam-beam interaction is strongly non-linear it is commonly parametrized by the tune shift ΔQ induced by its linear

part. We will here estimate the tune shift suffered by a proton of normalized energy γ traversing a bunch containing N_e electrons Gaußian distributed transversely to the beam axes with rms size σ_x and σ_z.

The focal length of such a "space charge" lens can be written as:

$$\frac{1}{f_u^p} = (k\,\ell)_u^p = \frac{2N_e}{(\sigma_{ex}^* + \sigma_{ez}^*)\,\sigma_{eu}^*}\,\frac{r_p}{\gamma_p} \qquad (9.33)$$

The stars indicate that beam sizes are evaluated at the crossing point, u = x or y.

The tune shift caused by a lens of focal strength $f = \frac{1}{k\ell}$ located at a position where the amplitude function has the value β is given by:

$$\Delta Q = \frac{\beta\, k\ell}{4\pi} \qquad (5.13)$$

Introduce the strength of the lens from eq. 9.27 yields:

$$\Delta Q_u^p = \frac{N_e}{2\pi(\sigma_{ex}^* + \sigma_{ez}^*)\sigma_{eu}^*}\,\frac{r_p}{p}\,\beta_u^*$$

To find the effect of the electron beam on the proton beam one may to first order simply replace p by e in the formulae above.

It is clear that the ultimate tune shift limit must depend on the details of the machine and the tune advance between crossings. However, it has been found experimentally at the high energy electron machines that a tune shift of $\Delta Q^e \leq 0.025$ is acceptable

for electrons. At the CERN SPS $p\bar{p}$ collider a tune shift of 0.003 has been obtained for bunched proton beams. The factor ten difference between the electron and the proton tune shift limits is presumably due to the radiative damping of the electron beam.

10. Layout and Performance of HERA

In this last chapter we briefly discuss the choice of the main parameters for HERA[5] and evaluate the luminosity.

10.1 The Lattice

The present choice of lattice for the electron and the proton ring are shown in Fig. 10.1. Both machines have a periodic FODO cell structure consisting of equidistant focusing and defocusing quadrupoles with as much as possible of the intervening space filled with bending magnets. The main lattice parameters are listed in Table 10.1. They can be derived to a good approximation using the formulas listed in chapter 4.5.

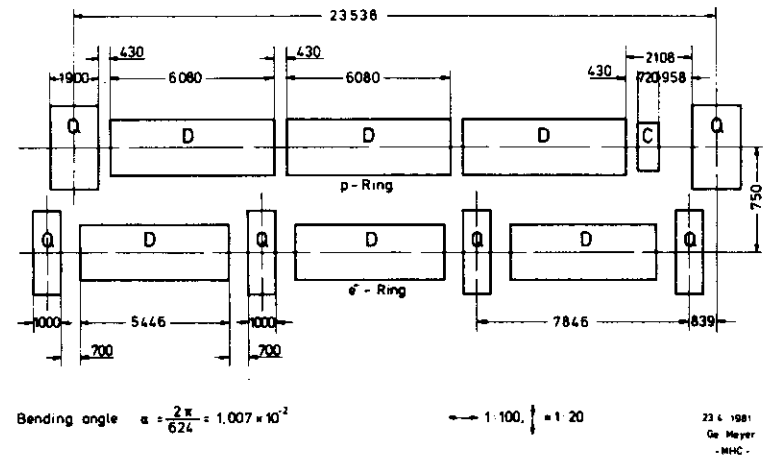

Fig. 1 HERA normal cell lattice

Fig. 10.1 - Lattice for the electron and the proton ring HERA.

Fig. 10.2 shows a cross section through the tunnel in the arcs with the proton machine installed above the electron ring.

In the e^+e^- mode of HERA the cell length is a free parameter which, for a given emittance and hence luminosity, may be chosen for minimum cost. In the ep case, the proton cell length should be an integral multiple of the electron cell length. The electron emittance and hence the focal length should be chosen such that it is possible to match the electron and the proton beam sizes at the interaction point for a given horizontal/vertical coupling of the electron beam. It can be shown that the optimum cell length is around 10 m for an aperture limited e^+e^- design luminosity of $4 \cdot 10^{31}\ m^{-2}s^{-1}$ at $2 \cdot 25$ GeV. Since the minimum is rather flat we have chosen a cell length of 15.692 m for mechanical reasons. In an octant of the electron ring there are 34 1/2 periodic cells and 2 dispersion suppressing cells in the arcs and 2 1/2 cells are incorporated into the spin rotator.

The large number of electron cells per octant reflects the need to have a dense focusing structure for the electrons. In the electron ring the beam emittance is determined by the equilibrium of synchrotron radiation and focusing strength (eq. 7.39). A dense focusing structure leads to a small beam emittance, low synchrotron frequency and a lower r.f. voltage. It is also possible to match the vertical electron beam size to that of the proton in the interaction point by varying the emittance.

Table 10.1 - HERA lattice parameters

	p-ring	e-ring
Circumference (m)	6336	
Number of superperiods	4	
Lattice	FODO	
Straight section length	360 m	
Normal cells /octant	9	34.5*
Dispersion suppressing cells/ octant	4	2
Number of dipoles / cell	6	2
Magnetic length of dipole (m)	6.08	5.446
Aperture of bending magnet (mm)	60.0 ϕ	70 x 40
Bending radius (m)	603.8	540.9
Bending angle (mrad)	10.07	
Magnetic length of quadrupole (m)	1.90	1.00
Aperture of quadrupole (mm)	60.0 ϕ	50.0 ϕ
Betatron phase advance/cell	90^0	60^0
Momentum compaction	$1.315 \cdot 10^{-3}$	$0.495 \cdot 10^{-3}$
Transition energy (GeV)	25.9	
Working point Q_x/Q_z	32.15/35.19	48.3/48.2
Cell quadrupole focal length (m)	16.6	7.8
Cell quadrupole gradient (T/m)	91.2	12.7
Amplitude function β^{max} (m)	80.4	27.2
β_{min} (m)	13.8	9.1
Dispersion D^{max}(m)	1.9	0.39
D_{min}(m)	0.92	0.24

* The horizontal bend of each spinrotator is equivalent to that of 2.5 normal cells.

The chromaticity is compensated using two families of sextupoles located adjacent to the focusing quadrupoles.

The useful aperture of the proton ring is presumably limited by non linearities rather than the geometric aperture:

These non linearities result from:

- The sextupoles needed to compensate the natural chromaticity. At least two families are needed and their strength can be written as

$$m_F = s_F \ell_F = \frac{1}{D_F}\left(\frac{1}{f} + \frac{4\pi\,(\xi_{IR})}{N_c\,(\beta_F - \beta_D)}\right) \qquad (10.1)$$

$$m_D = \frac{D_F}{D_D} m_F$$

ξ_{IR} is the chromaticity resulting from the straight sections and N_c is the number of cells.

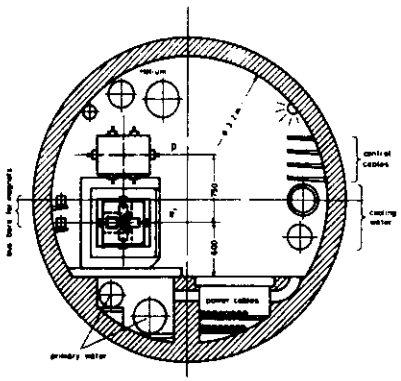

Fig. 10.2 - A cross section through the beam tunnel in the arcs.

- The higher field harmonics caused by the approximation to a cosθ current distribution in the dipole magnets and by positioning errors of the wires. The field can be written as a sum of the harmonic coefficients b_n for normal multipole fields and a_n for skew multipole fields. These coefficients are obtained from the Fourier expansion of the azimuthal field component.

$$B_\theta(r,\theta) = B_o \sum_{n=1}^{\infty} \left(\frac{r}{r_o}\right)^{n-1} (b_n \cos n\theta - a_n \sin n\theta) \qquad (10.2)$$

B_o is the induction on the axis and r_o = 2.5 cm is the reference radius.

The tolerances on the field components were taken to be the same as those imposed on the FNAL magnets:

Normal and skewed quadrupole: a_2, $b_2 = 2.5 \cdot 10^{-4}$

Sextupole : $b_3 = 6 \cdot 10^{-4}$

Skewed sextupole and all higher multipoles including the 18-pole $= 2 \cdot 10^{-4}$

This distribution was assumed to be a Gaußian centered at zero with a rms value a third of the tolerances listed above. A cold iron magnet has much higher values of the multipole components and their relative strength also changes with current due to iron saturation.

- Persistent currents. These currents induce mainly a constant setupole field with a strength proportional to the filament diameter. For the 10μm filaments used in the HERA cables the relative strength of the persistent current sextupole relation to the dipole field is $-2 \cdot 10^{-3}$ at the injection energy of 40 GeV. If left uncorrected these sextupoles would introduce a chromaticity of $\xi_H = -181$ and $\xi_V = 143$. We assume that the mean value of the persistent current sextupoles are compensated by a bucking field such that only the $\pm$ 10% fluctuations must be included in the computations must be included in the computations.

The resulting nonlinear aperture was investigated using a fast tracking programme[40]. The particles, with a given initial amplitude are tracked around the ring and their amplitude checked after each sextupole. If at least one particle is found outside the goemetric aperture then the amplitude is unstable, if all particles (in general 16) survived 100 turns then the amplitude was called stable.

The stable amplitude for the cell depicted in Fig. 10.1 is plotted versus momentum in Fig. 10.3. The computation was done at the injection energy of 40 GeV for a phase advance of 60^0 and 40^0 per cell.

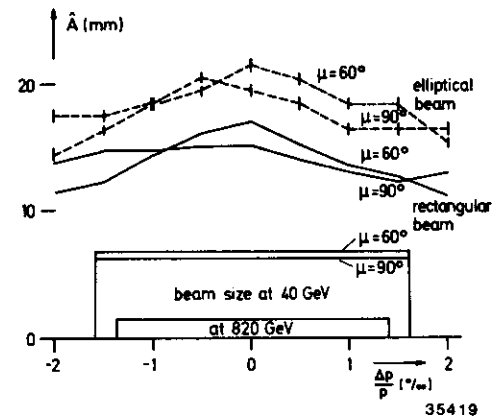

Fig. 10.3 - The stable amplitude limits at the injection energy of 40 GeV are plotted versus momentum for a phase advance of 60^0 corresponding to Q_x/Q_z = 33.15 / 35.18 and a phase advance of 90^0 yielding Q_x/Q_z = 25.16 / 29.23 The limits are evaluated for a rectangular and an elliptical phase space distribution. The maximum horizontal beam size ($2.2\sigma_x$) at 40 GeV and 820 GeV are shown for comparison.

Within the accuracy of the computation the non linear aperture is the same for 60^0 and 90^0 phase advance. For a rectangular beam phase space and $\varepsilon_x = \varepsilon_z$ the non linear aperture is on the order of 14 mm. It might be more realistic to assume an elliptical phase space and in this case the aperture is around 18 mm. The aperture at 820 GeV is slightly larger since persistant current effects can be neglected

at high energies. The values should be compared to the geometric aperture of $\pm$ 28 mm. Measurements at the ISR found a beam lifetime on the order of 18.5 hours with the vertical collimators set at 2.2σ. This aperture is indicated at the injection energy of 40 GeV and at 820 GeV. This aperture, even at 40 GeV, is comfortably smaller than the non linear aperture determined by the tracking programme. The emittance growth due to beam-gas and intra beam scattering has been evaluated and found to be negligible for injection times on the order of half an hour.

At present the computation time is about 5000 times longer than the natural revolution time such that only short storage times may be investigated. We are now building a dedicated computer which will enable us to investigate storage times on the order of several hours.

10.2 The r.f. System

The r.f. system for the electron ring is based on the 500 Mhz system used in PETRA. Indeed r.f. equipment like klystrons, cavities, waveguides and other components will be transferred from PETRA to HERA.

At the nominal energy of 30 GeV the particle loose 142.3 MeV per turn in synchrotron radiation. For a phase advance of 60^{o} the peak voltage must be 166.7 MV per turn to ensure a beam life of 24 hours due to quantum fluctuations. The stable r.f. phase is 58.6^{o}. The number of synchrotron oscillation per turn is 0.038 and the r.m.s. bunch length is 9.3 mm.

The injection system for the protons is designed to fill HERA with 210 bunches of protons with $3 \cdot 10^{11}$ protons per bunch using the following sequency of accelerators:

Proton Linac (50 MeV) → DESY (7.6 GeV) → PETRA (40 GeV) → HERA

The bunches with the final number of particles per bunch are formed in DESY such that a complicated stacking procedure, which may lead to an emittance growth, is avoided. To reach the highest luminosity the proton r.f. system must be designed not only to accelerate but also to produce a short proton bunch with a high line density. The stable bunch length shrinks from about 100 m at low energies to a fraction of 1 m at the peak energy of HERA. Some of the shrinkage is provided by the natural evolution of the bunch length during acceleration but in addition the frequency is increased twice during the acceleration sequence.

These frequency changes are done at transfer. The first step is from 2.8 MHz in DESY to 10.37 MHz in PETRA as the beam is transferred. The second step from 10.4 MHz to 208 MHz occurs between PETRA and HERA. In order for the PETRA bunch to fit into the much shorter HERA bucket a bunch rotation is applied to the bunch before transfer.

We now give some of the parameters for the r.f. systems as presently planned. We assume that adiabatic capture works with an efficiency of 70% and that 10% of the protons are lost during each transfer. To reach the design value of $3 \cdot 10^{11}$ protons/bunch a total of $1.6 \cdot 10^{3}$ protons are injected from the Linac in a single turn

into DESY. At DESY the protons are captured into three 100 m long bunches. The momentum spread is $1.2 \cdot 10^{-3}$ corresponding to a bunch area of 0.005 rad. A peak voltage of 1.43 kV at a frequency of 0.891MHz (h=3) is needed at injection.The protons are accelerated through transition (γ_{tr} = 5.680) and transferred bunch by bunch into PETRA. Note that the protons are injected at 7.6 GeV which is above the the transition energy (γ_{tr}=6.0) in PETRA. The frequency at injection is 2.817 MHz and the peak voltage is 11.22 kV. Such a system can easily be realized using ferrite loaded cavities. Longitudinal instabilities do not appear to be a problem - the Laslet Q shift is -0.103 at injection and (Z/n) must be less than 40Ω to avoid the microwave instability.

PETRA is loaded with 18 out of 20 possible bunches spaced 384 ns apart. PETRA will then accelerate the protons to 40 GeV, limited by the saturation of the dipole magnets. At injection the r.f. frequency is 10.33 MHz with a peak voltage of 19.8 kV. At the end of the accelerating cycle the r.f. frequency is 10.41 MHz and a peak voltage of 8.35 kV. The Laslet Q shift is only -0.040 at injection and (Z/n) must be less than 14.4 Ohm at 40 GeV.

Since the required frequency swing is only 0.6% cheap reentrant r.f. cavities can be used instead of ferrite loaded cavities. At 40 GeV the bunches can be made short without creating a large Q-shift and it is therefore possible to go directly to the final r.f. frequency of 208 MHz in HERA. At 40 GeV in PETRA the bunch is 10 m

long. Clearly the bunches must be compressed to about 1.3 m before they are transferred to HERA. The simplest way to do this is to perform a one quarter bunch rotation in an abruptly increased bucket. This requires much less voltage than adiabatic compression of the bunch and the voltage is only required during the short time of one quarter synchrotron oscillation. The bunches must then be transferred between PETRA and HERA in one go and this is possible since the ratio of the circumference is 80 to 220. The bunch rotation can be done by simply pulsing the accelerating cavities to some 500 kV for about a msec.

The PETRA cycle is repeated 12 times until HERA is loaded with 210 bunches spaced uniformly by 96 ns except for a notch 1 μs long. The notch is needed for the risetime of the beam abort kickers.

There are several reasons for choosing a rather low r.f. frequency in HERA.

Firstly we have seen that a low frequency makes the final bunch compression in PETRA easier.

The inductive wall impedance shift the coherent synchrotron frequency according to eq. 9.19. Landau damping breaks down if this shift exceeds the incoherent frequency spread of the particles in the bunch. The voltage required to prevent this (eq. 9.19) is proportional to $\omega_{r.f.}^2$ for a given ratio of bunch length to bucket length. Even for a (Z/n) as low as 5 Ω the r.f. peak voltage must be 100 MV for a r.f. frequency of 208 MHz and a bunch length of 38 cm. Lower frequency r.f. cavities are difficult to fit into the ring due to their larger diameter.

10.3 Interaction Region

The interaction region in an electron-proton collider is complex. It must bring the two different beams into a small angle low beta

collision geometry and it must turn the electron spin to be either parallel or antiparallel to the beam direction at the interaction point. Furthermore, the dispersion in the lattice must be made to disappear in the straight section, and sufficient space for r.f. cavities, injection and ejection system must be found.

In the design we must first decide whether to use a head on collision geometry, or to opt for a crossing angle. Since luminosity and beam-beam tune shift vary in the same manner with crossing angle, a larger angle would simply achieve the same conditions as a head on collisions but requires more protons and electrons. To optimize the luminosity, the interaction region must be designed to produce a small value of the betatron function at the interaction point. The minimum value of the betatron function is presumably limited by the maximum chromaticity introduced by the vertically focusing quadrupoles. The vertical chromaticity introduced by the eight vertically focusing quadrupoles is given by:

$$\xi_y^{IP} = -\frac{8}{4\pi}\frac{f}{\beta^*} \qquad (10.3)$$

f is the focal length and β^* the value of the betatron function at the interaction point. The quadrupoles must thus be positioned as close as possible to the interaction point. To set the scale, the arcs contribute $\xi_y^a = 30$ to the vertical chromaticity. The arbitrary assumption that the interaction region should make a smaller contribution yield the inequality $\xi < 45\beta^*$.

Rather strong quadrupole fields are needed to focus the proton beam and it therefore seems advisable not to pass the electrons through the field of the proton quadrupoles.

In the head on collision geometry the electron and the proton beam must be separated by a dipole magnet. In order not to flood the interaction region with synchrotron radiation this bend must be rather gentle and the vertically focusing proton quadrupole will therefore be located rather far from the interaction point.

In the present layout (Fig. 3.2) we have chosen to cross the beams at an angle of $\pm$ 10 mrad in the horizontal plane. A horizontal crossing is advantagous since the width of the electron beam is much larger than its height. The large crossing angle makes it possible to install the proton quadrupoles directly following the electron quadrupole. In the present layout the front face of the vertically focusing quadrupoles are positioned at $\pm$ 7.5 m and at $\pm$ 10 m with respect to the IP for electrons and protons respectively. It is possible to detect particles down to 13 (32) mrad. This is more than sufficient (Fig. 2.12) to measure the formfactors with high precision at values of Q^2 which overlap with present data. Note that the two machines are totally independent. It is thus possible to inject into one ring while leaving the other at high energy. It is also possible to vary the center of mass energy by changing the proton energy and keeping the electron fixed at 27.5 GeV where polarisation is expected to occur.

The next problem is to incorporate the spin rotators. Several possible designs exist. The solution presently adoped is shown schematically in Fig. 10.4.

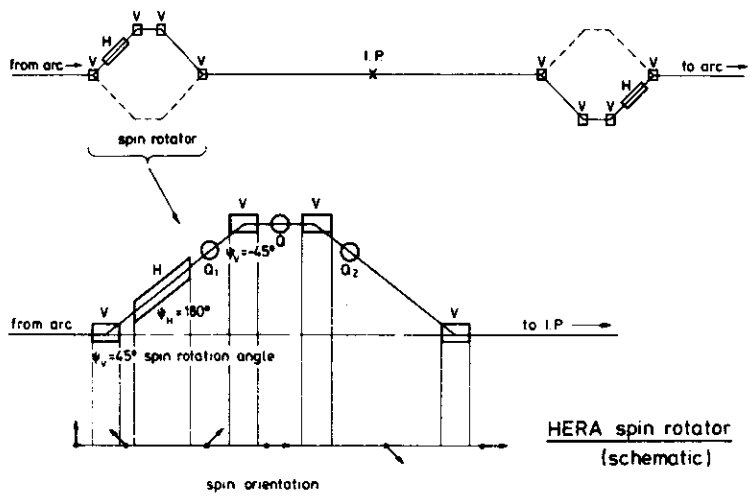

Fig. 10.4 - Principal layout of the spin rotators.

The essential part of the rotator is a horizontal bending magnet which causes the spin to precess by π around the vertical axis and is surrounded by two vertical bending magnets of opposite sign that generate a spin rotation of $\pm \pi/4$ about the radial axis. A pair of vertical bending magnets restores the original beam direction without changing the spin direction. There is again one such rotator at each end of the straight section; the first turns the spin longitudinal and the second restores the transverse polarisation. For

opposite helicity at the interaction point, all vertical bends are inverted, while the horizontal bends remain unchanged. Since these horizontal bends are rather strong, they are designed to be a part of the normal bending in the arc. In the HERA design each horizontal rotator magnet replaces exactly 5 of the 78 normal cell bending magnets per octant.

The horizontal bending magnets must thus deflect the particles through a well defined angle. α = 50.32 mrad and precess the spin around the vertical direction by $\phi_y = \pi$. Since $\phi_y = (\gamma a)\,\alpha$, both conditions can only be satisfied for a single energy E_0 = 27.8 GeV corresponding to a spin tune $\nu = (\gamma a)$ = 62.4 GeV.

To operate the rotator at a different energy requires two correction bends to feed the beam band into its nominal position in the arcs. With such correctors it is possible to properly operate the rotators in an energy range of, say 0.5 GeV around E_0 and explore the optimum between depolarising resonances.

The final layout of the interaction regions is shown in Fig. 3.2. The spin rotators are located at the ends of the $\pm$ 180 m long straight sections. With the expections of the vertical spin rotator bends the electron ring stays in the plane. Note that the 1st bending magnet is located nearly 120 m from the IP. Detailed calculations show that it is possible to position detector elements

within a few cm of the beam without being swamped by synchrotron radiation.

10.4 Luminosity

The luminosity of an electron - proton colliding beam machine with the beams crossing in the horizontal plane at an angle 2ϕ is given by:

$$L = \frac{f_o\, n_b\, N_e\, N_p}{2\pi(\sigma_{xp,eff}^2 + \sigma_{xe}^2)^{1/2}\,(\sigma_{zp}^2 + \sigma_{ze}^2)^{1/2}}$$

In this formula f_o is the revolution frequency, n_b the number of bunches in the ring, N_e and N_p the number of electrons and protons per bunch respectively, $\sigma_{xp,eff} = (\sigma_{sp}^2 + (\sigma_{sp}\,\phi)^2)^{1/2}$ with σ_{sp} denoting the proton bunch length, σ_{xe} is the width of the electron beam and σ_{zp} and σ_{ze} the heights of the proton and the electron beam respectively. The beam sizes are all defined in the interaction point and are calculated from the beam emittances and the values of the amplitude function at the interaction point. The emittance of the proton beam is determined by the injectors, whereas the emittance of the electron beam is given by the electron energy and the phase advance per cell.

We will now discuss the choice of the various parameters which enter the luminosity computation.

The ultimate limit to the luminosity is given by the maximum allowed value of the beam-beam tune shifts. The tune shifts, derived

in chapter 9, can be expressed for the vertical direction as:

$$\Delta Q_{ze} = \frac{\beta_{ze}^*\, r_e\, N_p}{2\pi\gamma_e(\sigma_{xp,eff}^* + \sigma_{zp}^*)\,\sigma_{zp}^*}$$

$$\Delta Q_{zp} = \frac{\beta_{zp}^*\, r_p\, N_e}{2\pi\gamma_p(\sigma_{xe}^* + \sigma_{ze}^*)\,\sigma_{ze}^*}$$

Here γ_e and γ_p are respectively the electron and the proton energy measured in units of the rest energy and β_e^* and β_p^* are the values of the amplitude function at the origin. ΔQ is quoted per interaction region.

For head-on collisions a tune shift limit of 0.025 has been observed at high energy e^+e^- colliders compared to approximately 0.003 observed at the CERN $p\bar{p}$ collider. We will use $\Delta Q_e = 0.025$ and $\Delta Q_p = 0.0025$ as the limiting values also in the case of a finite crossing angle.

The luminosity was evaluated with $\beta_{ze}^* = 0.15$ m, $\beta_{xe}^* = 3.0$ m, $\beta_{zp}^* = 0.30$ m and $\beta_{xp}^* = 3.0$ m. The vertical chromaticities evaluated according to eq. 10.3 yields:

$$\xi_{ze}^{IP} = 31.8 \qquad \xi_{zp}^{IP} = 21.2\ .$$

The effective horizontal beam size is determined by the crossing angle and the length of the proton bunch. With the 100 MV r.f. system as proposed the bunch is 9.5 m long (σ_s) at 820 GeV.

The vertical emittance for the electron beam is determined by the vertical and horizontal coupling. Couplings as small as 1% have been observed at PETRA. The spinrotator will increase the vertical coupling and with the present rotator we find a value of 10%. This can be reduced and we assume a coupling of 4% for the calculations here. To maximize the luminosity the phase advance per cell is adjusted in discrete steps of 30^0, 45^0, 60^0 and 90^0.

The luminosity is also proportional to the number of bunches per beam. In the case of a crossing geometry the number of bunches is a free parameter. In the present design we have limited the number of bunches to 210 corresponding to a spacing of 28.8 m between adjacent bunches.

The electron current at high energy is limited by the available r.f. power. At HERA we assume that at most 12 MW is available at the r.f. cavities. It takes about 4.0 MW to establish the required circumferential voltage of 166.7 MV at 30 GeV. With an average energy loss of 142.3 MeV per turn the remaining 8 MW is sufficient to accelerate a current of 56 mA.

For the protons we assume a limit of $3 \cdot 10^{11}$ protons per bunch. As a comparison 10^{11} protons per bunch have been stored at the SPS collider. The hope for increase in protons is based on a very smooth beam pipe with a low (Z/n), a high r.f. peak voltage to produce a

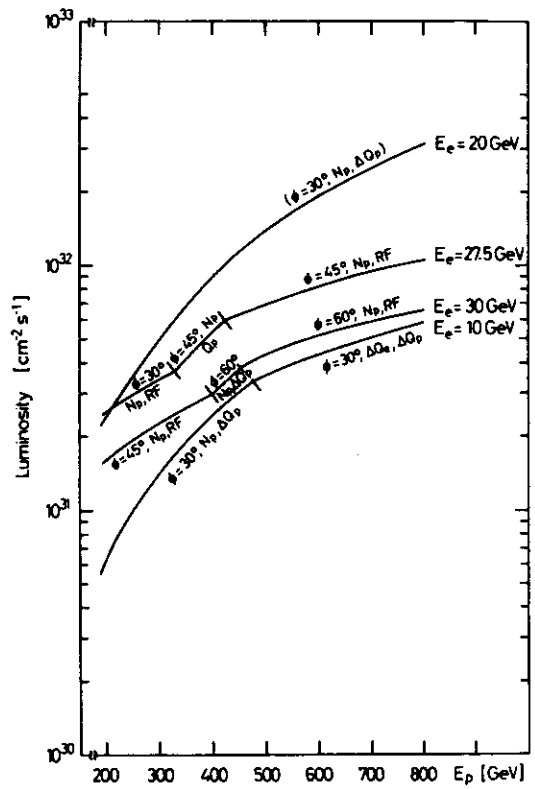

Fig. 10.5 - Luminosity as a function of proton energy for various electron energies. The luminosity limiting parameters are indicated.

high line density and the use of octupoles and feed back systems to stabilize the beam.

The luminosity is plotted in Fig. 10.5 versus the proton energy for electron energies of 10, 20, 27.5 and 30 GeV. Listed in the brackets is the phase advance per cell in the electron beam which with the parameter in the proton respectively in the electron beam which limits the luminosity. Note that at 30 GeV the luminosity is limited by the available currents - i.e. the luminosity can be increased by either storing a higher current or by moving the quadrupoles closer and lower the vertical β function. Indeed at 30 GeV and 820 GeV the tune shifts are rather low Q_{xe}/Q_{ze} = 0.008/0.014 and Q_{xp}/Q_{zp} = 0.0006/0.0009.

At E_e = 20 GeV sufficient electron current can be stored to reach the proton tune shift limit. In this case a peak luminosity of $3 \cdot 10^{32}$ $cm^{-2}s^{-1}$ is realistic.

With the luminosity predicted at HERA we should thus be able to explore the kinematical region $Q^2 > 10000$ GeV^2 where surprizes are expected to occur. With some luck this may happen before the end of the decade.

References

1) H.G.Hereward, K.Johnsen, A.Schoch and C.J. Zilverschon, Proc. 3rd Internat.Conf. on High Energy Accelerators, Brookhaven, 1961.

2) L.Goldzahl and E.G.Michaelis, CERN 66-12 (1966).

3) C.Pellegrini, J.Rees, B.Richter, M.Schwartz, D.Möhl and A.Sessler, Proc. 8th Internat.Conf. on High Energy Accelerators, CERN, 1971, p. 153.

4) H.Gerke, H.Wiedemann, B.H.Wiik and G.Wolf, DESY H-72/22 (1972)

R.Chasman and G.A.Voss, IEEE Trans.Nucl.Sci. NS-20, No.3 (777) 1973

EPIC Machine Design Study Group, 9th Intern.Conf. on High Energy Accelerators, Stanford, 1974.

T.L.Collins, P.A.Edwards, J.Ingebretsen, D.E.Johnson, S.Ohnuma, A.G.Ruggiero and L.C.Teng IEEE Trans.Nucl.-Sci. NS-22, No. 3 (1911) 1975

5) Report of the Electron-Proton Working Group of ECFA, Study of the Proton-Electron Storage Ring Project HERA ECFA 80/42, DESY HERA 80/01 - 1980 HERA - A Proposal for a large Electron-Proton Colliding Beam Facility at DESY - DESY HERA 81/10

6) T.Nishikawa, Proc. of 9th Int.Conf. on High Energy Accelerators, May 1974, Stanford, California, Report of the TRISTAN ep ($e\bar{e}$) Working Group UTPN-165 / UT-345 July 1980

7) Electron-Proton Interaction Experiment, Fermilab Proposal 659, Spokesman: W.Y.Lee, R.R.Wilson. A more ambitious proposal was put forward by a group of Canadian Physicists but terminated due to lack of funds.

CHEER - A feasibility Study for an Electron Ring at a High Energy Proton Accelerator.

8) P.E.Faugeras, CERN / SPS / DI-MST 81-16 and LEP Note 303.

9) M.Sands - The Physics of Electron Storage Rings - SLAC-121

10) H.Bruck, Accelerators Circulaire des Particules Press Universitaires de France, Paris, 1966

11) Theoretical Aspects of the Behaviour of Beams in Accelerators and Storage Rings. - Proceedings of the First Course of the International School of Particle Accelerators, Erice 10-22 Nov. 1976 - CERN 77-13

12) Physics of High Energy Particle Accelerators, edited by: R.A.Carrigan, F.R.Huson and M.Month, American Institute of Physics - 1982

13) J. Le Duff: Stanford Summer Institute 1981

14) The various proposals listed above contain a discussion of the physics which can be carried out with a large electron-proton colliding ring - for an early complete discussion see: C.H.Llewellyn-Smith and B.H.Wiik, DESY 77/38 (1977) CHEEP-An ep facility in the SPS: J.Ellis, B.H.Wiik and K.Hübner CERN 78-02. Most figures and rules shown below are taken from this work and from reference 5.

15) Superconducting Accelerator Design Report - Fermi National Accelerator Laboratory (1979)

16) S.L.Glashow, Nucl.Phys. 22, 579 (1961)

S.Weinberg, Phys.Rev.Lett. 19, 1267 (1967)

A.Salam, Proc. 8th Nobel Symposium, Stockholm, Almquist and Wiksells, Stockholm 1968 p. 363

17) A.J.Buras and K.J.F.Gaemers, Nucl.Phys. B 132, 249 (1978)

18) M.Kobayashi and T.Maskawa, Proc. Theor.Phys. 49, 652 (1973)

19) L.F.Abbott and E.Fahri, Nucl.Phys. B 189, 547 (1981)

20) For an early account on the observation of pointlike constituents see: W.K.H.Panofsky, Proceedings of the XIV International Conference on High Energy Physics, Vienna, Austria, 1968

21) For an early report on Scaling Violation see: R.E.Tylor in Proc. of the Int.Symposium on Lepton and Phtoton Interactions at High Energies, Stanford 1975 and J.Drees, Proc. of the Int. Neutrino Conference, Aachen 1976.

22) H.Fritzsch, M.Gell-Mann and H.Leutwyler, Phys.Lett. 47B. 365 (1973) D.J.Gross and F.Wilczek, Phys.Rev.Lett.30, 1343 (1973) H.D.Politzer, Phys.Rev.Lett. 30, 1346 (1973) S.Weinberg, Phys.Rev.Lett. 31, 31 (1973)

23) Yu. A.Gal'fand and E.P.Likhman, JEPT Lett. 13, 323 (1971) P.V.Volkov and V.P.Akalov, Phys.Lett. 46B, 109 (1973) J.Wess and B.Zumino, Nucl.Phys. B70, 39 (1974)

24) For a recent review and a complete set of references see: M.E.Peskin, 1981 International Symposium on Lepton and Photon Interactions at High Energies, Bonn, August 1981

25) J.C.Pati and A.Salam, Phys.Rev. D8, 1240 (1973) and Phys.Rev.D10, 275 (1974)

26) J.Schwinger, Phys.Rev.125, 397, 2286 (1973)

R.Jackiew and K.Johnson, Phys.Rev. D8, 2286 (1973)

J.M.Cornwall and R.E.Norton, Phys.Rev.D8, 3338 (1973)

M.A.Beg and A.Sirlin, Ann.Rev.Nucl.Sci 24, 379 (1974)

S.Weinberg, Phys.Rev. D13, 979 (1976) and Phys.Rev. D19, 1277 (1979)

L.Susskind, Phys.Rev.D20, 2619 (1979)

27) S.Rudaz and J.Vermaseren, CERN Preprint TH-2961 (1981).

28) G.Barbiellini et al., ECFA/LEP Specialized Study Group 9, DESY Report 79/67.

29) S.K.Jones and C.H.Llewellyn-Smith, University of Oxford Preprint 73/82.

30) E.D. Courant and H.S.Snyder; Ann. Physics 3, 1 (1958)

K.G.Steffen in Proc. Int. School "Enrico Fermi", Course XLVI, Physics with Intersecting Storage Rings, Academic Press (1971)

E.Keil in ref. 11.

31) A.Schock, CERN Report 57-1 (1978)
G.Guignard, CERN 78-11 (1978)
E.J.N.Wilson in ref. 11.

32) B.W.Montague in ref. 11.

33) K.Robinson, Phys.Rev. 111, 373 (1958)

34) I.M.Ternov, Yu.M.Loskutov and L.I.Korvina, Sov.Phys. JETP, 14, 921 (1962)

A.A.Sokolov and I.M.Ternov, Sov.Phys.Dokl. 8, 1203 (1961)

A.W.Chao in ref. 12 - Talks given at the Polarized Electron Acceleration and Storage Workshop Hamburg, March 22-27, 1982 DESY M-82/09.

35) H.D.Bremer et al., DESY 80/76 and DESY 82/26.

36) V.Bargman, L.Michel and V.L.Telegdi, Phys.Rev.Lett. 2, 435 (1959)

37) V.N.Baier and Yu. F.Orlov, Sov.Phys.Dokl. 10, 1145 (1966)

Ya. S. Derbenev and A.M.Kondratenko, Sov. Phys. JETP 37, 968 (1973)

38) A.W.Chao and K.Yokoya, KEK-81-7;

K.Steffen, Internal Report CBN 81-29, Newman Lab. Cornell - November 1981.

39) For a review on instabilities including references see: A.Hofmann, B.Zotter and F.Sacherer in ref. 11.

40) A.Wrulich - DESY HERA 82/07.